Forschungszentrum Karlsruhe
in der Helmholtz-Gemeinschaft

Wissenschaftliche Berichte
FZKA 6988

Melt Dispersion and Direct Containment Heating (DCH) Experiments in the DISCO-H Test Facility

L. Meyer, G. Albrecht, M. Kirstahler
M. Schwall, E. Wachter, G. Wörner

Institut für Kern- und Energietechnik
Programm Nukleare Sicherheitsforschung

Mai 2004

Forschungszentrum Karlsruhe

in der Helmholtz-Gemeinschaft

Wissenschaftliche Berichte

FZKA 6988

Melt Dispersion and Direct Containment Heating (DCH) Experiments in the DISCO-H Test Facility

L. Meyer, G. Albrecht, M. Kirstahler

M. Schwall, E. Wachter, G. Wörner

Institut für Kern- und Energietechnik

Programm Nukleare Sicherheitsforschung

Forschungszentrum Karlsruhe GmbH, Karlsruhe

2004

Impressum der Print-Ausgabe:

Als Manuskript gedruckt

Forschungszentrum Karlsruhe GmbH
Postfach 3640, 76021 Karlsruhe

Mitglied der Hermann von Helmholtz-Gemeinschaft
Deutscher Forschungszentren (HGF)

ISSN 0947-8620

urn:nbn:de:0005-069882

Experimente in der DISCO-H Versuchsanlage zur Dispersion der Kernschmelze und der direkten Aufheizung des Sicherheitsbehälters (DCH)

Zusammenfassung

Die Versuchsanlage DISCO-H wurde im Forschungszentrum Karlsruhe gebaut um Experimente durchzuführen, zur Untersuchung der Dispersion der Kernschmelze und der direkten Aufheizung des Containments bei Versagen des Druckbehälters bei niedrigem Systemdruck während eines schweren Störfalles eines Leichtwasser Druckreaktors. Es werden die fluiddynamischen, thermischen und chemischen Prozesse modelliert, die bei einem Versagen der Bodenkalotte des Reaktordruckbehälters (RDB) und dem anschließenden Ausströmen der Schmelze auftreten. Eine Eisen-Aluminiumoxid Schmelze wird durch Dampf bei Drücken bis zu 2.2 MPa ausgetrieben. Vorausgegangen war eine detaillierte Untersuchung der Strömungsvorgänge mit kalten Modellflüssigkeiten bei verschiedenen Drücken und Geometrien in der DISCO-C Anlage.

Die wichtigen Komponenten der Anlage sind im Maßstab 1:18 zu einem großen europäischen Reaktor modelliert. Folgende Größen werden im Versuch bestimmt: die Druck- und Temperaturverläufe im RDB, in der Reaktorgrube, den Reaktorräumen und dem Sicherheitsbehälter; die Schmelzeanteile an allen Orten, zusammen mit der Größenverteilung der Partikel; Videofilme im Reaktorraum und im Sicherheitsbehälter zur Bestimmung der Dauer des Partikelfluges und der Wasserstoffflamme; und Gasanalysen an drei Orten vor, während und nach dem Versuch.

Die Ergebnisse von sechs Experimenten werden präsentiert. Alle Versuche wurden mit 10,6 kg Eisen-Aluminiumoxid Schmelze (skaliert 16 m³ Corium) und Löchern von 56 mm (skaliert 1 m) bzw. 28 mm Durchmesser im Zentrum der Bodenkalotte durchgeführt. Zum Vergleich mit einem ähnlichen Experiment im Maßstab 1:10 wurde das Referenzexperiment mit einem direkten Ausgang aus der Reaktorgrube in den Sicherheitsbehälter durchgeführt (offene Grube). Die Atmosphäre im Sicherheitsbehälter war weitgehend prototypisch, mit einem großen Dampfanteil und 3% Wasserstoff. Hier und in anderen Tests wurde zusätzlich Wasserstoff gebildet und verbrannt. In einem Versuch wurde dieser Effekt ausgeschlossen, indem die Schmelze durch Stickstoff ausgetrieben wurde und eine reine Luftatmosphäre im Sicherheitsbehälter herrschte. In zwei Versuchen wurde der direkte Weg aus der Grube in den Sicherheitsbehälter verschlossen.

Der Druckanstieg im Sicherheitsbehälter war am höchsten bei einer offenen Grube und mit Wasserstoffverbrennung. Bei einer geschlossenen Reaktorgrube müssen die Schmelzepartikel zuerst in den Reaktorraum gelangen und von dort durch relativ kleine Querschnitte in den Sicherheitsbehälter. In diesem Fall wird wesentlich weniger Wasserstoff erzeugt und verbrannt. In dem Versuch ohne Dampf gab es keinen Wasserstoffeffekt, jedoch war der direkte Weg in den Sicherheitsbehälter offen. Dadurch wurde ein großer Anteil der Schmelze fein verteilt in den Sicherheitsbehälter ausgetragen, und konnte dort durch effizienten Wärmeaustausch die Atmosphäre aufheizen und den Druck erhöhen. Bei geschlossener Grube verblieb mehr Schmelze in der Grube und fast der gesamte Rest wurde im Reaktorraum aufgefangen. Die Partikel, die in den Sicherheitsbehälter gelangen, haben einen kleinen mittleren

Durchmesser von 0.15 bis 1.4 mm, während die Partikel im Reaktorraum einen mittleren Durchmesser meist größer 2 mm haben.

Die skalierten Experimente mit nahezu prototypischen Bedingungen haben den großen Einfluss eines direkten Weges zwischen Reaktorgrube und Sicherheitsbehälter gezeigt. Existiert dieser Weg nicht, so kann es zwar einen beträchtliche Schmelzeaustrag in die Pumpen- und Dampferzeugerräume geben, jedoch kaum in den Sicherheitsbehälter. Als Folge wird der Druckanstieg gering sein und unter dem Auslegungsdruck der meisten Sicherheitsbehälter bleiben.

Abstract

The DISCO-H Test Facility at Forschungszentrum Karlsruhe was set up to perform scaled experiments that simulate melt ejection scenarios under low system pressure in Severe Accidents in Pressurized Water Reactors (PWR). These experiments are designed to investigate the fluid-dynamic, thermal and chemical processes during melt ejection out of a breach in the lower head of a PWR pressure vessel at pressures below 2 MPa with an iron-alumina melt and steam. In the past, a detailed study of pressure and geometry effects on the fluid dynamics of the melt dispersion process had been performed with cold model fluids in the facility DISCO-C.

The main components of the facility are scaled about 1:18 linearly to a large European pressurized water reactor. Standard test results are: pressure and temperature history in the RPV, the cavity, the reactor compartment and the containment, post test melt fractions in all locations with size distribution of the debris, video film in reactor compartment and containment (timing of melt flow and hydrogen burning), and pre- and post test gas analysis in the cavity and the containment.

The results of six experiments are presented here. All experiments were done with 10.6 kg of iron-alumina melt (scaling to 16 m³ corium), and a hole of 56 mm diameter (1 m scaled) or 28 mm at the center of the lower head. For comparison with a similar experiment conducted in a larger scale (1:10), the basis experiment was performed with an open path from the reactor pit to the containment (open pit), with prototypical conditions concerning the steam driven ejection out of the RPV, and a containment atmosphere, that was part air and part steam at an elevated pressure, with 3 mole-% hydrogen. In this and other tests, hydrogen production and combustion occurred. In one experiment the hydrogen effect was excluded by using only nitrogen as driving gas and a pure air atmosphere in the containment. In some tests the direct path to the containment was closed (closed pit).

The pressure rise in the containment is highest with an open pit and hydrogen combustion. With a closed pit the gas and the debris has to flow first into the subcompartment and then through relatively small cross sections into the containment. Considerable less hydrogen was produced and burned in this case. In the test without steam, no hydrogen effect was present, but, with the direct path to the containment open, a large amount of debris was dispersed into the containment, and efficiently transferred heat to its atmosphere. With the closed pit more melt remained in the pit and almost all the rest was trapped in the subcompartment. The size of the debris particles ejected into the containment is very small, with the bulk of the mass having diameters between 0.15 and 1.4 mm, whereas the melt fraction found in the subcompartment had larger particles with diameters mainly above 2 mm.

The experiments performed with nearly prototypical conditions in a small scale showed the importance of the direct path from the reactor pit to the containment. If that path does not exist, there may be a considerable ejection into the pump and steam generator rooms, but almost nothing into the open space of the containment. The pressure increase will stay moderate and well below the design pressure of most containments.

CONTENTS

TABLES

FIGURES

ACKNOWLEDGMENTS

We want to thank Günter Jacobs, who for many years promoted the idea to investigate experimentally the problem of Direct Containment Heating for the European reactors. The strong support from Prof. Günter Kessler finally lead to the initiative to start the program.

We are grateful to Tom Blanchat, Sandia National Laboratories, for his advice and information on experimental procedures. The authors express their gratitude to Markus Greulich, who was involved to a large extend in setting up the test facility and performing the first tests.

This work was partially funded by the German VdEW and Siemens under the contract for the Collaboration in Research and Development for the Investigation of the Events in Severe Accidents in LWRs, and part of the work was supported by the European Commission under the contract FIKS-CT-1999-00003 (ECOSTAR, 5th EC-Framework Program).

NOMENCLATURE

CPV	containment pressure vessel
DCH	Direct Containment Heating
RCS	reactor cooling system
RPV	reactor pressure vessel
TÜV	Technischer Überwachungsverein
A	surface (m^2)
d	diameter (m)
M	molecular weight (kg/kmol)
m	mass of melt (kg)
p	pressure (MPa)
Δp	pressure difference between RPV and cavity (MPa)
R	gas constant (J/kmol/K)
R	gas constant (J/kg/K)
ΔT	temperature difference (K)
Δt	time interval (s)
u	velocity (m/s)
V	volume (m^3)
ε	contraction factor of a jet
ρ	density (kg/m^3)

1 Introduction

The conditions in the reactor pressure vessel (RPV) in the late phase of a core melt accident can differ significantly depending on the failure history of the core. If a failure of the RPV lower head occurs, the condition of the molten core, i.e. temperature, composition, distribution, and mass of the melt, together with the design of the lower head, determines the location, shape and size of the breach. The decisive parameter for the mode of melt release is the system pressure at the time of RPV-failure. If the pressure is at the same level as the pressure in the containment, or only slightly above, the molten part of the core inventory will flow into the reactor pit by gravity. The release of radioactive aerosols will be small and the further development of the accident is determined by the specific plant provisions. The assumption that the system pressure at core melt accidents will be low (<20 bar) in German plants is justified, due to the pressure reduction system provided and the fact that a failure of the surge line is expected in such cases [Roth94]. However, if the pressure is between 5 and 20 bar, e.g. because of late reflooding and rapid steam generation, the melt will be ejected forcefully into the reactor pit and possibly beyond, even at these low pressures, accompanied by the blowdown of the reactor cooling system. In this case it depends on the cavity geometry whether the melt will be trapped without severe consequences in places with long term cooling capabilities or whether it will be dispersed into the containment atmosphere with unfavorable effects upon the accident progress. The finely fragmented melt particles lead to efficient debris-to-gas heat transfer, hydrogen generation by metal/steam reactions in the reactor pit and hydrogen combustion in the containment. These processes, referred to as Direct Containment Heating (DCH), may cause a rapid increase in temperature and pressure in the containment and may have an impact on vital safety components (see sketch below).

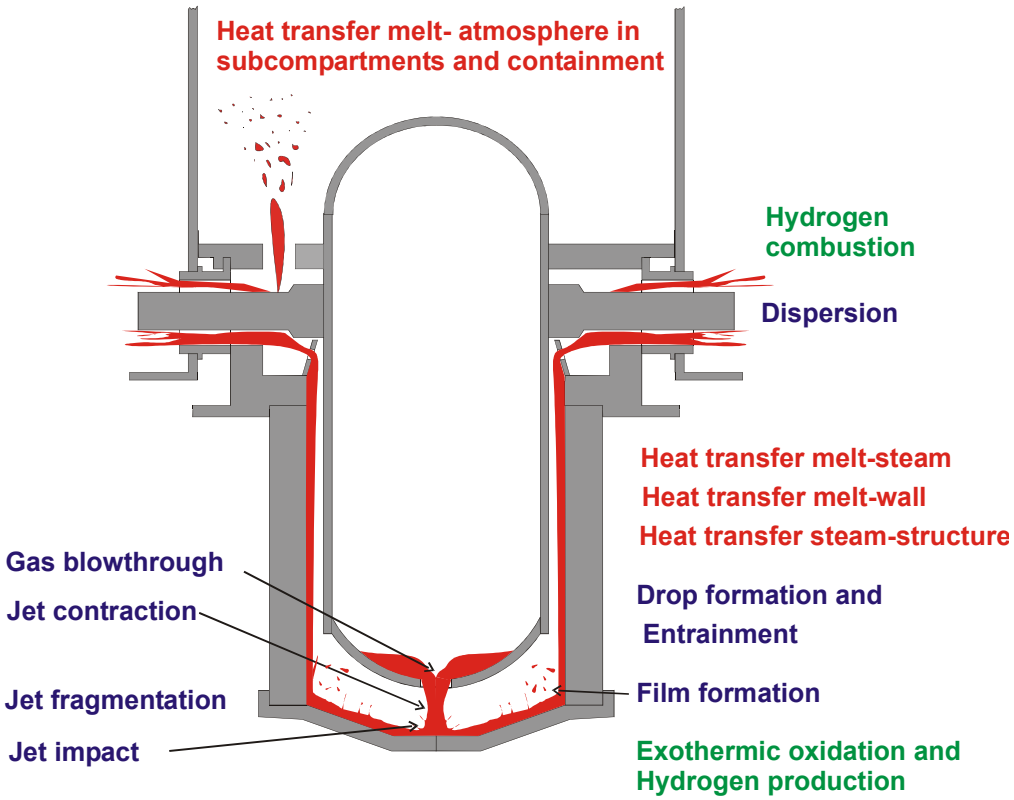

DCH is a relatively well resolved issue for reactor plants with cavity designs without a direct path to the containment, where a large instrument tunnel is connected to reactor sub-compartments. A research program devoted to high pressure melt ejection (HPME) in US-reactor designs, relating to small holes centered at the lower head, was concluded in 1998 with two important findings [Pil96].

1. The main part of the corium is trapped in these intermediate rooms, and the DCH-processes have less impact due to constraints in available volume and time, thus the pressure build up in the containment stays below the design pressure.

2. The results concerning melt dispersion and DCH are extremely dependent on geometric parameters.

Experiments, carried out with cavities partially open to the containment through the annular space between the vessel and the pit, have shown that a considerable amount of melt can be dispersed into the containment and the containment pressure can increase rapidly by several bars [Bla99].

At Forschungszentrum Karlsruhe (FZK), experiments were performed with cold model fluids in a test facility (DISCO-C) scaled 1:18 to a large PWR, to study the fluid dynamic processes with different failure modes of the bottom head under low pressure conditions ($p \leq 15$ bar). The fluids employed were water or a bismuth alloy instead of corium, and nitrogen or helium instead of steam. The main results from the cold experiments were: large holes ($Ø \geq 0.5$ m, scaled) at the base of the bottom head lead to high dispersed melt fractions (> 50%). The maximum dispersed fraction for such breaches is reached already at pressures below 20 bar. A certain amount is trapped in the reactor pit depending on its geometry. With breaches at the side of the lower head, the dispersed melt fraction is lower and, even with unzipping of the bottom head, the dispersed fraction is smaller than with central holes [Mey03].

In a second facility (DISCO-H) selected experiments in the same scale were performed with an iron-alumina melt, steam and a prototypic atmosphere in the containment. These experiments are designed to investigate the fluid-dynamic, thermal and chemical processes during melt ejection out of a breach in the lower head of a PWR pressure vessel at pressures below 2 MPa. The results of the first six experiments performed in the DISCO-H facility are presented in this report.

2 Facility and Experiment Description

2.1 Components of the facility

2.1.1 The containment pressure vessel (CPV)

The containment pressure vessel is a TÜV-approved cylindrical pressure vessel made of 15 mm steel and is rated at 1.0 MPa and 200°C. It has an outer diameter of 2.20 m and a height 4.60 m; with the pedestal and the top port its total height is 5.80 m (see **Fig. 1** and 2, for data see **Table 1**).

The pressure vessel consists of two segments and a lower and an upper head. Each segment has six instrument penetration ports at two levels labeled A through D. One of the level C ports is closed with a safety rupture disk (diameter 200 mm), with a burst pressure of 1 MPa. The lower head is filled with concrete that forms a level floor. All internal structures are bolted to that floor. At the center of the floor is a large vertical pipe that contains the condensate draining piping and has a connection to the bottom port. The connection of this pipe with the containment volume is via a 10 mm hole in the concrete cavity floor. The entire vessel is insulated against heat loss on the outside by a 100 mm thick fiberglass insulation. The empty volume of the containment vessel is 14.18 m³.

2.1.2 Subcompartment

The subcompartment is an annular space around the cavity. The flow path from the cavity is along the eight stubs modeling the main cooling lines. The top cover of the subcompartment has four openings with a diameter of 130 mm (**Fig. 2** and 3), that are covered by a wire mesh.

2.1.3 The pressure vessel modeling the RCS and RPV volume

The RCS-RPV pressure vessel models the volumes of both the reactor cooling system (RCS) and the reactor pressure vessel (RPV) (**Fig. 2**, 3 and 5) and has a total volume of 0.076 m³. A disk holding 8 pipes (46 mm I.D., 255 mm length) separates the two partial volumes. This arrangement models the main cooling lines with respect to the flow constriction between RCS and RPV. The cylinders (I.D. 200 mm) modeling the RCS and RPV are heated electrically, and are insulated over the whole length and on the top.

2.1.4 The RPV model

The RPV model, that serves as crucible for the generation of the melt, is bolted to a plate carrying the RCS-RPV pressure vessel (**Fig. 5**, **6** and **8**). An insulation material of magnesium oxide (MagneRam®) is filled between the outer shell of the RPV model and an inner steel cylinder, that contains the thermite powder. The hole at the bottom of the melt generator is formed by a graphite annulus. It is closed with a brass plate (**Fig. 9**).

2.1.5 The reactor pit

The cavity and RPV-hold-down were designed to withstand a pressure of 10 MPa with a safety factor of 2 to yield. The reactor pit is made of concrete (**Fig. 7** and **8**) and is installed inside a strong steel cylinder (30 mm thick wall). This cylinder is clamped by 8 bolts (56 mm diameter) between a base plate and a top plate, both 90 mm thick (see **Fig. 2**). Besides the flow path along the main cooling lines there is the option of a flow out of the cavity straight up into the containment through eight openings with a total cross section of 0.052 m². Depending on the reactor design that is to be investigated this cross section is a variable (**Table 2** and **Fig. 4** and **8**).

2.1.6 Steam accumulator

The steam accumulator is a TÜV-approved cylindrical pressure vessel placed outside of the containment pressure vessel with approximately the same volume as the RCS-RPV pressure vessel and is rated at 2.0 MPa and 250°C (**Fig. 2** and **10**). Both vessels are connected by a 25 mm diameter pipe with an electro-pneumatically actuated valve. The vessel is electrically heated from the outside and is insulated by fiberglass. The required amount of steam is generated inside the steam accumulator. A high pressure metering pump is connected to the accumulator that can inject very accurate amounts of water into the heated vessel to reach that required pressure.

2.1.7 Steam generator

The steam generator serves for heating up the containment vessel and providing the steam for the initial containment atmosphere. It has a capacity of 42 kg/h steam (32 kW) at 1 MPa. The steam generator is also used to vent the steam accumulator of air (**Fig. 10**).

2.2 Instrumentation and Measurements

2.2.1 Temperature

Generally, type-K thermocouples (chromel-alumel) are installed in the facility. They are steel sheathed thermocouples with insulated wires. The outer diameter of the sheath is given in **Table 3**. At some positions in the reactor pit some high temperature thermocouples were used (WRe), but the measured data were not promising. A large number of thermocouples is installed at the outside of the steam accumulator tank and the RCS-RPV pressure vessel to control the electric heaters. These temperatures are monitored at the heater control board.

The data acquisition system records the signals of the 22 thermocouples that are listed in **Table 3**, at a rate of 2000 samples per second per channel. The steam temperature in the accumulator tank is measured by two thermocouples, one near the top and one near the bottom. There is one thermocouple within the draining pipe at the bottom to measure the water temperature, if water is present. There are two thermocouples within the RCS-RPV pressure vessel, one in each compartment (RCS and RPV). A total of 11 thermocouples are located at different levels in the containment pressure vessel (CPV, level A through D) to measure the bulk gas temperature. Two of them are within the subcompartment, one is at

the floor and the rest is either close to the wall or in the space between the RCS-RPV pressure vessel and the containment wall.

Six thermocouples (No. 17-22) are at two locations near or inside the concrete wall of the cavity (**Fig. 7**). The thermocouples sticking 2 mm out of the wall measure the arrival of the melt. They are destroyed by the melt. The thermocouples placed at two different depths within the concrete were expected to measure the transient heat flux entering the concrete. However, the results were ambiguous, therefore no data are presented in this report.

2.2.2 Pressure

A total of 15 strain gauge-type pressure transducers (Kulite) with ranges of 0–1.7 MPa, 0–3.4 MPa and 0–7.0 MPa are used to measure steam and gas pressures (**Table 4**). The compensated operating temperature range is 27°C – 232°C, with a thermal drift of +/- 5% of full scale output. The transducers are being adjusted at the operating temperature just before the start of the experiment. The data acquisition system records data at a rate of 2000 data points per second per channel. All gages are mounted in tapped holes that are connected gas tight with the outside atmosphere at their backsides. In case of the transducers in the RCS-RPV pressure vessel, the compartment, and the cavity this connection is achieved by flexible steel hoses. The gages in the containment pressure vessel are mounted in the blind flanges of the ports at different levels (see **Fig. 2** and **Table 4**).

2.2.3 Gas composition

Ten pre-evacuated 500-cm³ gas grab sample bottles are used to collect dry-basis gas samples at three positions, in the cavity, in the subcompartment, and in the upper part of the containment. The sample lines and the sample bottles are at room temperature, thus the bottles are being filled with non-condensable gases and steam, that condenses. One pretest sample collects background information just prior to the start of the melt ejection. One sample at all three stations each is taken during the blow down and one 20 seconds or later after the blow down. The gas samples are analyzed at the Engler-Bunte-Institut at the University Karlsruhe.

2.2.4 Additional measurements

Three video cameras are used in the experiment. One camera looks down from the dome into the containment, one is installed at the level B port looking at the top of the subcompartment and the openings in the top plate, that represent the direct path from the cavity into the containment. A third camera looks into the compartment from the side by means of an endoscope.

Break wires are placed across the RPV exit hole (**Fig. 9**) and at the annular gap exit. The break wires were intended to give timing information on entry of debris into and out of the cavity.

The total debris mass dispersed into the DISCO vessel and the debris mass in specific locations is determined by a posttest debris recovery procedure. A posttest sieve analysis of the debris recovered from different locations is performed for each test.

2.3 Conduct of the Experiment

The containment model (**Fig. 2**) is heated over a time period of 10 to 20 hours by filling with steam additional to the atmospheric air until the vessel pressure reaches 0.2 MPa. The condensate water is drained at the bottom of the vessel from time to time. The average gas temperature and the wall temperature inside the vessel is 373 K (100°C) at the end of the heat-up. A metered amount of hydrogen gas (approximately 3 mol%) is added to the vessel at the end of heat-up while fans are running inside the vessel. A gas sample is taken just before the start of the experiment.

The pressure vessel modeling the RPV and RCS volume, which is inside the containment vessel, is electrically heated to the saturation temperature of steam at the planned blowdown pressure, e.g. to 453 K (180°C at 1.0 MPa). Before the initiation of the experiment it contains nitrogen at that temperature at 0.1 MPa.

The steam accumulator is outside of the containment vessel. It is heated electrically to the saturation temperature of twice the planned burst pressure, e.g. 486 K (213°C at 2.0 MPa). The accumulator is filled with a measured amount of water by a high pressure metering pump to reach that pressure. The RCS pressure vessel and the accumulator are connected by a 25 mm diameter pipe with an electro-pneumatically actuated valve.

The model of the RPV that is directly flanged to the RCS pressure vessel contains aluminum-iron oxide thermite. The experiment is started by igniting the thermite electro-chemically (Pyrofuze®) at the upper surface of the pressed thermite powder. When a pressure increase in the RPV-RCS pressure vessel verifies that the thermite reaction has started, the valve in the line connected to the accumulator is opened and steam enters the pressure vessel. The valve is closed again after two seconds, by that time the pressure in the RPV-RCS vessel and the accumulator has equilibrated. The amount of steam that is initially in the RCS-RPV pressure vessel is determined by the amount of water originally in the accumulator minus the water left in the accumulator. The steam flow takes approximately one second. During that time and thereafter the thermite reaction progresses until it reaches the bottom of the RPV vessel. 3 to 8 seconds after ignition the brass plug at the bottom of the RPV vessel is melted by the 2400 K hot iron-alumina mixture. That initiates the melt ejection. By that time the pressure in the RCS-RPV pressure vessel will be higher than the preset value due to radiation heat transfer from the hot melt to the steam. The melt is driven out of the breach by the steam and is dispersed into the cavity and the containment. Due to the melt-to-gas heat transfer, exothermic metal/oxygen reactions, and hydrogen combustion the pressure and temperature in the containment pressure vessel will rise. 10 seconds after blow-down, the fans, which had been shut down before the start of the test, are started again, and at 20 or 30 seconds the post test gas samples are taken.

2.4 Scaling considerations

The geometrical linear scale is 1:18, thus volumes of gas and liquid are scaled accordingly (length scale to the power of 3). The initial pressure can be scaled 1:1, and the duration of the blowdown is scaled as the length scale. Then, the gas velocity and the droplet size are mainly functions of the properties of the model fluids used. **Table 5** shows the composition of

the used thermite and of the reaction product melt. Before ejection, the melt separates into the two main components, iron on the bottom and alumina on top. Note that the melt has excess aluminum. The maximum potential hydrogen produced by the reaction with steam is 101 moles with iron and 6 moles with aluminum. The properties of the melt mixture are listed in **Table 6** together with those of a typical corium mixture [Bla99]. Important for the similarity of the thermal and chemical processes is the energy content of the melt. The chemical energy is that by the exothermic steam/metal reaction and a part of the hydrogen combustion, determined by the two-cell equilibrium (TCE) model [Pil91]. The combined thermal and chemical energy is 1.47 MJ/kg for corium and 2.83 MJ/kg for the model melt. Thus the scaling of melt mass is difficult, as is shown in **Table 7**. The scaled up mass of 10.6 kg melt gives 62000 kg, that has a volume of 16 m³ and a combined energy of 175000 MJ. The volume of 16 m³ corium would have a mass of 128000 kg and a total energy of 188000 MJ. The volume and energy content is scaled relatively correct, while the mass scaling is off by a factor of 2.

2.5 Thermite Composition and Burn Tests

2.5.1 Thermite composition

For a comparison of the experiments performed in the DISCO-H facility with the Sup1 and Sup2 tests performed in the Surtsey facility in Sandia National Laboratory (SNL) identical compositions of the melt should be used. **Table 8** and **Table 9** give the respective composition of the SNL-tests [Bla99]. The stoichiometric reaction is:

$$119\,mol\ Fe_3O_4 + 216\,mol\ FeO + 8\,mol\ Fe_2O_3 + 511\,mol\ Al + 37\,mol\ Al_2O_3 \rightarrow 239\,mol\ Al_2O_3 + 590\,mol\ Fe + 33\,mol\ Al + 37\,mol\ Al_2O_3 \qquad (2.1)$$

This specific mixture has been chosen to achieve a certain ratio of iron and alumina with a predetermined temperature and energy content, respectively. Instead of using three different iron oxides we used only two, Fe_3O_4 and Fe_2O_3. By mixing these with the other components, Fe, Al and Al_2O_3 in a certain ratio, we can obtain the identical melt composition and energy content per melt mass. The theoretical temperature for both mixtures taking into account realistic reaction rates, was 2562°C. Because of heat losses a temperature of 2230°C was determined for the SNL experiments. The heat losses due to radiation and conduction lead to a temperature reduction given roughly by

$$\Delta T \sim A\,\Delta t / m, \qquad (2.2)$$

with A, the total surface of the melt, Δt, the length of time between start of the reaction and ejection of the melt, and m, the mass of the melt. These parameters are not the same in the two experiments because of the different scales. Therefore the effect on the temperature was estimated and the composition of the melt was chosen accordingly.

The time Δt is unknown and depends on the following parameters: the height and diameter of the thermite bed, the density of the thermite, the grain size, and the system pressure. Although many test series have been performed at SNL to find correlations for Δt, no reliable correlation containing all parameters are available. Therefore, two thermite burn tests in the DISCO-geometry were performed outside the containment vessel, in the open air.

2.5.2 Preparation of the thermite

The grain size of the used components (Al, Fe, Fe_3O_4, Fe_2O_3) was 44 μm. The iron oxide powder is dried for 18 hours at 200°C. The powders are sieved and mixed for 15 minutes. The density of the thermite powder is 0.8 g/cm³. The mixture is filled into the RPV-crucible (**Fig. 11**) and pressed. The main reason for the compaction of the powder is to reduce the probability for a channeling of the chemical reaction, which could lead to a premature melt plug failure. The ignition wire (about 20 cm of Pyrofuze® wire) is placed onto the surface of the pressed thermite, and is covered with a layer of thermite powder.

2.5.3 Results of the burn tests

The tests were performed with the RPV-RCS pressure vessel connected to the RPV-model (**Fig. 5**). The vessel contained nitrogen at 1 bar and 20°C prior to ignition. The crucible (RPV-model) contained 11.5 kg of thermite. The first test was performed in a crucible with an I.D. of 220 mm (**Fig. 11**) and a thermite density of 1.17 g/cm³. After ignition the pressure increased up to 6.1 bar and fell to 5 bar at melt plug failure, which occurred 4.2 sec after ignition (**Fig. 13**). The gas temperature reached more than 1000°C in the lower part of the vessel and about 300°C in the upper part (**Fig. 14**). A mass exchange between the two parts has taken place after two seconds, connected with a decrease of the pressure, a temperature drop in the lower part and an increase in the upper part. The melt temperature could not be measured with sufficient reliability, but all signals pointed to a temperature ≥ 1950°C.

The hole diameter was 56 mm, formed by a graphite ring. Post test, a 0.8 mm thick crust covered the inside of the ring, no traces of the brass melt plug were found within the hole. The brass plug immediately melts and vaporizes, as can be seen in the photographs taken from the side of the crucible and from below by a mirror (**Fig. 17**). The steel liner (wall thickness 4 mm) inside the RPV had melted at a few locations near the bottom, exposing the MgO insulator.

From the gradient of the pressure curve after melt plug failure (**Fig. 15**) we can infer two phases of the ejection process, first 340 ms ejection of the melt and gas as a two-phase jet, and second, blow down of the single-phase gas, lasting 440 ms. These data compare well with data from cold tests with water (D06) and Woods metal (M03) [Mey03].

The time from ignition to melt plug failure was 4.3 seconds. Because this seemed too short for the real test, where steam has to be filled into the RCS/RPV vessel during that time, a second test was performed with a reduced inner diameter of the crucible (**Fig. 12**). Thereby, for the same melt mass the height of the thermite bed grows. However, this time the compaction pressure was increased and the density was 1.96 gr/cm³, which lead to about the same height as in the first test (**Table 11**).

The maximum pressure during the reaction time was 4.6 bar (**Fig. 16**), lower than in the first test, due to the smaller free surface, which reduced the heat transfer to the vessel gas The time from ignition to melt plug failure was 10.1 seconds, long enough for a real test. Therefore the crucible design of the second test was used for the DISCO-H tests.

2.5.4 Discussion of the melt temperature

To obtain a similar melt temperature as in the SNL experiments the heat losses and the different melt mass must be taken into account. There is the heat loss due to radiation and conduction, that is proportional to the respective surfaces, the heat sink by melting part of the liner and by vaporizing part of aluminum and brass. It is impossible to determine those losses without a large uncertainty, but they are smaller in DISCO than in the larger scale of the SNL experiment. On the other hand, the melt mass in DISCO is only about 1/6 of that in the SNL experiment, which would lead to a higher temperature reduction. The time between ignition and plug failure is shorter in DISCO, by 30% in the second burn test (10.1 versus 13.3 seconds). However, in the subsequent six DISCO-H experiments this time was always shorter with an average of 5.4 seconds. The reason is not known, maybe because of the higher system pressure. If we introduce the respective data into the relation 2.2, we see that the temperature of the melt in DISCO should be similar to the temperature in the SNL experiments.

$$\frac{\Delta T_{DISCO}}{\Delta T_{SNL}} = \frac{A_D}{A_S} \cdot \frac{\Delta t_D}{\Delta t_S} \cdot \frac{m_S}{m_D} = \frac{2002}{4422} \cdot \frac{5.4}{13.3} \cdot \frac{62}{10.6} = 1.07 \qquad (2.3)$$

By variation of the amount of the components of the thermite powder or by adding different amounts of Fe or Al_2O_3, we can increase or decrease the melt temperature. The thermite composition chosen for the DISCO experiments is shown in **Table 5**.

Table 1. Geometric parameters of the test facility

Containment Pressure Vessel		
Diameter (inner)	m	2.170
Height of a segment	m	1.650
Height of upper head	m	0.640
Total inner height	m	3.940
Diameter of portholes (DN 200)	m	0.199
Length of ports	m	0.215
Length of lower port (vertical pipe)	m	1.601
Volume of lower port (vertical pipe)	m³	0.050
Total empty volume of containment	m³	14.180
Volume of internal structures (RPV, cavity, etc)	m³	0.300
Total freeboard volume (incl. subcompartment)	m³	13.880[1]
Subcompartment		
Outer diameter (inside)	m	1.810
Inner diameter	m	0.600
Height	m	0.785
Volume	m³	1.740
RCS and RPV pressure vessel		
Inner diameter	m	0.200
Height of RCS	m	1.586
Volume of RCS	m³	0.0498
Volume of the line connecting to accumulator	m³	0.0013
Height of upper RPV (same diameter as RCS)	m	0.430
Volume of upper RPV	m³	0.0135
Inner diameter of lower RPV (crucible)	m	0.168
Height of lower RPV (crucible)	m	0.514
Volume of lower RPV (crucible)	m³	0.0114
Total volume of RCS and RPV	m³	0.0760
Volume of the steam accumulator	m³	0.0820

[1] Total freeboard volume in the SNL experiment was 91.6 m³; scaled to DISCO this is 15.7 m³

Table 2. Geometric flow parameters in the cavity

Height of cavity	m	0.612
Diameter of cavity (lower part, concrete wall)	m	0.342
Height of lower part (concrete wall)	m	0.462
Diameter of cavity (upper part, steel wall)	m	0.540
Height of upper part (steel wall)	m	0.150
Length from RPV bottom (lower head) to cavity floor	m	0.066
Length of annular cross section	m	0.316
Gap width between RPV and cavity wall	m	0.021
Cut out diameter at nozzles (around main cooling lines)	m	0.086
Cold/hot leg diameter (main cooling lines)	m	0.050
Flow area of annulus	m^2	0.0212
Flow area in upper part of cavity	m^2	0.1583
Flow area at nozzles ($8 \times$ cut out area – $8 \times$ cold/hot leg area)	m^2	0.0308
Flow area into containment (where existing, 8 holes)	m^2	0.0520
Empty volume of cavity (without RPV)	m^3	0.0748
Free volume of cavity	m^3	0.0365

Table 3. Thermocouple Summary

No. T	Channel	Location	Type diameter mm	Range (0 - 5 Volt) °C	Position Height cm	Position from wall cm	Position angular degree
1	03	accumulator low	K 1.0	0 - 500			
2	04	accumulator high	K 1.0	0 - 500			
3	05	RCS high (10 cm)	K 0.5	-100 -1350			
4	06	RCS low (170 cm)	K 0.5	-100 -1350			
5	07	accumulator (bottom)	K 1.0	0 - 500			
6	08	CPV A1	K 0.35	0 - 500	0	3	45
7	09	CPV-A2 (subcomp.)	K 0.35	0 - 1000	45	50	135
8	10	CPV-A3 (subcomp.)	K 0.35	0 - 500	46	61	225
9	11	CPV-B1	K 0.35	0 - 1000	116	56	45
10	12	CPV-B2	K 0.35	0 - 1000	109	56	135
11	13	CPV-B3	K 0.35	0 - 500	116	52	225
12	14	CPV-C1	K 0.35	0 - 1000	211	9	45
13	15	CPV-C2	K 0.35	0 - 1000	212	71	135
14	16	CPV-D2	K 0.35	0 - 500	283	5	135
15	17	CPV-D3	K 0.35	0 - 500	277	8	225
16	18	CPV-D3	K 0.35	0 - 1000	280	61	225
17	19	Cavity	K 0.35	0 - 1000	362	-3	0
18	20	Cavity	K 0.35	0 - 1000	362	2	0
19	21	Cavity	K 0.35	0 - 1000	362	-1	0
20	22	Cavity	K 0.35	0 - 1000	62	-3	0
21	23	Cavity	K 0.35	0 - 1000	62	2	0
22	24	Cavity	K 0.35	0 - 1000	62	-1	0

Table 4. Pressure transducer Summary

No. P	Position	Channel	Line No.	Transducer No.	Pressure [bar]	Type	Position [cm/degree] Height	angular
1	Accumulator flange	33	D1	614	35	HEM-375-35 BAR A		
2	Accumulator flange	34	D2	228	70	HEM-375-70 BAR SG		
3	RCS flange	35	101	101	17	HEM-375-17 BAR A		
4	RCS flange	36	102	102	17	HEM-375-17 BAR A		
5	CPV A1	37	92	92	17	HEM-375-17 BAR A		
6	CPV A2	38	93	93	17	HEM-375-17 BAR A		
7	CPV B1	39	94	94	17	HEM-375-17 BAR A		
8	CPV C2	40	98	98	17	HEM-375-17 BAR A		
9	CPV B3	41	99	99	17	HEM-375-17 BAR A		
10	cavity – 1	42	86	86	17	HEM-375-17 BAR A	162	0
11	cavity – 2	43	87	87	17	HEM-375-17 BAR A	412	0
12	cavity – 3	44	88	88	17	HEM-375-17 BAR A	162	180
13	cavity – 4	45	89	89	17	HEM-375-17 BAR A	412	180
14	compartment - 1	46	90	90	17	HEM-375-17 BAR A		
15	compartment - 2	47	91	91	17	HEM-375-17 BAR A		

Table 5. Thermite and Melt Composition

	Thermite		Melt					
	Mass kg	Moles	Mass kg	Moles	Volume cm³	Mass Fraction	Mole Fraction	Volume Fraction
Fe	0.30	5.37	5.64	101.03	887.2	0.53	0.66	0.33
Al	2.54	94.14	0.11	4.24	58.9	0.01	0.03	0.02
Fe_3O_4	4.00	17.28	-	-	-	-	-	-
Fe_2O_3	3.50	21.92	-	-	-	-	-	-
Al_2O_3	0.30	2.94	4.88	47.89	1733.5	0.46	0.31	0.65
Total	10.64	141.65	10.64	153.16	2679.6	1.00	1.00	1.00

Table 6. Material properties of the melt

Property			**Corium**	**Simulant melt**
Effective molecular weight	MW_{eff}	*kg/mole*	0.2247	0.0691
Specific heat of reaction	$\Delta e_{reaction}$	*MJ/mole*	0.0371	0.0160
Specific thermal ernergy	$\Delta e_{thermal}$	*MJ/mole*	0.2980	0.1820
Specific combined energy	$\Delta e_{combined}$	*MJ/mole*	0.3350	0.1980
Specific heat	C_p	*J/mole/K*	119.1	82.8
Specific heat	c_p	*J/kg/K*	525.7	1198.4
Thermal conductivity	k	*W/m/K*	5.0	19.7
Density	ρ	kg/m^3	8045	3878
Density	ρ	$mole/m^3$	3.58×10^4	5.61×10^4
Dynamic Viscosity	μ	*Pa s*	0.0151	0.0073
Kinematic Viscosity	$\nu = \mu/\rho$	m^2/s	1.88×10^{-6}	1.88×10^{-6}
Surface tension	σ	*N/m*	0.973	0.932
Melting point of oxide	$T_{mp,oxide}$	*K*	2450	2200
Temperature of melt	T_{melt}	*K*	2800	2500

Table 7. Scaling of melt mass

	SNL 1:10	DISCO 1:18	Prototype 1:1
Mass, Iron-Alumina (kg)	62	10.6	62 000
Volume, Iron-Alumina (m^3)	16×10^{-3}	2.74×10^{-3}	16
Volume × density of corium (8000 kg/m^3) (kg)			128 000
Thermal + chemical energy of 128000kg corium (MJ)			188 000
Thermal + chemical energy of simulant melt [1] (MJ)	175	30	175 000

The energy of 175 000 MJ is contained in **120 000** kg of corium.

[1] data for specific corium see NUREG/CR-5746, 1999
Thermal + chemical energy of simulant melt 2.83 MJ/kg
Thermal + chemical energy of corium 1.47 MJ/kg

Table 8. Thermite composition of the SNL-Sup Tests

SPECIES	MASS FRACTION	MASS (kg)	Molecular Weight (g/ mole)	Moles (mole)
Fe_3O_4	0.4441	27.54	231.5	118.97
FeO	0.2507	15.54	71.85	216.34
Fe_2O_3	0.0215	1.33	159.69	8.34
Al	0.2225	13.80	26.98	511.46
Al_2O_3	0.0612	3.79	101.96	37.17
Total	1.0000	62.00	N/A	892.28

Table 9. Thermite products in the SNL-Sup Tests

SPECIES	MASS FRACTION	MASS (kg)	Molecular Weight (g/ mole)	Moles (mole)	Moles H_2 per Moles Metal	Potential Moles H_2 (mole)
Fe	0.5315	32.95	55.85	589.93	1.0	590
Al_2O_3	0.4540	28.15	101.96	276.25		
Al	0.0145	0.90	26.98	33.30	1.5	50
Total	1.0000	62.00	N/A	899.48		640

Table 10. Composition of Corium[1]

Fraction	Mass	Mole	Volume
UO_2	0.8477	0.7056	0.7503
ZrO_2	0.1272	0.2323	0.2149
Zr	0.0251	0.0620	0.0348

[1]Corium mass fractions are based on the Calvert Cliffs scenario V upper bound limits, shown in NUREG/CR-6338 (Pilch et al. 1996).

Table 11. Parameter of thermite burn tests

Test	Mass [kg]	Volume [cm³]	Density [g/cm³]	Diameter [mm]	Height [mm]	Duration [s]	Burn rate [cm/s]	Max. pressure [MPa]
BT01	11.5	9 800	1.17	220	285	4.3	6.5	0.611
BT02	11.5	5 900	1.96	168	280	10.1	2.8	0.460

Fig. 1. The DISCO-H Test Facility

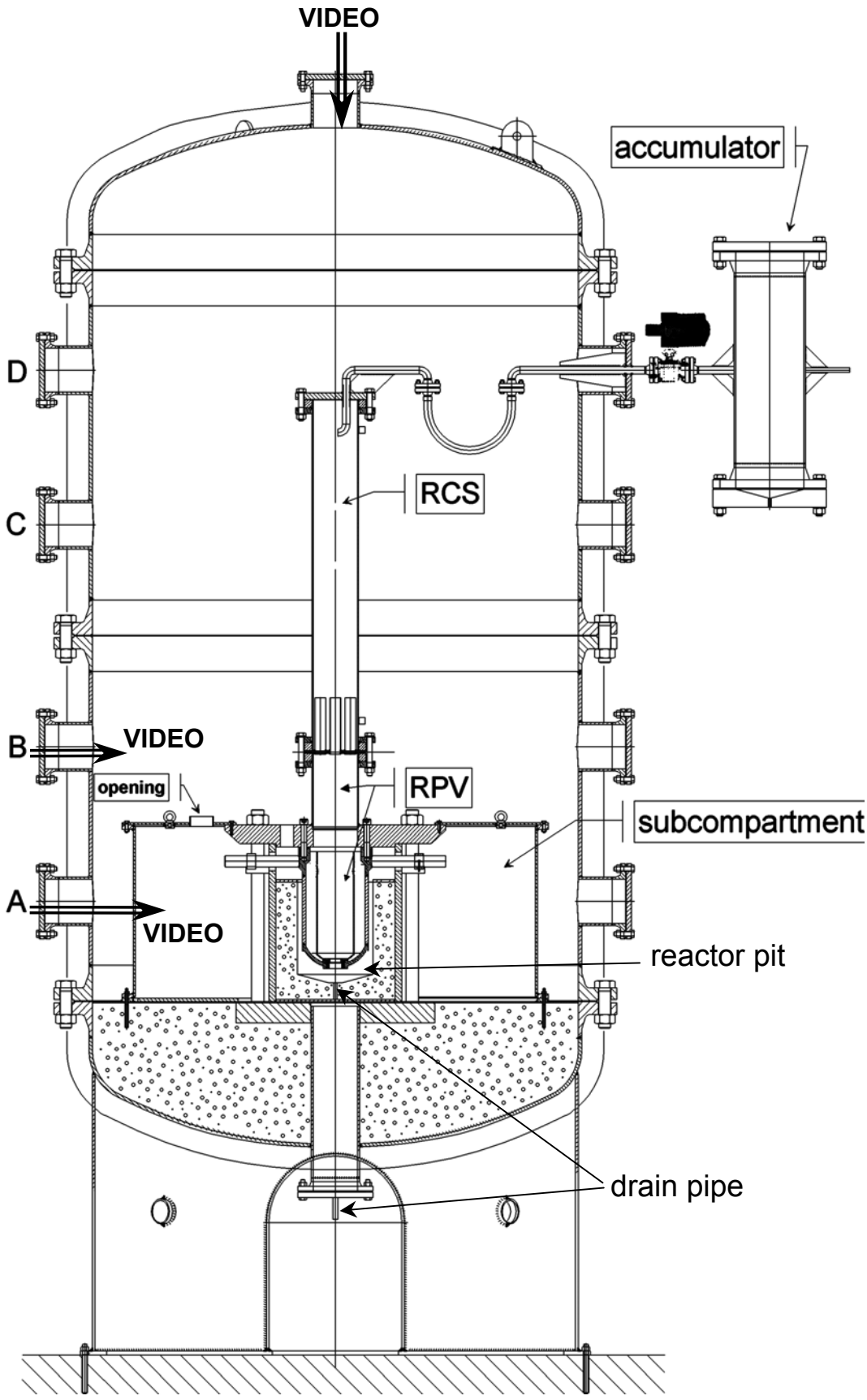

Fig. 2. The Containment pressure vessel with internal structures

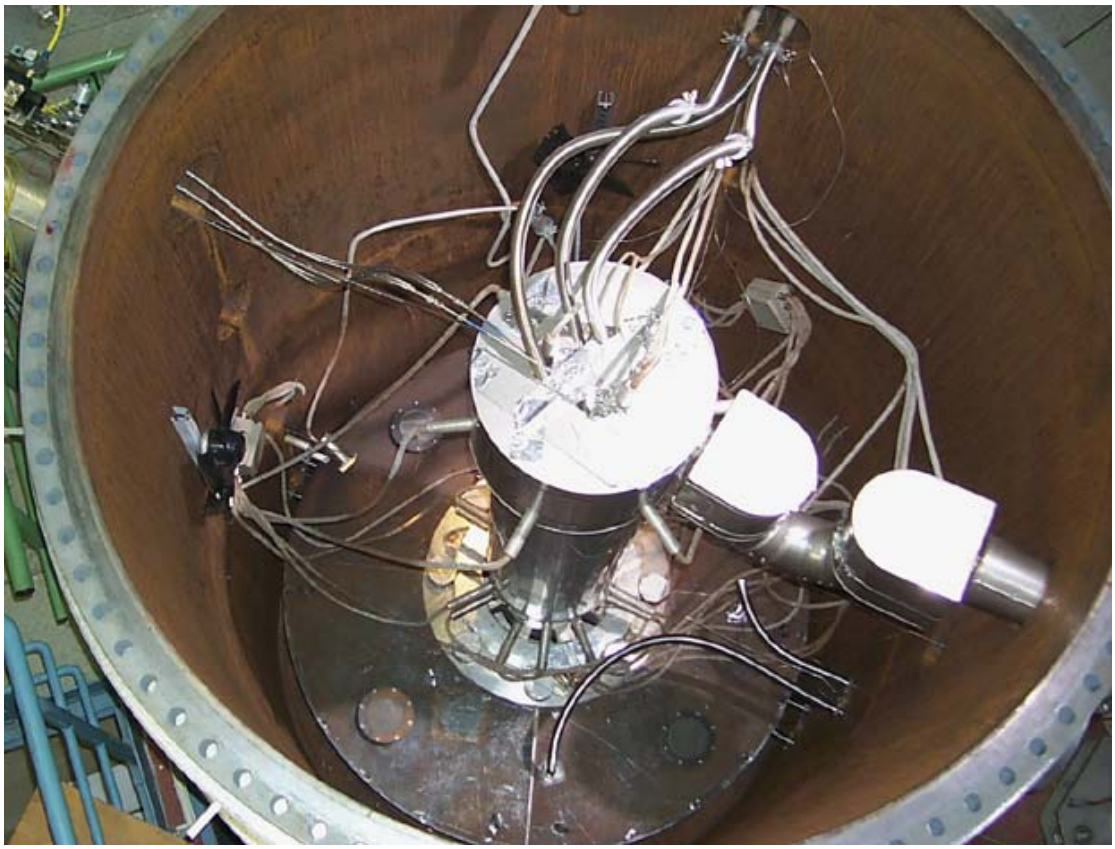

Fig. 3. View into Containment pressure vessel, with RCS-RPV pressure vessel

Fig. 4. Top view of the cavity top plate with exit holes leading into containment

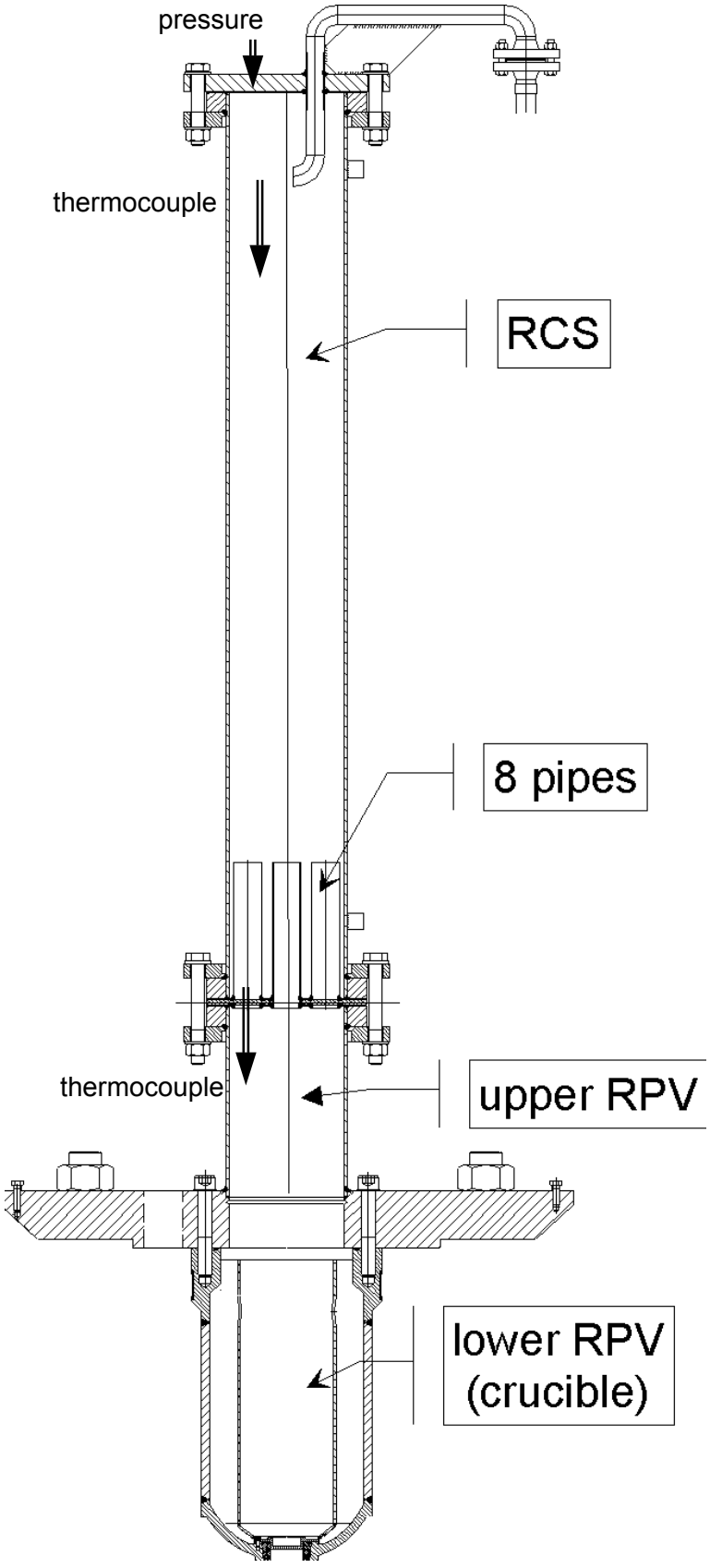

Fig. 5. The model of the RCS vessel and RPV

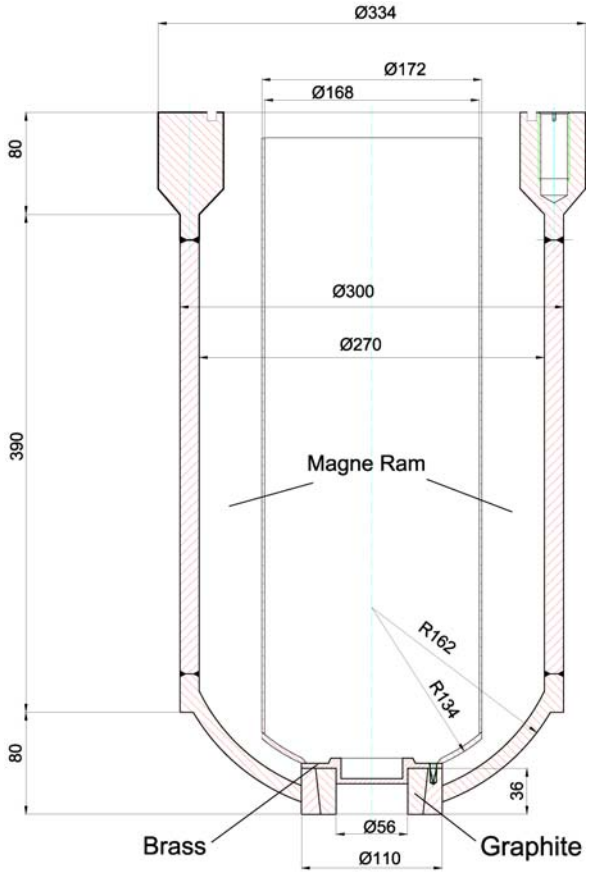

Fig. 6. The RPV model, crucible for the thermite melt

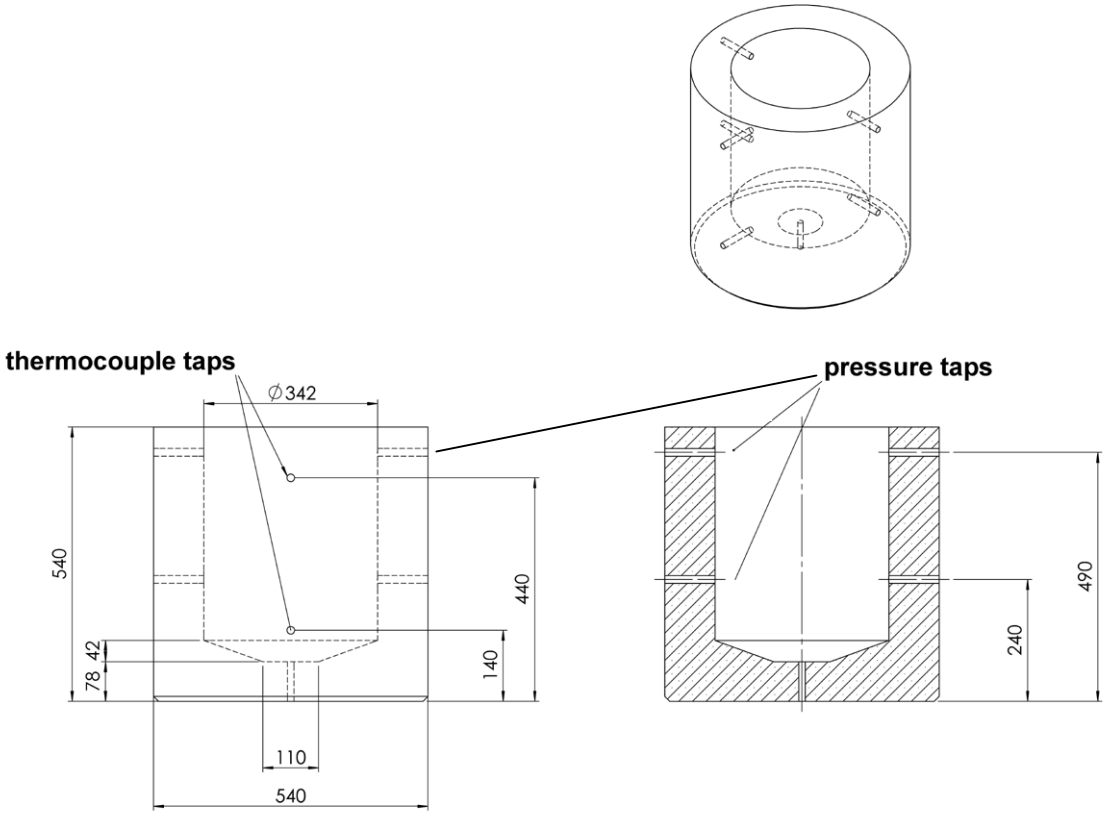

Fig. 7. The reactor pit made of concrete

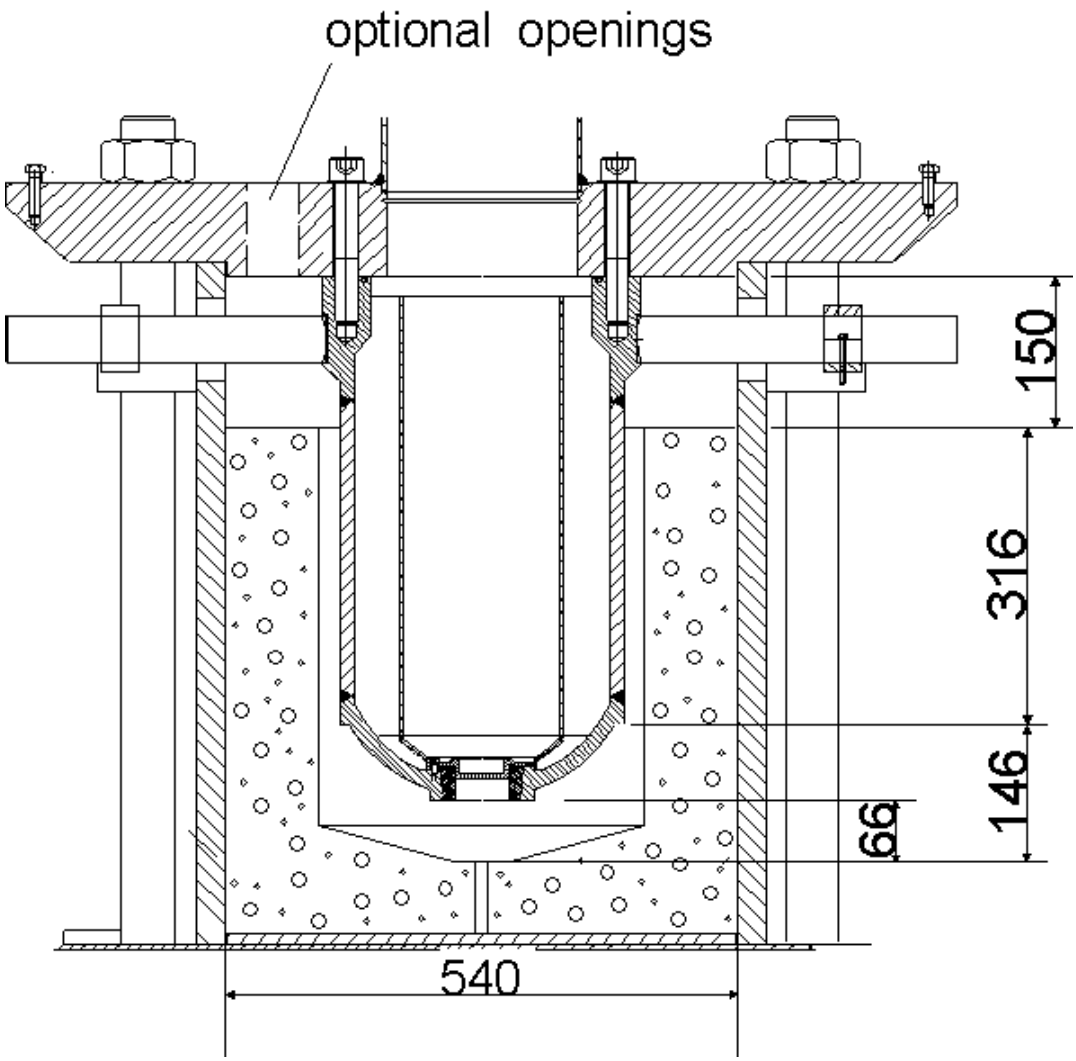

Fig. 8. The RPV-model (crucible) and cavity

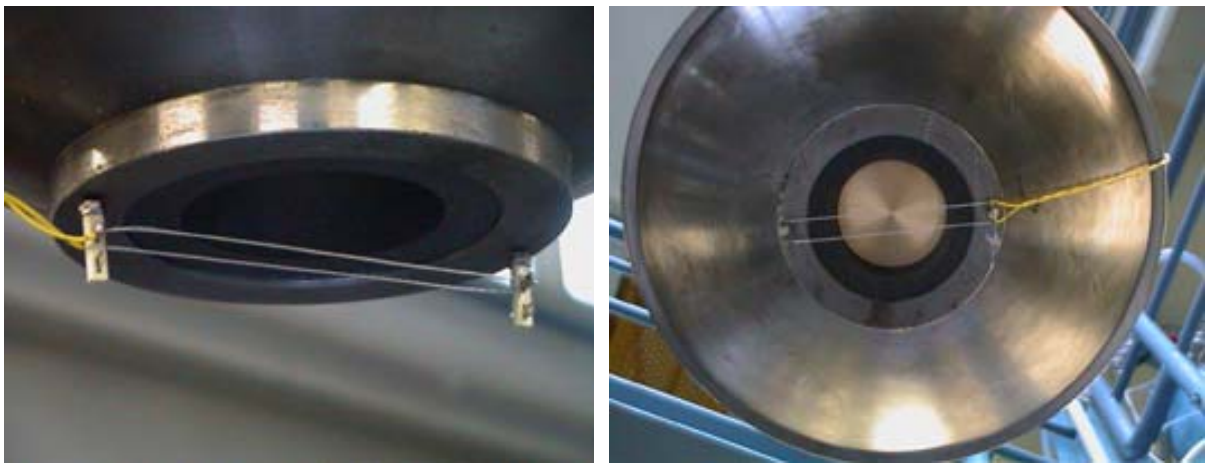

Fig. 9. Breakwires at the RPV exit hole

Fig. 10. The steam accumulator (left) and the steam generator (right)

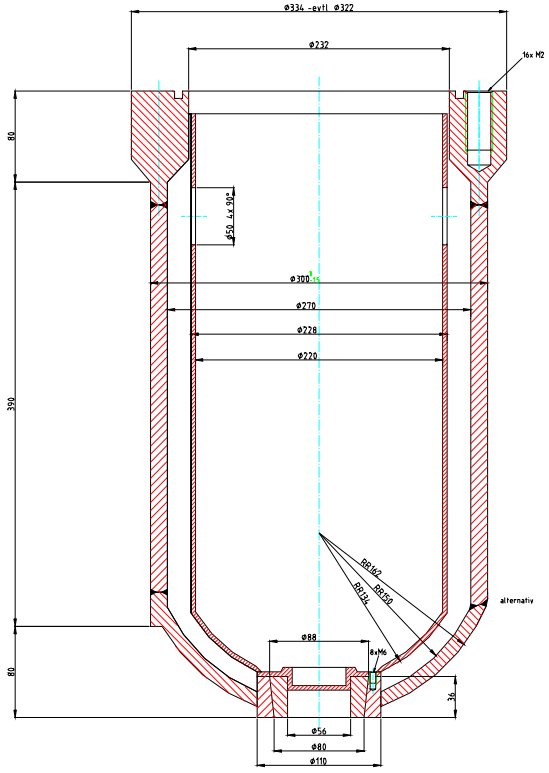

Fig. 11. Crucible of burn test BT1

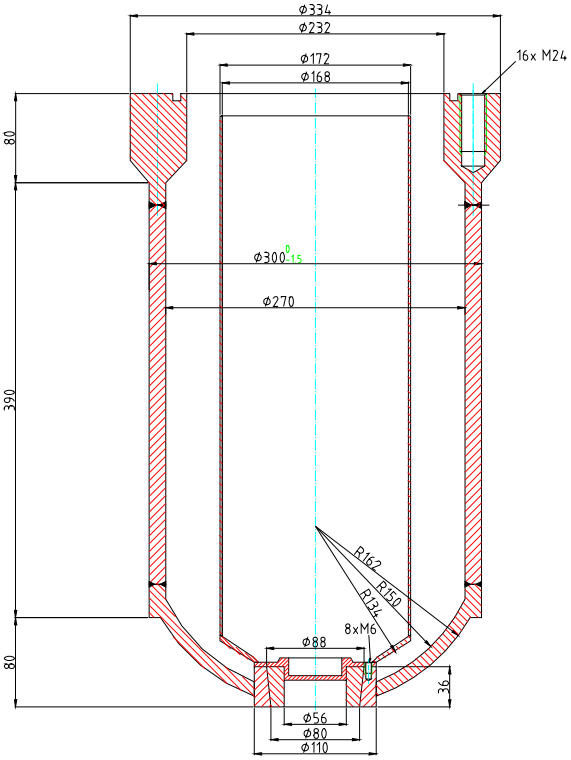

Fig. 12. Crucible with reduced diameter of BT2

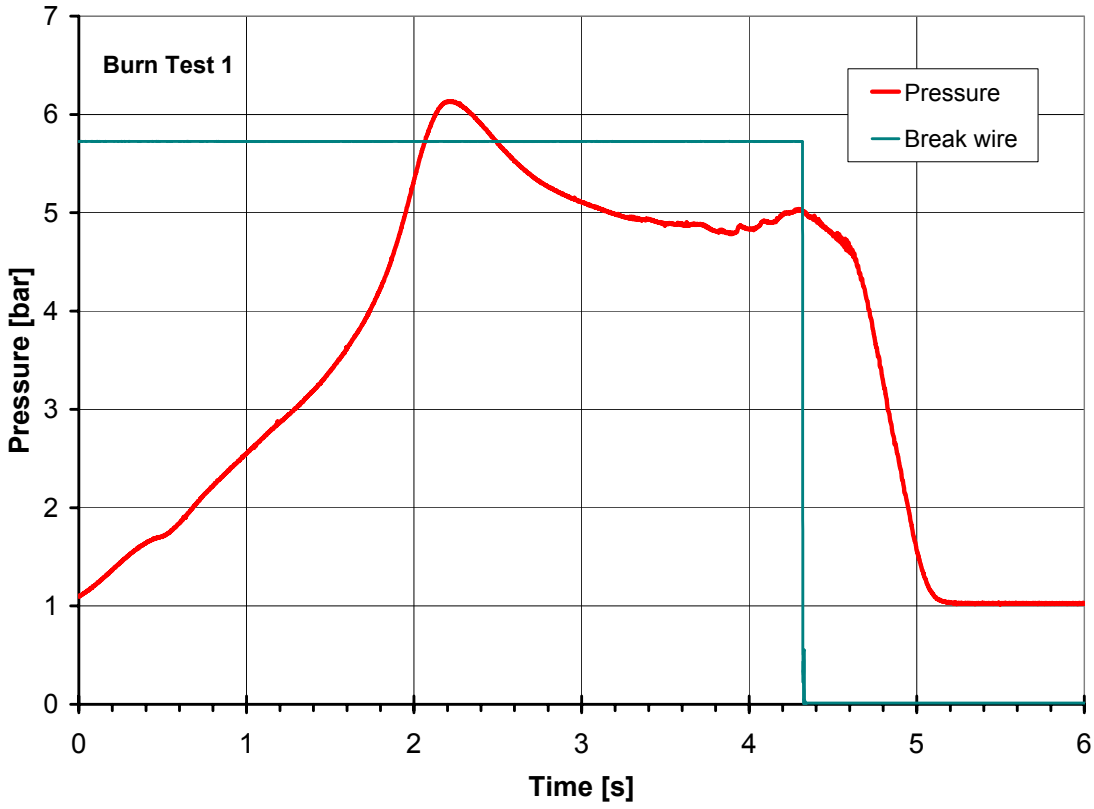

Fig. 13. Pressure in the RPV-RCS vessel during burn test BT1

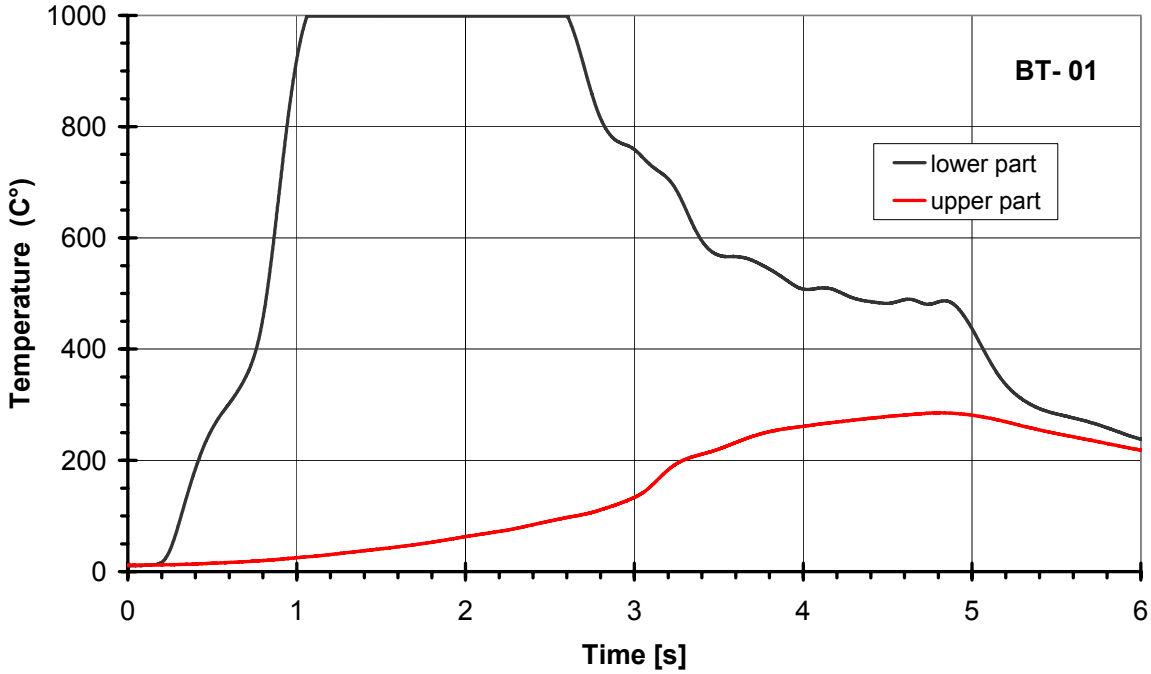

Fig. 14. Temperatures in the RPV-RCS vessel during burn test BT1

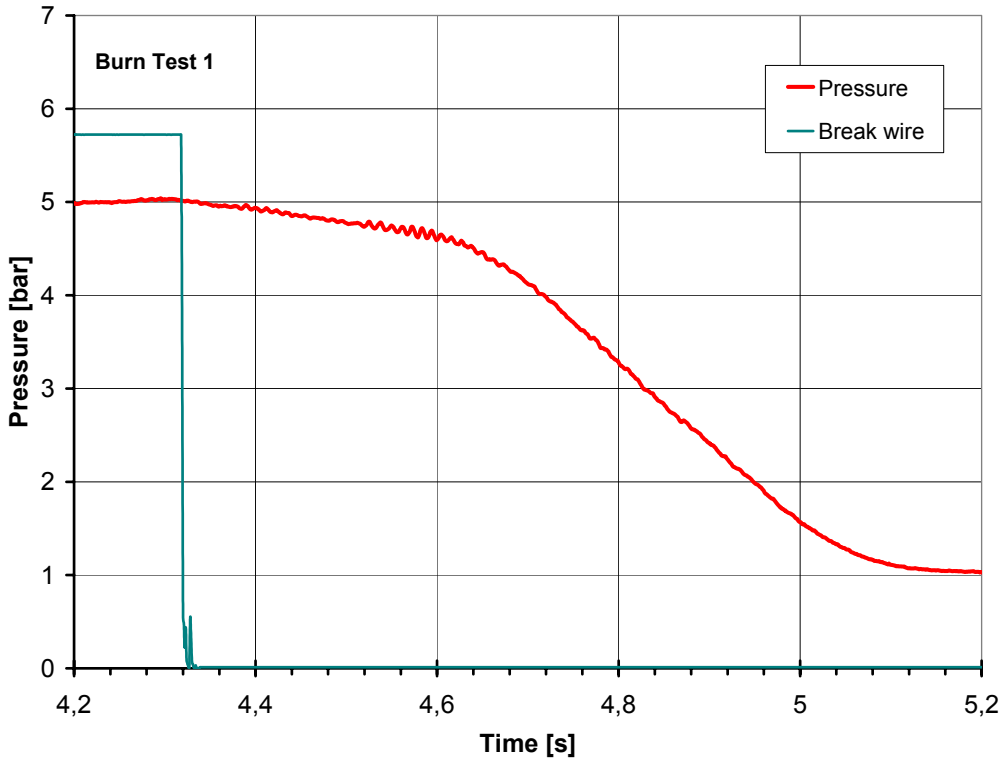

Fig. 15. Blow-down pressure in the RPV-RCS vessel during burn test BT1

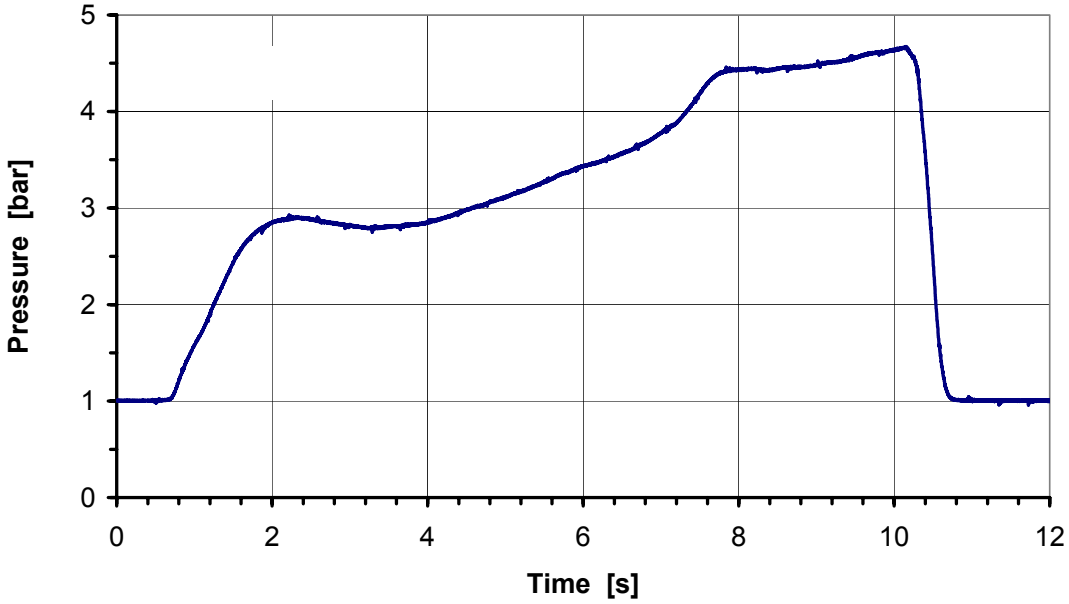

Fig. 16. Pressure in the RPV-RCS vessel during burn test BT2

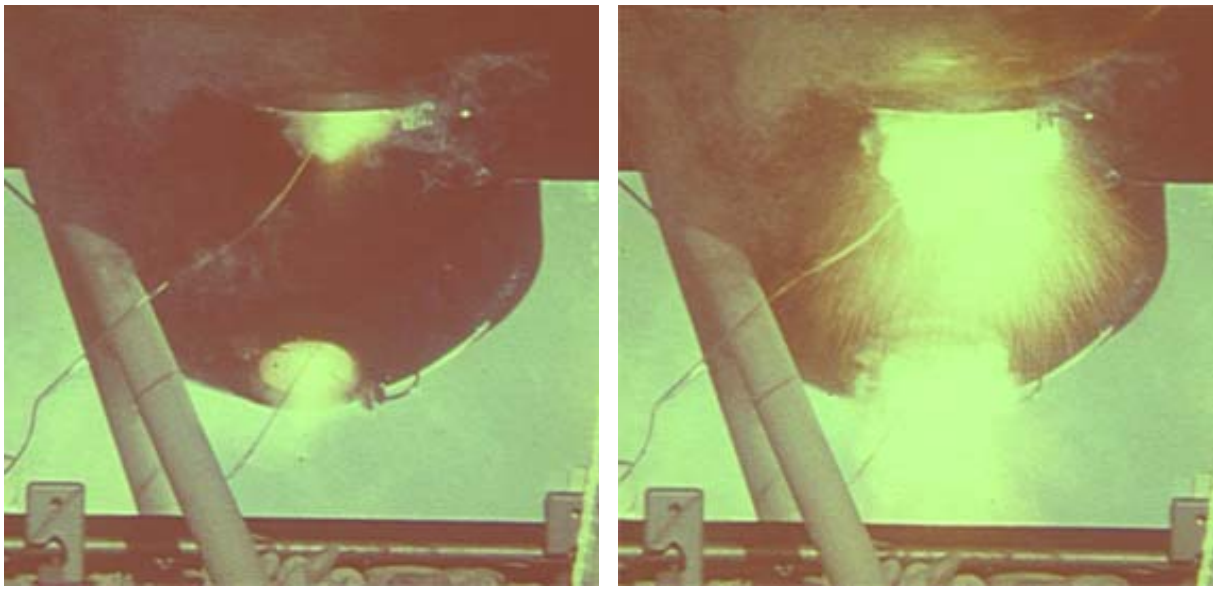

t = 0 ms t = 2 ms

Fig. 17. Melt plug failure in burn test BT1, view from side (top) and below by a mirror

3 Description of the Experiments and Results

3.1 Test Matrix: Variations to the base case

Six experiments are described in this report. Four parameters were varied in a systematic way:

1. Pressure at melt plug failure
2. Flow path out of the reactor pit (w. / w.o. direct path into the containment dome)
3. Driving gas and containment atmosphere (steam / nitrogen and w./w.o. steam in the containment)
4. Hole size in RPV bottom (56 or 28 mm)

The experiment named H02 can be considered to be the base case. This experiment was performed with an open direct path from the reactor pit to the containment, with prototypical conditions concerning the steam driven ejection out of the RPV, and a containment atmosphere, that was part air and part steam at an elevated pressure, with 3 mole-% hydrogen. Test H01 had less steam in the RCS/RPV vessel, the pressure at failure was only 0.8 MPa, versus 1.2 MPa for the base case. In test H03 the direct path to the containment dome was closed, but the thermodynamic conditions were the same as in H02. In these tests, hydrogen production and combustion occurred. In the experiment H04 the hydrogen effect was excluded by using only nitrogen as driving gas and a pure air atmosphere in the containment. The only chemical reaction is the oxidation of iron in the containment atmosphere. The conditions of this experiment may not be prototypical, but it is important to separate the thermal effects from the chemical effects, to validate the respective models. Tests H05 and H06 were both performed with a smaller hole, 28 mm instead of 56 mm. Additionally, in H05 the direct path to the containment was closed again, while in H06, with an open path, the pressure at failure was raised to 2.2 MPa by filling more steam into the RCS/RPV vessel. A quick reference table is given below; the exact initial conditions are listed in **Table 12**, **13** and **Table 14**.

	Base case H02	**H01**	**H03**	**H04**	**H05**	**H06**
Pressure	***1.2***	**0.8**	1.2	0.9	1.2	**2.2**
Cavity	***open***	open	**closed**	open	**closed**	open
Driving gas	***steam***	steam	steam	**nitrogen**	steam	steam
Hole size	***56 mm***	56	56	56	**28 mm**	**28 mm**

3.2 Pressure and Temperature Data

Figures 18 to **23** give the pressure and temperature history of the RCS/RPV-pressure vessel and the cavity from thermite ignition till 5 to 10 seconds after plug failure. For tests H02 and H03 the pressure in the steam accumulator is also shown. The sequence of events as described in chapter 2.3 can be perceived in the data curves (see e.g. **Fig. 19**). After ignition of the thermite the pressure and temperature in the RPV starts to rise. The temperature signal is well above 1000°C. When the valve has opened and steam flows from the accumulator into the RCS/RPV-vessel, the pressure increases rapidly until it balances with the pressure in the accumulator, which has decreased at the same time. The temperature in the lower part of the RCS/RPV-vessel drops due to the relatively cold steam flow, while in the upper part the temperature increases up to the steam temperature of 213°C. The temperature in the lower part behaves differently in the different tests, depending on the mixing of the hot and cold steam and the duration of the thermite reaction. Although the thermite properties were nominally the same, the reaction times were different:

H01	H02	H03	H04	H05	H06
7.8 s	4.0 s	4.3 s	4.1 s	9.5 s	2.9 s

This can only be explained by small differences in the compaction density of the thermite powder and different gas/steam pressures. After closing of the valve the pressures in the accumulator and the RCS/RPV-pressure vessel diverge again. When the brass melt plug fails, the blow-down starts, both the pressure and the temperature in the vessel drops.

Figures 24 to **29** give the blow-down pressure and the pressures in the cavity and containment. The blow-down ends when the RPV-pressure curve meets the rising cavity pressure. It lasts approximately 0.5 seconds in the four tests H01 through H04 with the 56-mm-hole, and 1.4 and 2.0 seconds for tests H05 and H06, respectively, which both have a 28-mm-hole, but in H06 the pressure at failure was higher. Three distinct stages can be recognized in the curves of the RPV pressure: first, a slow decrease, second, a steep drop up to a maximum slope, and third a slowing down of the pressure drop. These stages can be detected better if the pressure gradient dp/dt is plotted versus time, as shown in **Fig. 30** for all six experiments. Except in test H01, an almost constant low gradient exists for a certain time at the beginning of the blow-down, which can be interpreted as a liquid single-phase or nearly single-phase jet. The second stage is a two-phase flow, starting slowly and reaching a peak volume flow when the single-phase steam flow begins. At this point of time the pressure ratio of the vessel pressure and cavity pressure is still supercritical, and choked flow prevails. In **Table 15** the times of these three flow stages are listed. Also given is the theoretical velocity of the liquid jet determined by the driving pressure difference Δp and the density of the melt, ρ_M,

$$u_L = (2\,\Delta p/\rho_M)^{1/2}, \tag{3.1}$$

and the duration of the melt ejection, provided that all melt is ejected single-phase,

$$t_s = V_M / (\varepsilon\,\pi\,d^2/4\,u_L) \tag{3.2}$$

with $V_{M,}$ the volume of the melt and ε, the contraction factor. However, the two components of the melt probably have separated, with the iron *(ρ = 6.35 g/cm^3)* at the bottom and the alumina *(ρ = 2.8 g/cm^3)* on top. Therefore, the iron will be ejected first with a lower velocity and the alumina second. The velocity ratio is 1.5. Since the volume ratio of iron to alumina is 0.5, the duration of the iron ejection is approximately 43% and that of the alumina 57% of the total ejection time, provided that all melt is ejected single-phase. The total ejection time does not change significantly whether the well mixed melt or the separated components are ejected. The ejection time was calculated with *ε= 0.8.* But regardless of the chosen value, 0.5 or 0.9, the resulting times t_s are shorter than those taken from the measured data (t_{bl}), with the exception of test H01. The only plausible explanation is a larger liquid volume due to gas that was previously dissolved in the thermite melt. By contrast, in the experiments with cold water or Wood´s metal as model fluids, the theoretical time was longer than the measured time of single-phase liquid flow [Mey03]. This was attributed to the gas blow-through which occurs at a certain liquid height before all liquid is blown out. Because of the large and variable divergence between theoretical and measured liquid discharge times, all models based on these theoretical data should be used with care. The last column in **Table 15** lists the time signal of the second break wire, that was installed at the cavity exit leading directly to the containment. The signal indicates the arrival of melt particles that are large enough to break the wire by a direct hit.

Figures 31 through **36** allow a closer inspection of the pressure transients in the cavity, subcompartment and containment. During the ejection of the melt the pressure in the cavity is generally higher, by a maximum of 0.1 MPa, than in the other locations, especially in tests H02, H03 and H04. This hints to a rapid heating of the cavity atmosphere and a flow obstruction by the narrow annular cross section around the RPV. In tests H05 and H06 the melt flow is too small to cause a substantial overpressure in the cavity. Shortly after the end of the single-phase melt ejection the pressure in all locations changes uniformly. The differences in the curves are due to faulty transmitter signals.

The maximum pressure is reached at t = 1.75 s in all tests with an open cavity, and at t = 1.2 in tests H03 and H05 with a closed cavity (**Table 16**). Due to heat losses to the vessel walls the pressure decreases again. After approximately 10 s the pressure increase has dropped to half of its maximum value.

The pressure rise in the containment is highest with an open pit and hydrogen combustion (**Figs. 37 and 38**). With a closed pit the gas and the debris has to flow first into the subcompartment and then through relatively small cross sections into the containment. Considerable less hydrogen was produced and burned in this case (see Table 16). In test H04, without steam, no hydrogen effect was present, but, with the direct path to the containment open, a large amount of debris was dispersed into the containment, and efficiently transferred heat to its atmosphere. The smaller breach in tests H05 and H06 leads to a longer blow down, but to a smaller pressure rise, due to less melt dispersion out of the cavity.

The gas temperatures in the containment correspond to the pressure rises (**Fig. 39**) It is, however, difficult to determine a representative temperature in the containment vessel, especially during the first 4 to 10 seconds. **Figures 40 to 45** show the vessel gas temperatures from 11 thermocouples distributed at 4 height levels and different axial and circumferential

positions (see **Table 3**, No.6-16). Some thermocouples in the compartment (T8) and in the lower part of the containment (T9-T11) registered very high gas temperatures (see e.g. Fig.42). The temperature in the compartment is high (>800°C) because of the heat transfer from the high load of melt particles to the gas inside the small space of the compartment. The thermocouples T9-T11 are close to the compartment exit holes and are within or near the hydrogen flame, that could be observed during the first 2 seconds in test H03. Unfortunately some thermocouples went out of range. Thus, the average was determined by those data, that were not extreme. Those from positions where the flame was burning or near the floor were not considered. Of course, this choice introduces a large uncertainty into the average temperature data.

3.3 Gas Analyses

The objective of the gas composition measurements and gas analysis is to obtain data on the chemical reactions taking place during the blow-down, that is, the production of hydrogen by the metal/steam reaction and the hydrogen combustion. We cannot distinguish these processes from direct metal/oxygen reactions, but in terms of total energy release, it makes little difference that direct metal/oxygen reaction initially deposits more energy in the debris and less in the gas, because, for small particles that react efficiently, heat transfer is also efficient.

The composition of the gas in the vessel was measured in four tests, H02, H03, H05 and H06. The gas samples were taken from an atmosphere containing a mixture of steam and noncondensible gases. For the noncondensible part of the mixture, the measured mole % of nitrogen, oxygen and hydrogen are listed in **Tables 17** to **20**. The uncertainty in the evaluation of the gas samples is 0.1 vol% for H_2, 0.6 for O_2 and 0.8 for N_2. Therefore, the theoretical values in **Table 14**, and the measured in **Table 21** are not exactly identical.

The pretest composition of the vessel atmosphere is known and the amount of each gas in moles can be calculated with the volume of the vessel V, the atmosphere pressure p_0 and temperature T_0, and the measured amount of added hydrogen:

Initial number of moles of hydrogen	[kmol]	$N^0_{H2} = m_{H2} / M_{H2}$	(3.3)
Initial number of moles of air	[kmol]	$N^0_{air} = p_0\, V / (\mathbf{R}\, T_0)$	(3.4)
Initial mass of air	[kg]	$m_{air} = N^0_{air} \cdot M_{air}$	(3.5)
Pre-test partial pressure of air	[MPa]	$p_{1\,air} = p_0\, T_1 / T_0$	(3.6)
Pre-test partial pressure of hydrogen	[MPa]	$p_{1\,H2} = m_{H2}\, R_{H2}\, T_1 / V$	(3.7)
Pre-test partial pressure of steam	[MPa]	$p_{1\,steam} = p_1 - p_{1\,air} - p_{1\,H2}$	(3.8)
Number of steam moles	[kmol]	$N^0_{steam} = p_{1steam}\, V / (\mathbf{R}\, T_1)$	(3.9)
Mass of steam	[kg]	$m_{steam} = N^0_{steam}\, M_{H2O}$	(3.10)
Total number of gas moles	[kmol]	$N_{total} = N_{air} + N_{H2} + N_{steam}$	(3.11)
Number of nitrogen moles	[kmol]	$N_{N2} = 0.7803\, N_{air}$	(3.12)
Number of oxygen moles	[kmol]	$N_{O2} = 0.2099\, N_{air}$	(3.13)
Number of argon moles	[kmol]	$N_{Ar} = 0.0093\, N_{air}$	(3.14)

The constants are the molecular weights, M_{H2} = 2.02 kg/kmol, M_{air} = 28.96 kg/kmol, M_{H2O}=18.02 kg/kmol, and the gas constants, **R** = 8314 J/kmol/K and R_{H2} = 4116 J/kg/K.

The results are given in **Table 14**.

The amount of hydrogen, that is produced and burned during the test, can be determined by the nitrogen ratio method [Bla94]. The data and assumptions required for this method are listed below:

1. The total pretest moles of noncondensible gases must be known.
2. The measured ratios of the pretest and posttest noncondensible gases must be known.
3. It must be assumed that nitrogen is neither produced nor consumed by chemical reactions.

With the measured data of the pretest mole fractions (**Table 17** to **20**) of species i, X^0_i, the initial number of gas moles N^0_i is:

$$N^0_i = X^0_i \, (N^0_{air} + N^0_{H2} + N_{N2\ RCS/RPV}) \tag{3.15}$$

with $N_{N2\ RCS/RPV}$ from **Table 13**. The calculation was performed separately for the subcompartment and the rest of the containment volume. The sum of moles per species may deviate from the values in **Table 14**, due to incomplete mixing of the components and the uncertainty in the acquisition and analysis of the gas samples. With the assumption that the number of nitrogen moles has not changed, the post test number of moles of oxygen and hydrogen can be determined from the measured post test mole fractions X^2_i:

$$N^2_{O2} = N^0_{N2} \, X^2_{O2} / X^2_{N2} \tag{3.16}$$

$$N^2_{H2} = N^0_{N2} \, X^2_{H2} / X^2_{N2} \tag{3.17}$$

The number of moles of burned hydrogen is linked to the decrease of oxygen moles,

$$N^2_{H2\ burned} = 2 \, (N^0_{O2} - N^2_{O2}) \tag{3.18}$$

and the balance of hydrogen gives the moles of produced hydrogen:

$$N^2_{H2\ produced} = N^2_{H2} - N^0_{H2} + N^2_{H2\ burned}. \tag{3.19}$$

The fraction burned is $$F_{H2} = N^2_{H2\ burned} / (N^0_{H2} + N^2_{H2\ produced}). \tag{3.20}$$

The results (**Table 21**) show that more hydrogen is produced and burned if a direct path to the containment dome exists and if the breach is large. The pressure rise in the containment is correlated to the amount of burned hydrogen (**Fig. 46**).

Not all metal in the melt was oxidized, or in other terms, more hydrogen could have been produced with the existing metal. The potential maximum hydrogen production would be 101 moles by iron and 6 moles by aluminum (see **Table 5**). The ratio of hydrogen moles produced to iron moles oxidized depends on the kind of iron oxide formed. Based on the experience at the Sandia National Laboratories, Blanchat [Bla99] gives a ratio of 1:1, which implies that in a first step only FeO is formed. For aluminum it is 1.5:1, 3 moles of hydrogen are produced by the oxidation of 2 moles of aluminum with water (**Table 9**).

3.4 Video observation results

Not all three video cameras that were installed delivered useful pictures in each test. Therefore a selection is presented here. Note that the cameras had a fixed exposure setting, except for the camera looking at the cavity exit from the side (level B port), which had an automatic amplification.

H01: No useful pictures are available.

H02: A typical sequence of pictures from the subcompartment taken through an endoscope is shown in **Fig. 47**. The first very small melt particles appear at t = 100 ms, bigger ones are seen at t = 120 ms entering the subcompartment, the maximum density is at t = 220 ms. For a short time (< 30 ms) at t = 400 ms a melt stream appears. Around t = 600 ms, the particles flow subsides.

The view directly at the cavity exit into the containment from the level B port is shown in **Fig. 48**. At t = 20 ms a first glow is seen at the exit (the light on the left comes from the electric illumination). Between t = 40 ms and t = 540 ms, the light of the melt is too bright to distinguish any details. The automatic exposure setting is too slow to follow the quick changes in brightness. Thereafter we can see melt particles raining down until t = 2000 ms. Starting at t = 1700 ms, a pulsating yellow-orange flame can be observed. For 300 ms it turns into a greenish tone around t = 3600 ms and slowly subsides at t = 6000 ms.

H03: Pictures from the endoscope camera looking into the subcompartment are not shown here. At t = 220 ms smoke can be seen that is lighted by the melt particles, which lasts until t = 550 ms.

In **Fig. 49** the view from the side at the compartment cover is shown. At each exit from the compartment to the containment a blue flame can be observed. Between t = 100 ms and 340 ms the light is too bright. Up to t = 2000 ms an orange light can be seen with occasional melt particles crossing the picture. We interpret this light as a hydrogen flame.

H04: Pictures from the level B port are shown in **Fig. 50**. Up to 600 ms the light was too bright, or the automatic exposure setting too slow. For approximately 3 seconds we see a particle flow with changing density, brightness and background color. At t = 1550 ms there is a peak in the brightness and at t = 1600 ms the color turns into blue for about 200 ms. The change of direction of the particle flow cannot be determined, because the interval of 25 ms between two pictures is too long.

H05: No useful pictures are available.

H06: The top view is shown in **Fig. 51**. The dark round object at the center is the top of the RCS-vessel. The cavity exit openings, which are 2 meters below, can be seen in the first picture. Up to t = 840 ms melt particles are airborne. Between t = 1160 ms and t = 1240 ms a bright orange glow hints to a hydrogen flame (note that the camera has a fixed exposure setting).

3.5 Debris Recovery Data

Debris in the DISCO vessel was recovered from five locations: (1) all cavity surfaces (**Fig. 52** and **53**) , (2) all surfaces in the subcompartment, (3) on the cover of the subcompartment

(**Fig. 55**), (4) on the vessel wall (**Fig. 56**), dome surface, and structures inside the containment, and (5) in the vertical annulus between the containment vessel wall and the subcompartment wall and on the small annular floor. The RPV-vessel (crucible) was weighted pre- and post-test (**Fig. 54**).

The color of the debris was gray in all tests except in test H04, where no steam was present. Here the debris had a brown color (**Fig. 57**– **60**). Note, that Fe_3O_4 and FeO are black and Fe_2O_3 are red.

A posttest sieve analysis was performed separately of the debris that was recovered from the subcompartment and the containment. A standard set of 17 sieves was used (10 mm to 40 µm, **Fig. 61**). Only debris particles that had diameters smaller than 10 mm were analyzed.

Table 22 gives the debris recovery summary and compares the mass balance and transport fractions. A recovery factor greater than one indicates that the total mass available for dispersal into the DISCO vessel was greater than the initial thermite charge, caused by ablation of concrete in the cavity, melting of the crucible steel wall, contaminants (break wires, melt plug, thermocouples, etc.), and oxidation of metallic debris. Also listed are the fractions of the debris with diameters smaller than 10 mm in the subcompartment and the containment. The particle sieve mass median diameter (SMMD) of these fractions is given in the last three lines.

The debris in the cavity was found on the pit floor and on top of the concrete annulus below the main cooling lines. The melt film in the vertical cavity wall was thin (~ 1 mm). Much of the debris in the subcompartment was found at the vertical wall and below, opposite of the cooling line stubs. The debris in the containment was generally collected as small particles on the walls, the top cover and on the floor. Only where melt had hit some hosepipes, melt films had formed.

The particle size distribution is shown in **Figures 62** to **73**, separate for the particles collected in the subcompartment and the containment. In tests H01, H02, H04 and H06, much more melt was ejected directly into the containment than into the subcompartment. On the other hand, without a direct path from the pit into the containment (H03, H05) the gas and the debris has to flow first into the subcompartment and then through relatively small cross sections into the containment. Thus, most of the melt that was dispersed from the pit was trapped in the subcompartment, and very little mass reached the containment, with small particle sizes (median diameter 0.15 mm). Note, that a wire mesh covered the exits to the containment. Only few holes were burned into that mesh by melt particles. In contrast, the melt particles carried into the subcompartment have a median diameter of 3.5 mm and 4.8 mm, respectively. **Fig. 74** shows the cumulative particle size distribution of the total amount of debris found outside the reactor pit for all six experiments. The mean diameter of the debris particles in tests with the open cavity is 1.5 mm, while for test H03 and H05 this parameter is controlled essentially by the particles found in the subcompartment and consequently is much larger.

Table 12. Pre- and post-test data

		H01	H02	H03	H04	H05	H06
Pre-test accumulator pressure	MPa	2.023	2.057	1.992	-	2.054	3.44
Pre-test accumulator temperature	°C	215	221	221	-	221	242
Pre-test water in accumulator	gr	leak	786	986	-	800	1375
Post-test water in accumulator	gr	leak	510	616	-	426	747
Difference	gr	-	276	370[2]	-	374	628
Pre-test pressure in RCS/RPV vessel	MPa	0.101	0.10	0.1	0.381	0.1	0.121
Pre-test temperature in RCS/RPV vessel	°C	179	184	179	16.1	184	225
Containment temperature at closing valves	°C	30.5	26.5	22	16.1	16.3	20
Atmosphere pressure	MPa	0.1	0.1	0.1	0.1	0.101	0.1
Pre-test pressure in containment vessel	MPa	0.206	0.206	0.201	0.1	0.203	0.210
Pre-test temperature in containment vessel	°C	103	103	100	16.1	101	102
Weight of hydrogen bottle before filling	gr	15239.8	15191.2	14722.5	-	16933.3	16859.0
Weight of hydrogen bottle after filling	gr	15191.7	15144.1	14673.8	-	16881.0	16801.0
Difference	gr	48.1	47.1	48.7	-	52.3	58
Temperature of hydrogen bottle before filling	°C	23	21.6	22.5	-	20.3	19.7
Temperature of hydrogen bottle after filling	°C	23	18.4	15	-	17.0	17.0
Pressure in bottle before filling[3]	MPa	20.0	13.7	16.2	-	20.0	12.5
Pressure in bottle after filling	MPa	13.0	7.15	9.0	-	12.2	5.0
Post test water in containment	kg	-	-	-	-	-	186

[2] Probably leaking valve

[3] Volume of hydrogen bottle 0.01 m³

Table 13. Compilation of the initial conditions

		H01	H02	H03	H04	H05	H06
Theoretical melt composition (mass %)							
alumina				45.9			
iron				53.0			
aluminum				1.1			
Melt mass	(kg)	10.64	10.64	10.68	10.64	10.72	10.72
Temperature of melt (approx. ± 100)	(K)			2200			
RCS/RPV pressure (t = 0 s)	(MPa)	0.78	1.22	1.25	0.89	1.21	2.16
RCS/RPV volume	(m³)			0.076			
RCS/RPV steam	(g·moles)	7.0*	15.0	16.0	0.0	20.7	34.9
RCS/RPV nitrogen	(g·moles)	2.0	2.0	2.0	12.0	2.0	3.2
Exit hole diameter	(cm)	5.6	5.6	5.6	5.6	2.8	2.8
Exit hole area	(cm²)	24.6	24.6	24.6	24.6	6.1	6.1
Annular gap area	(cm²)			212			
Flow cross section into subcompartments	(cm²)			308			
Flow cross section into containment	(cm²)	520	520	0	520	0	520
Vessel pressure	(MPa)	0.206	0.206	0.201	0.100	0.203	0.210
Vessel temperature	(K)	376	376	373	293	374	375
Vessel gas moles	(g·moles)	908	908	889	570	898	924
Gas composition	Steam	36.6	36.6	34.2	0	33.5	35.8
in the Containment vessel (mol%)	N_2	47.4	47.4	49.2	78.0	49.7	47.7
	O_2	12.8	12.8	13.2	21.0	13.4	12.8
	H_2	2.6	2.6	2.7	0	2.9	3.1
	Other	0.6	0.6	0.6	1.0	0.6	0.6

*Because of leaking valve, water mass had to be calculated

Table 14. Initial Gas Composition in the Containment vessel

			SNL-Sup1	H01	H02	H03	H04	H05	H06
Containment volume	V	(m^3)	91.6	13.75	13.75	13.75	13.75	13.75	13.75
Initial air temperature	T_0	(K)	293	299.5	299.5	295	290	289.4	293
Atmospheric pressure	P_0	(MPa)	0.084	0.100	0.100	0.100	0.100	0.100	0.100
Temperature at start	T_1	(K)	372	375	375	374	290	374	376
Pressure at start	P_1	(MPa)	0.213	0.206	0.206	0.201	0.100	0.203	0.210
Added hydrogen	m_{H2}	(kg)	0.426	0.0481	0.0471	0.0487	0.0	0.0523	0.058
Air mass	m_{air}	(kg)	91.466	15.990	15.990	16.234	16.514	16.548	16.345
Steam mass	m_{steam}	(kg)	52.940	5.989	5.998	5.478	0.0	5.410	5.954[1]
Partial pressure of air	P_{1air}	(MPa)	0.107	0.125	0.125	0.127	0.100	0.129	0.128
Partial pressure H_2	p_{1H2}	(MPa)	0.00712	0.00540	0.00529	0.00545	0.0	0.00586	0.00653
Partial pressure steam	P_{steam}	(MPa)	0.09923	0.07539	0.07550	0.06877	0.0	0.06791	0.07514
Added hydrogen	N_{H2}	(kmol)	0.211	0.0238	0.0233	0.0241	0.0	0.0259	0.0287
Steam moles	N_{H2O}	(kmol)	2.939	0.332	0.333	0.304	0.0	0.300	0.330
Air moles	N_{air}	(kmol)	3.158	0.552	0.552	0.561	0.570	0.571	0.564
Total gas moles	N_{total}	(kmol)	6.308	0.908	0.908	0.889	0.570	0.898	0.924
Nitrogen moles	N_{N2}	(kmol)	2.464	0.431	0.431	0.437	0.445	0.446	0.440
Oxygen moles	N_{O2}	(kmol)	0.663	0.116	0.116	0.118	0.120	0.120	0.118
Argon etc. moles	$N_{Ar\ etc.}$	(kmol)	0.030	0.005	0.005	0.005	0.005	0.006	0.005
Mol% of hydrogen	N_{H2}/ N_{tot}	%	3.34	2.62	2.56	2.71	0.0	2.88	3.11
Mol% of steam	N_{H2O}/ N_{tot}	%	46.59	36.60	36.65	34.21	0.0	33.45	35.78
Mol% of air	N_{air}/ N_{tot}	%	50.07	60.78	60.78	63.08	100.0	63.66	61.11
Mol% of nitrogen	N_{N2}/ N_{tot}	%	39.07	47.43	47.43	49.22	78.03	49.68	47.68
Mol% of oxygen	N_{O2}/ N_{tot}	%	10.51	12.76	12.76	13.24	20.99	13.36	12.83
Mol% of argon	N_{Ar} / N_{tot}	%	0.48	0.59	0.59	0.61	0.96	0.61	0.59

[1] In Test H06 the condensate water could not be drained fast enough, therefore the floor of the containment and subcompartment was covered by more than 100 kg of water.

Table 15. Characteristics of the blow down process

No.	d (mm)	Δp (Mpa)	u_{liquid} (m/s)	t_L (s)	t_{2ph} (s)	t_{end} (s)	t_s (s)	t_s/t_L -	$t_{breakwire}$ (s)
H01	0,056	0,580	17,3	0,050	0,240	0,470	0,107	1,34	-
H02	0,056	1,020	22,9	0,090	0,270	0,490	0,080	0,67	71
H03	0,056	1,050	23,3	0,135	0,350	0,560	0,079	0,44	-
H04	0,056	0,790	20,2	0,145	0,350	0,550	0,091	0,47	162
H05	0,028	1,010	22,8	0,260	0,580	1,600	0,323	0,93	-
H06	0,028	1,950	31,7	0,250	0,600	1,600	0,232	0,70	101

$\mathbf{u}_{Liquid} = (2\,\Delta p/\rho_M)^{1/2}$ (Eq. 3.1), theoretical velocity of liquid jet

$\mathbf{t}_L$ end of single-phase liquid jet (liquid discharge time) (from Fig.30)

$\mathbf{t}_{2ph}$ end of 2-phase jet (from Fig.30)

$\mathbf{t}_{end}$ end of blow down (from Fig.30)

$\mathbf{t}_s = V_M / (\varepsilon\,\pi\,d^2/4\,u_L)$, (Eq.3.2) theoretical liquid discharge time

$\mathbf{t}_{breakwire}$ time of break wire signal at cavity exit to containment

Table 16. Compilation of the main results

			H01	H02	H03	H04	H05	H06
Flow path to containment vessel			open	open	closed	open	closed	open
RPV pressure at failure		MPa	0.77	1.22	1.25	0.89	1.21	2.16
Gas composition in RPV	steam	mole	7.0	15.0	16.0	0	20.7	34.9
	N2		2.0	2.0	2.0	12.0	2.0	3.2
Containment vessel initial pressure		MPa	0.201	0.206	0.201	0.100	0.200	0.210
Containment vessel initial temperature		°C	101	102	101	17	101	103
Max. containment vessel pressure		MPa	0.370	0.442	0.315	0.256	0.290	0.404
Max. containment vessel pressure increase		MPa	0.170	0.236	0.114	0.156	0.090	0.194
Time of peak pressure		s	1.75	1.75	1.2	1.75	1.75	1.75
Pressure at time = 10 s		MPa	0.294	0.325	0.260	0.185	0.258	0.329
Max. average vessel temperature (approx.)		°C	360	530	300	450	225	450
Hydrogen in containment vessel and subcompartment	pretest	mole	-	26	27	0	29	35
	produced		-	54	33	0	32	39
	burned		-	66	35	0	26	49
Fraction of available hydrogen that burned			-	0.83	0.53	-	0.43	0.66
Duration of hydrogen combustion		s	3	6	2	0		2
Melt transport fractions	dispersed from cavity		0.355	0.605	0.458	0.753	0.377	0.486
	transported to containment		0.237	0.503	0.022	0.663	0.018	0.361
	transported to subcompart.		0.120	0.102	0.435	0.090	0.359	0.125

Table 17. Gas concentrations measured in the H02 experiment.

Time	Location	Species (mole %)			
		N2	O2	H2	rest
-20s	containment	75.9	18.2	4.9	1.0
	subcomp.	78.3	18.7	2.4	0.5
	cavity	77.3	18.2	3.4	1.1
0.2 s	cavity	60.9	14.2	18.1	6.8
0.4 s	containment	79.5	15.9	3.5	1.2
	subcomp.	80.5	16.1	2.9	0.5
	cavity	48.2	11.9	31.6	8.3
20 s	containment	81.7	13.3	2.8	2.2
	subcomp.	82.8	14.6	1.8	0.7
	cavity	73.4	18.5	7.0	1.1

Table 18. Gas concentrations measured in the H03 experiment.

Time	Location	Species (mole %)			
		N2	O2	H2	rest
-20s	containment	75.4	18.3	5.1	1.2
	subcomp.	79.1	19.0	0.8	1.1
	cavity	78.1	20.3	0.8	0.8
0.2 s	cavity	68.2	18.9	9.9	3.1
0.4 s	containment	78.1	16.9	4.5	0.5
	subcomp.	88.1	8.8	1.2	1.8
	cavity	53.9	12.8	25.3	8.0
20 s	containment	78.3	16.7	4.5	0.5
	subcomp.	83.4	11.1	4.7	0.8
	cavity	80.2	17.6	1.2	1.0

Table 19. Gas concentrations measured in the H05 experiment.

Time	Location	Species (mole %)			
		N2	O2	H2	rest
-20s	containment	77.0	17.6	5.4	0
	subcomp.	80.3	18.9	0.8	0
	cavity	81.4	18.0	0.6	0
0.2 s	cavity	79.9	20.1	0.0	0
0.4 s	containment	78.1	16.8	5.1	0
	subcomp.	86.5	13.0	0.5	0
	cavity	79.0	20.9	0.1	0
20 s	containment	78.0	16.6	5.4	0
	subcomp.	80.3	10.0	8.7	1.0
	cavity	77.3	19.8	2.4	0.5

Table 20. Gas concentrations measured in the H06 experiment.

Time	Location	Species (mole %)			
		N2	O2	H2	rest
-20s	containment	77.5	17.0	6.6	-1.1
	subcomp.	81.3	17.7	0.8	0.2
	cavity	79.8	21.0	0.0	-0.8
0.2 s	cavity	78.7	20.5	0.0	0.8
0.4 s	containment	84.4	11.2	3.0	1.4
	subcomp.	81.2	16.3	2.0	0.5
	cavity	79.5	21.0	0.0	-0.5
40 s	containment	81.5	13.5	4.5	0.5
	subcomp.	82.0	14.2	4.5	-0.7
	cavity	79.9	20.9	0.0	-0.8

Table 21. Gas analysis

containment vessel		SNL-S1	H02	H03	H05	H06
Measured pretest gas concentrations (dry basis)	N_2	0.743	0.759	0.752	0.770	0.775
	O_2	0.196	0.182	0.183	0.176	0.170
	H_2	0.062	0.049	0.051	0.054	0.066
Moles of preexisting gas (det. from concentration measurements) (3.15)	N_2 kmol	2.503	0.381	0.384	0.401	0.401
	O_2 kmol	0.660	0.092	0.093	0.092	0.088
	H_2 kmol	0.209	0.025	0.026	0.028	0.034
Measured posttest gas concentrations (dry basis)	N_2	0.841	0.817	0.781	0.780	0.815
	O_2	0.125	0.134	0.167	0.166	0.135
	H_2	0.020	0.028	0.045	0.054	0.045
Calculated posttest gas moles (Eq.3.16, 3.17)	O_2 kmol	0.372	0.062	0.082	0.085	0.066
	H_2 kmol	0.060	0.013	0.022	0.028	0.022
Moles of hydrogen produced (Eq.3.19)	H_2 kmol	0.427	0.047	0.018	0.012	0.031
Moles of hydrogen burned (Eq.3.18)	H_2 kmol	0.577	0.059	0.022	0.013	0.043
Fraction of available hydrogen that burned $N_{burn}/(N_{pre}+N_{prod})$ (3.20)		0.906	0.820	0.498	0.313	0.661
sub-compartment			**H02**	**H03**	**H05**	**H06**
Measured pretest gas concentrations (dry basis)	N_2		0.783	0.791	0.803	0.813
	O_2		0.187	0.190	0.189	0.177
	H_2		0.024	0.008	0.008	0.008
Moles of preexisting gas (det. from concentration measurements) (3.15)	N_2 kmol		0.057	0.059	0.061	0.061
	O_2 kmol		0.014	0.014	0.014	0.013
	H_2 kmol		0.002	0.001	0.001	0.001
Measured posttest gas concentrations (dry basis)	N_2		0.828	0.834	0.803	0.820
	O_2		0.146	0.111	0.100	0.142
	H_2		0.018	0.047	0.087	0.045
Calculated posttest gas moles (Eq.3.16, 3.17)	O_2 kmol		0.010	0.008	0.008	0.011
	H_2 kmol		0.001	0.003	0.007	0.003
Moles of hydrogen produced (Eq.3.19)	H_2 kmol		0.007	0.015	0.020	0.008
Moles of hydrogen burned (Eq.3.18)	H_2 kmol		0.007	0.013	0.014	0.005
Fraction of available hydrogen that burned Nburn/($N_{pre}+N_{prod}$) (3.20)	-		0.852	0.792	0.284	0.129
Total			**H02**	**H03**	**H05**	**H06**
Initial	H_2 kmol		**0.026**	**0.027**	**0.029**	**0.035**
Produced	H_2 kmol		**0.054**	**0.033**	**0.032**	**0.039**
Burned	H_2 kmol		**0.066**	**0.035**	**0.026**	**0.049**
Fraction burned	H_2 -		**0.824**	**0.576**	**0.432**	**0.656**

Table 22. Debris recovery data

	Mass Balance (kg)	Fractions	SNL-S1	H01	H02	H03	H04	H05	H06
a	Initial thermite charge		62.000	10.640	10.640	10.680	10.640	10.720	10.720
b	Cavity		15.180	6.940	4.758	6.455	2.065	7.672	6.058
c	Subcompartment		5.930	1.268	1.226	5.186	1.010	4.422	1.475
	Fraction smaller 10 mm in SC			*0.855*	*0.970*	*0.909*	*0.988*	*0.550*	*0.708*
d	Containment		47.500	2.550	6.066	0.265	7.077	0.217	4.255
	Fraction smaller 10 mm in Cont.			*0.781*	*0.903*	*1.000*	*0.908*	*1.000*	*0.855*
e	Total recovered[1]		68.610	10.758	12.050	11.906	10.892	12.311	11.788
	Recovery factor	f_{rec} = e/a	1.107	1.011	1.133	1.114	1.024	1.148	1.100
	Melt transport fractions								
	Dispersed from cavity	f_{disp}=(c+d)/e	0.779	0.355	0.605	0.458	0.742	0.377	0.486
	Transported to subcompartment	f_{disp}= c/e	0.086	0.118	0.102	0.436	0.093	0.359	0.125
	Transported to containment	f_{cont} = d/e	0.692	0.237	0.503	0.022	0.650	0.018	0.361
Particle size	SMMD Subcompartment [mm]			2.1	2.8	3.5	1.5	4.8	2.6
	SMMD Containment [mm]			1.1	1.3	0.16	1.4	0.15	1.4
	SMMD Total [mm]			1.4	1.5	3.1	1.4	4.5	1.5

1 The total mass is greater than the initial thermite charge caused by partial melting of the inner wall of the crucible, melting of the fusible brass plug (0.450 kg), ablation of concrete in the cavity and other contaminants (wires etc.)

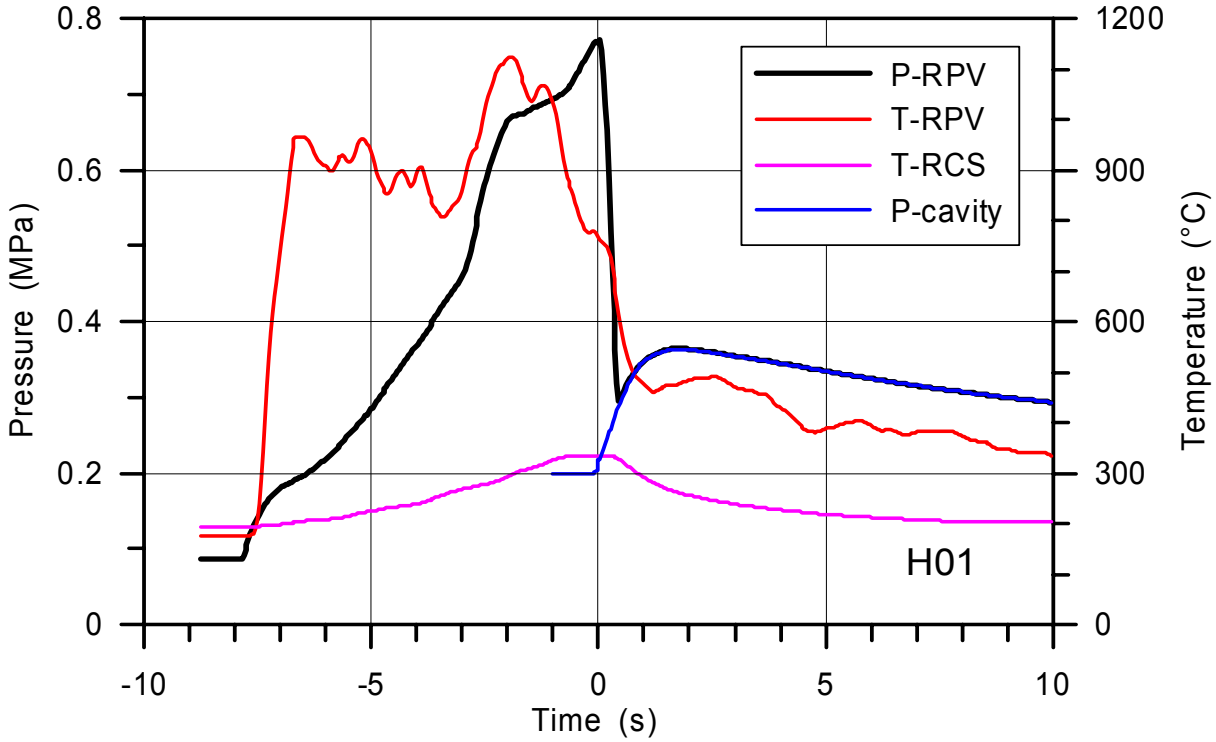

Fig. 18. Pressure and temperature in the RPV/RCS-vessel and the cavity in test H01

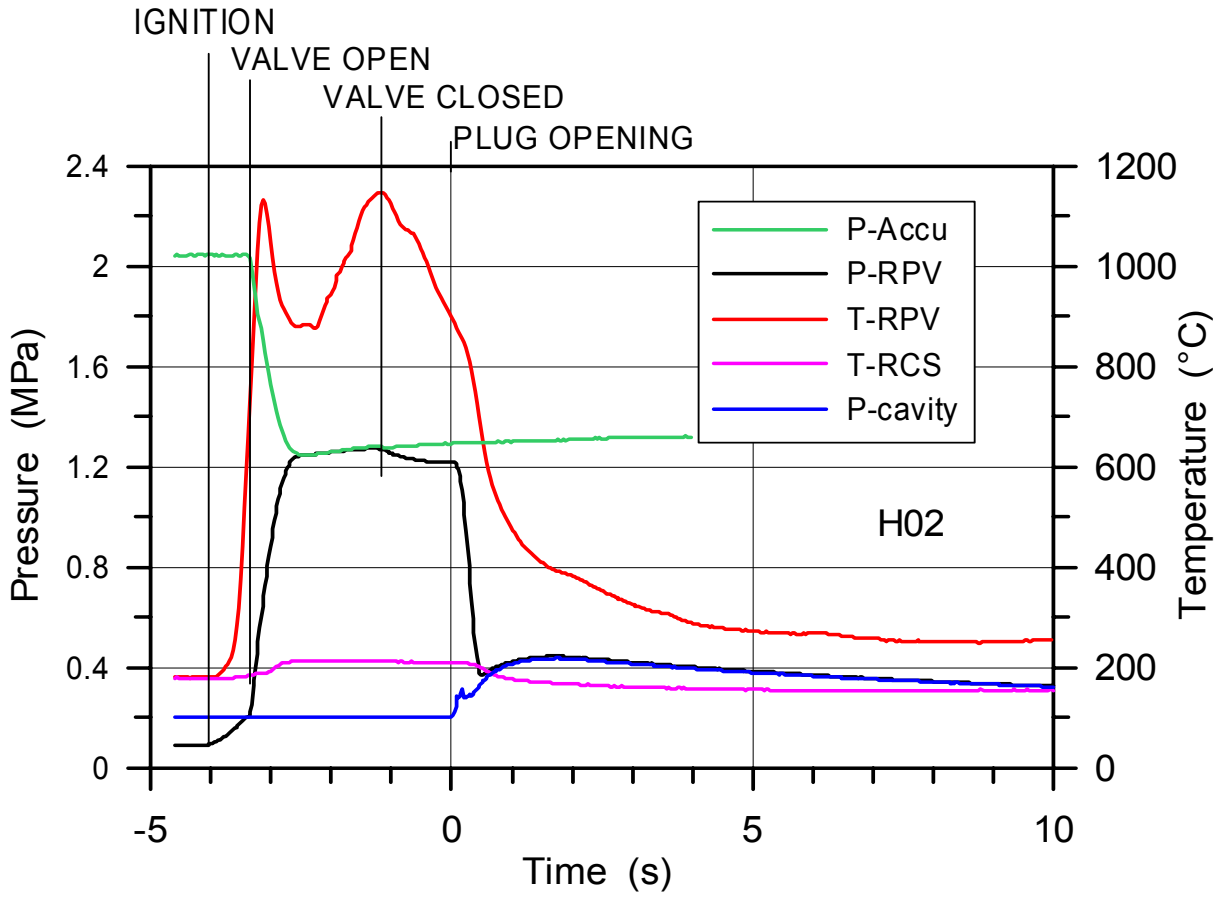

Fig. 19. Pressure, temperature and timing in H02

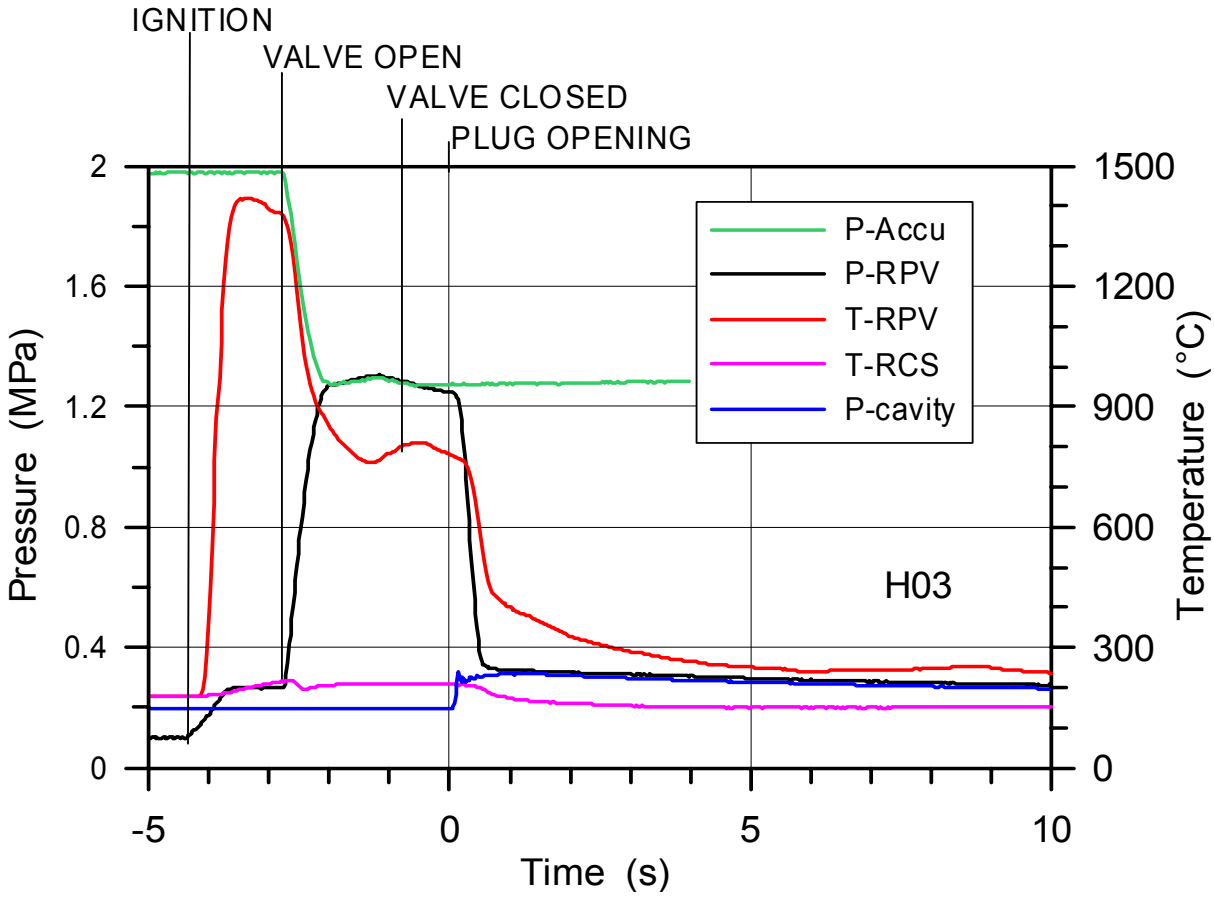

Fig. 20. Pressure, temperature and timing in H03

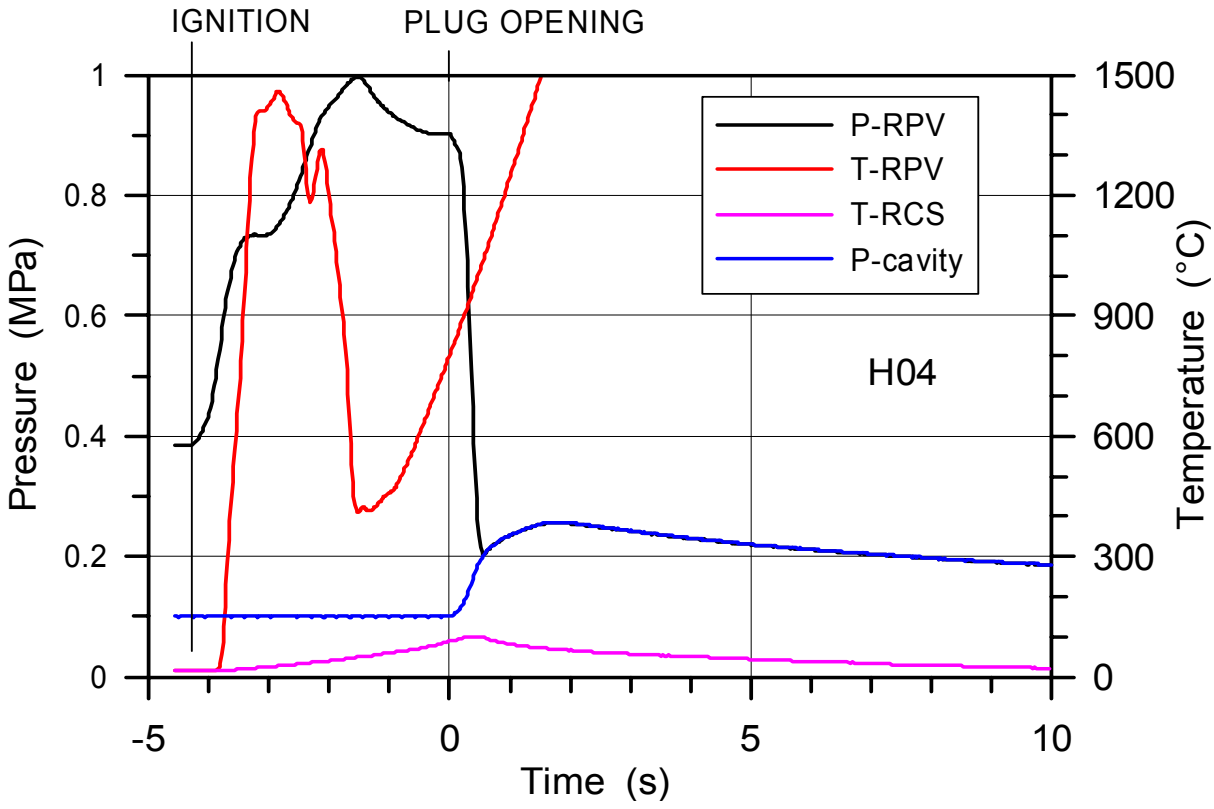

Fig. 21. Pressure, temperature and timing in H04 (no steam)

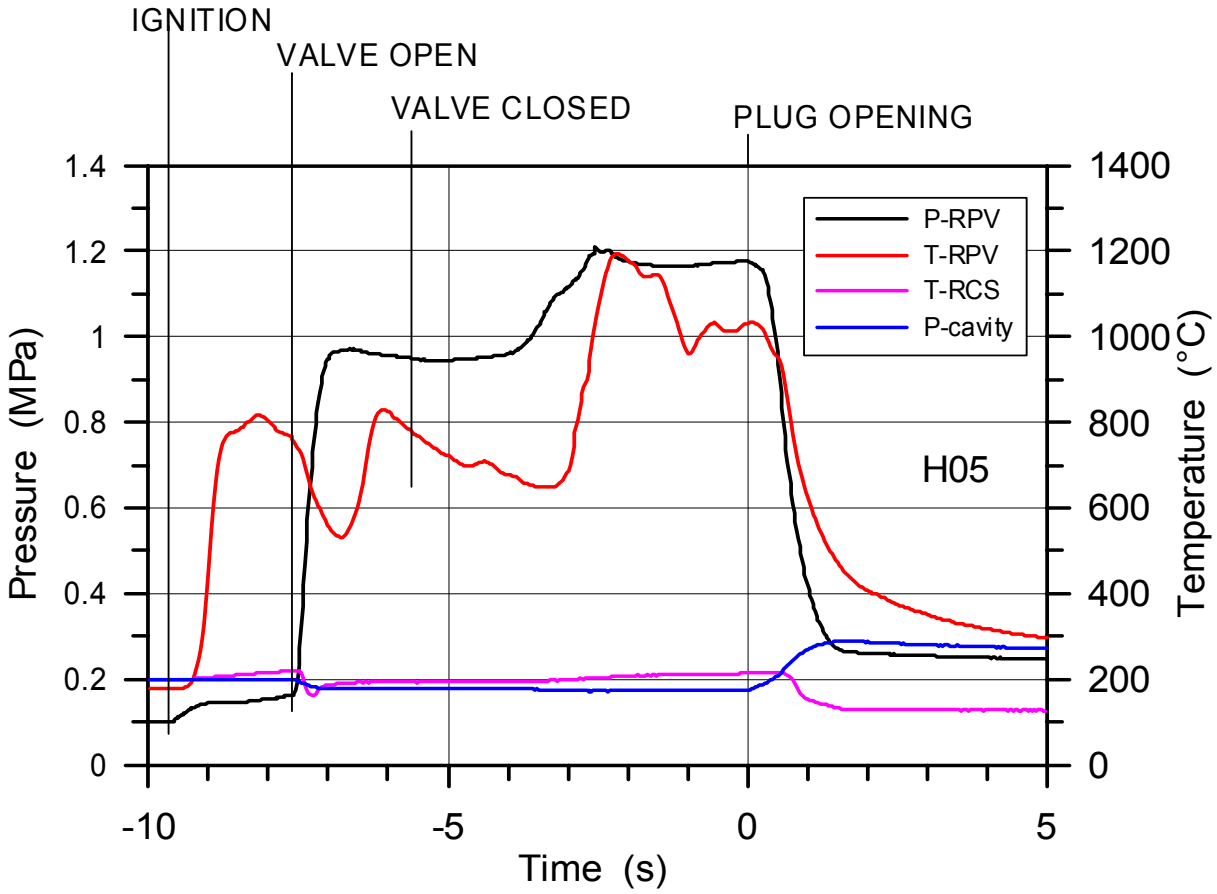

Fig. 22. Pressure, temperature and timing in H05

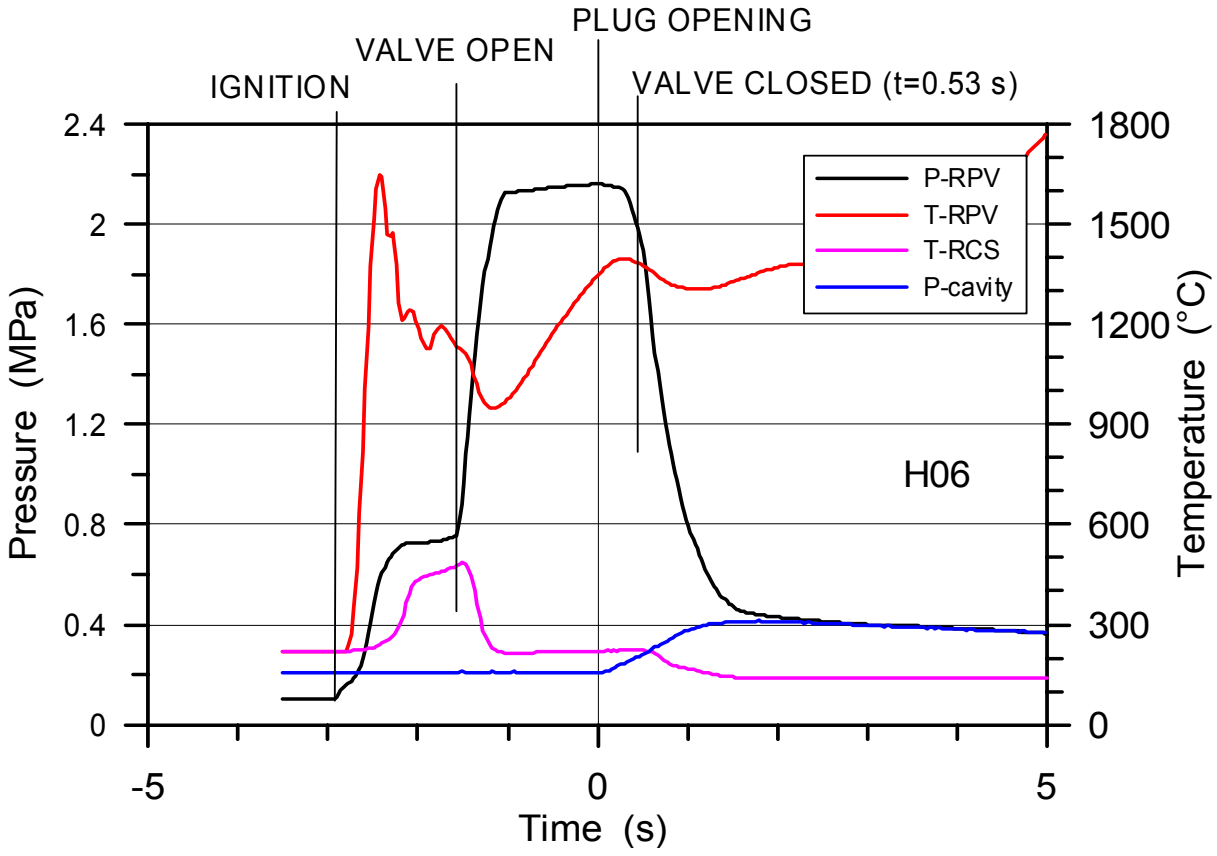

Fig. 23. Pressure, temperature and timing in H06

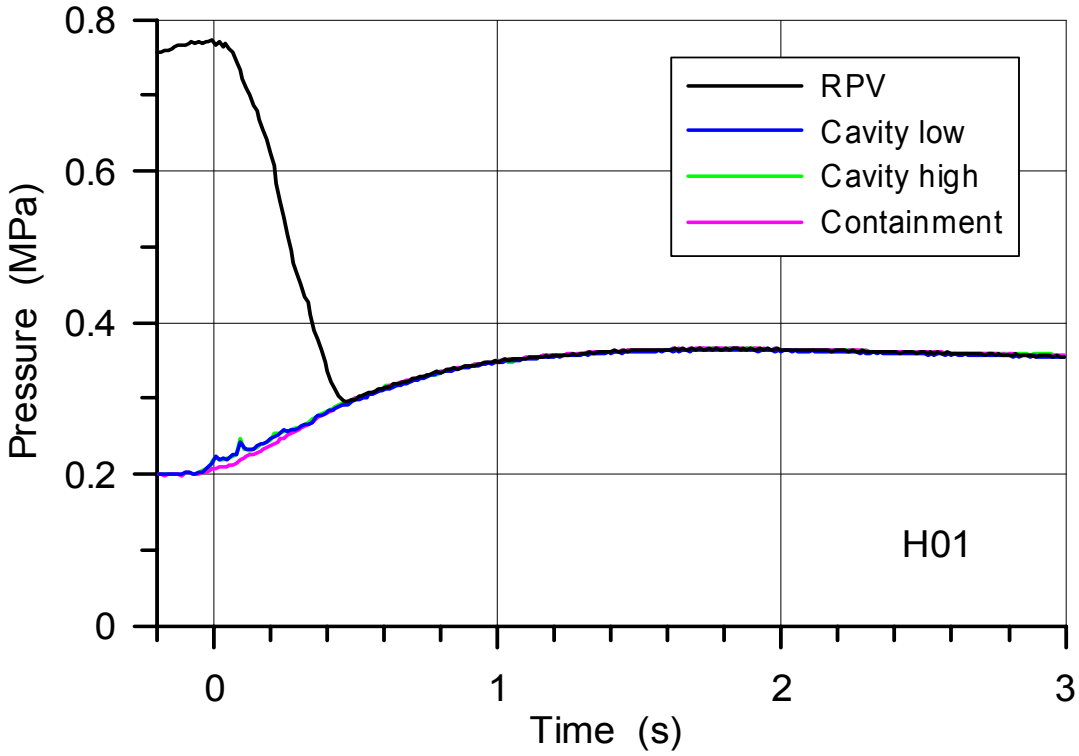

Fig. 24. Pressure in the RPV, cavity and containment in H01 (-0.2 to 3 s)

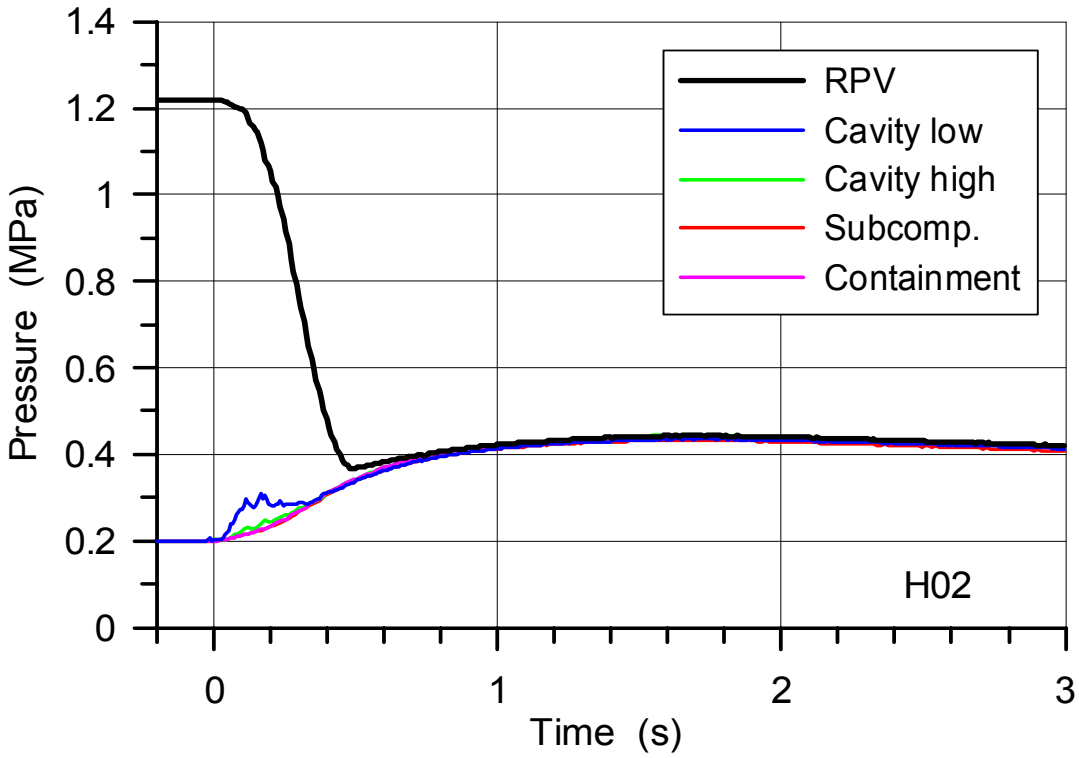

Fig. 25. Pressure in the RPV, cavity and containment in H02 (-0.2 to 3 s)

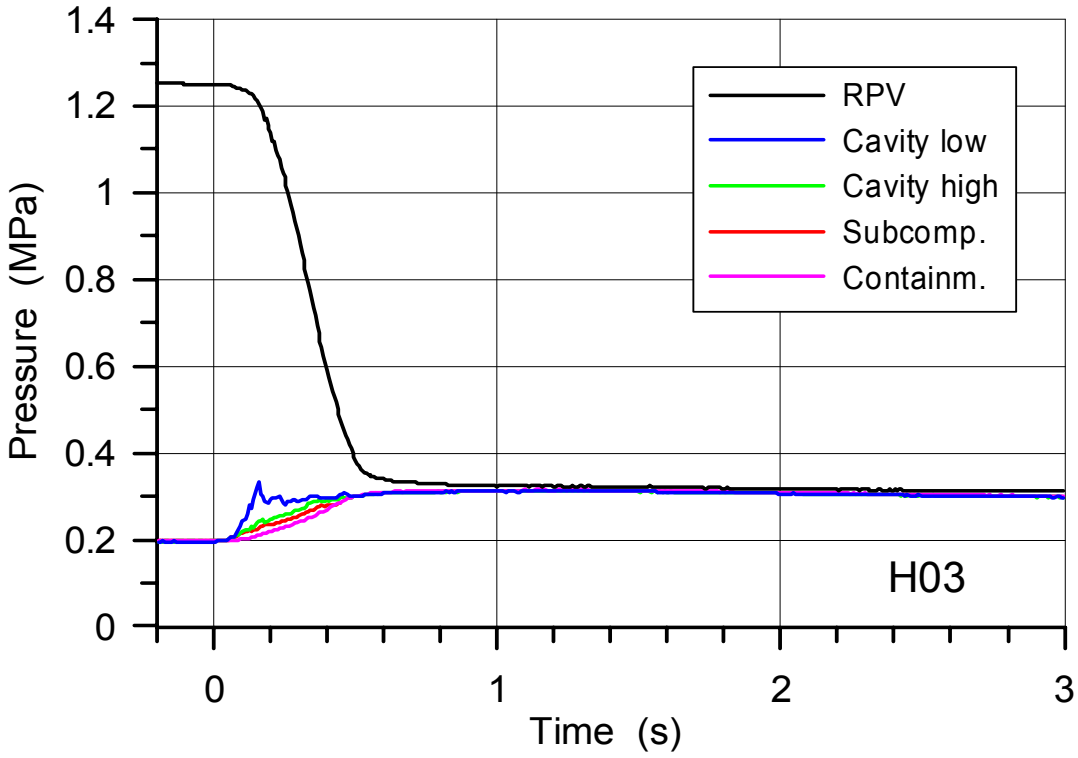

Fig. 26. Pressure in the RPV, cavity and containment in H03 (-0.2 to 3 s)

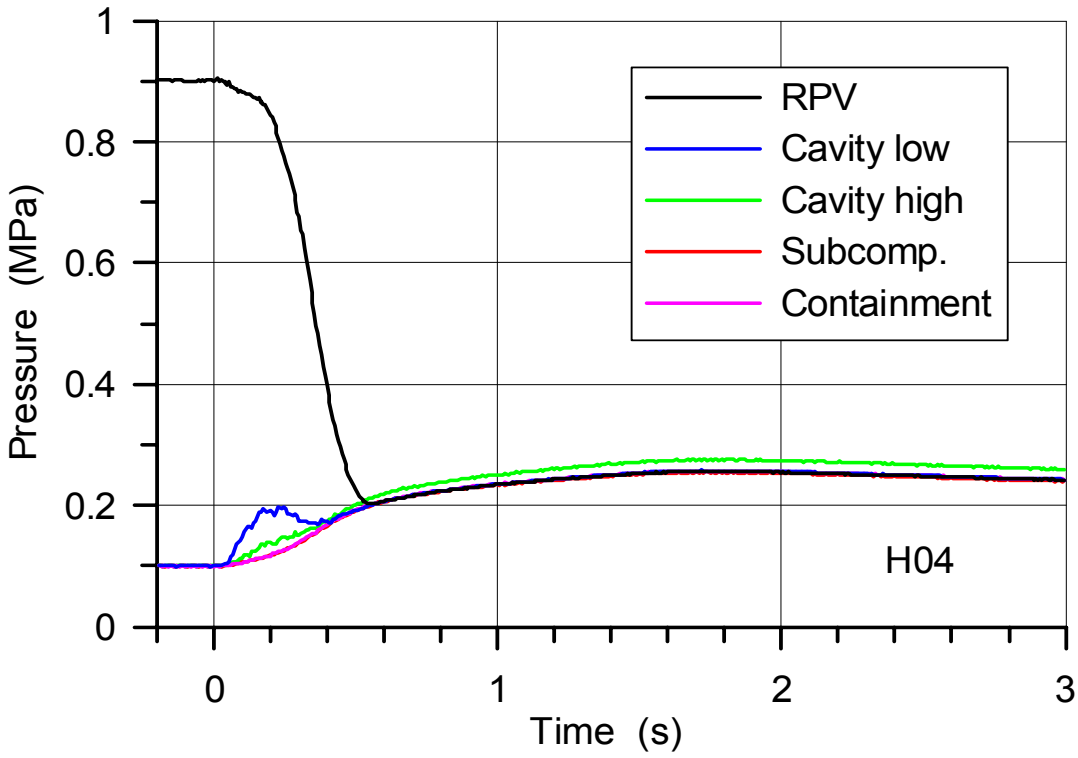

Fig. 27. Pressure in the RPV, cavity and containment in H04 (-0.2 to 3 s)

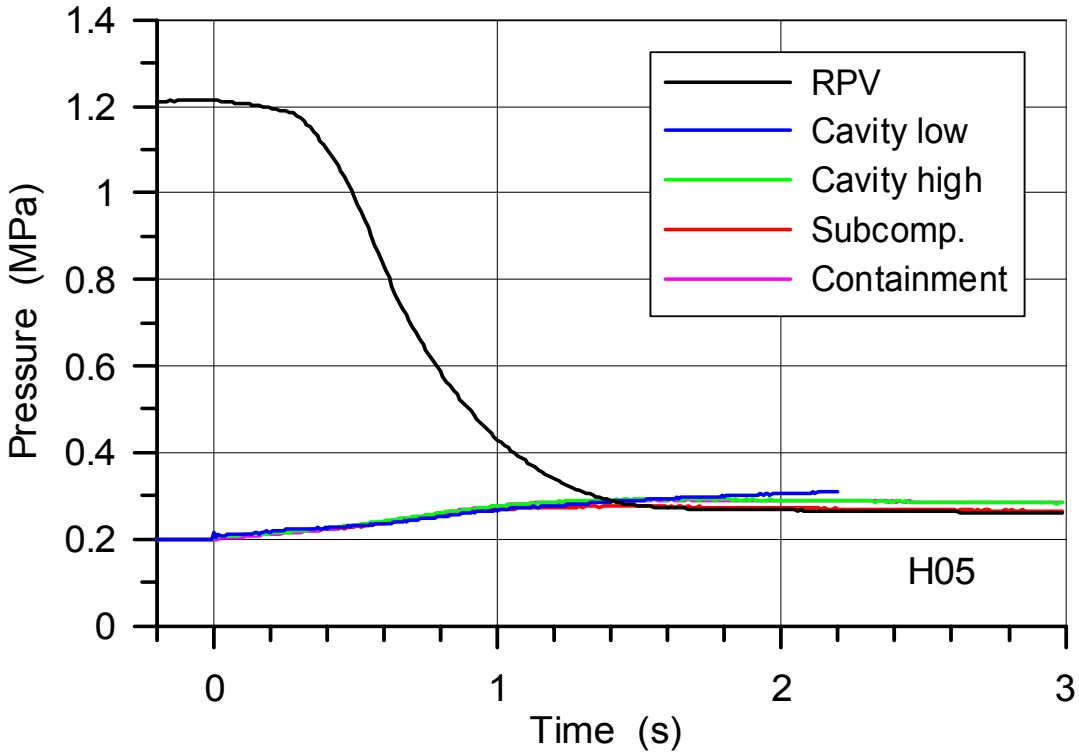

Fig. 28. Pressure in the RPV, cavity and containment in H05 (-0.2 to 3 s)

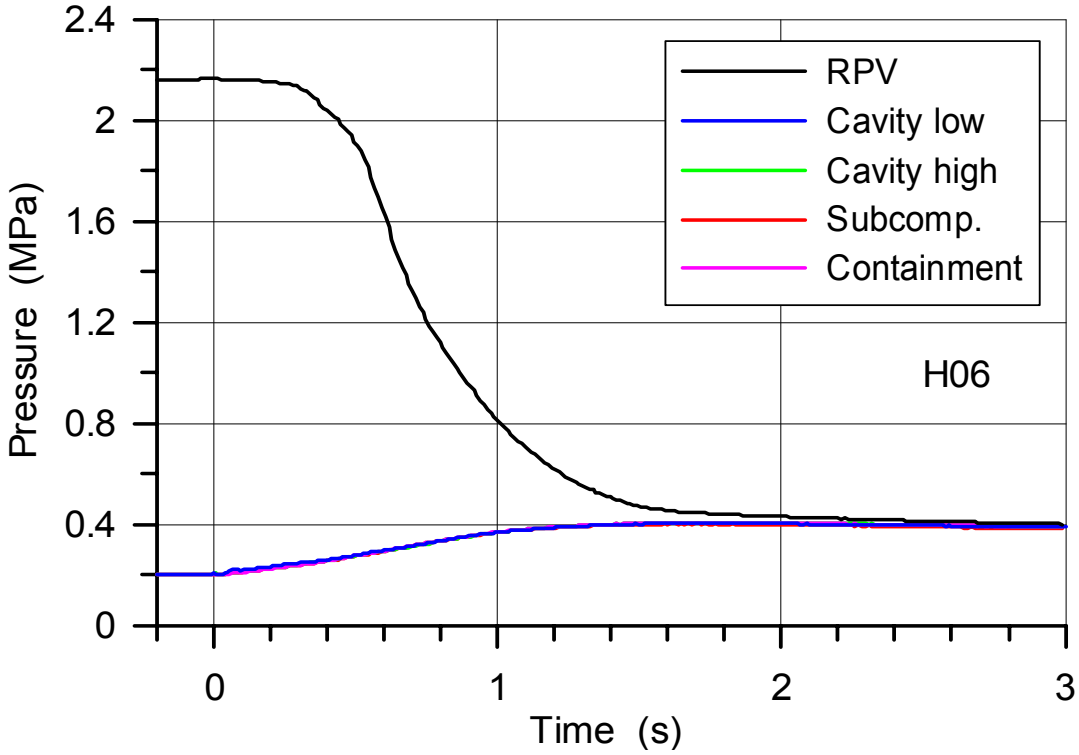

Fig. 29. Pressure in the RPV, cavity and containment in H06 (-0.2 to 3 s)

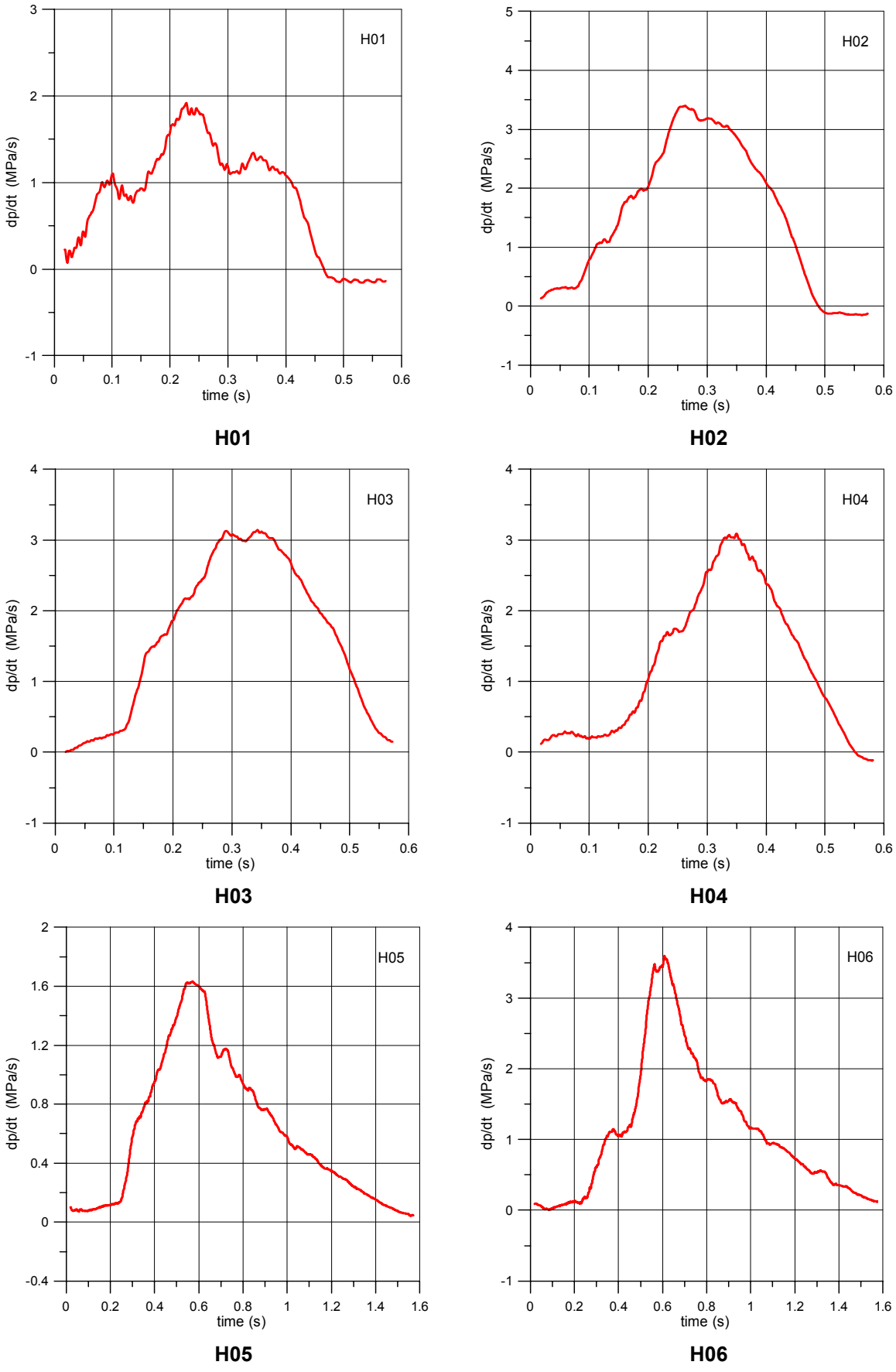

Fig. 30. Pressure gradient in RPV vessel

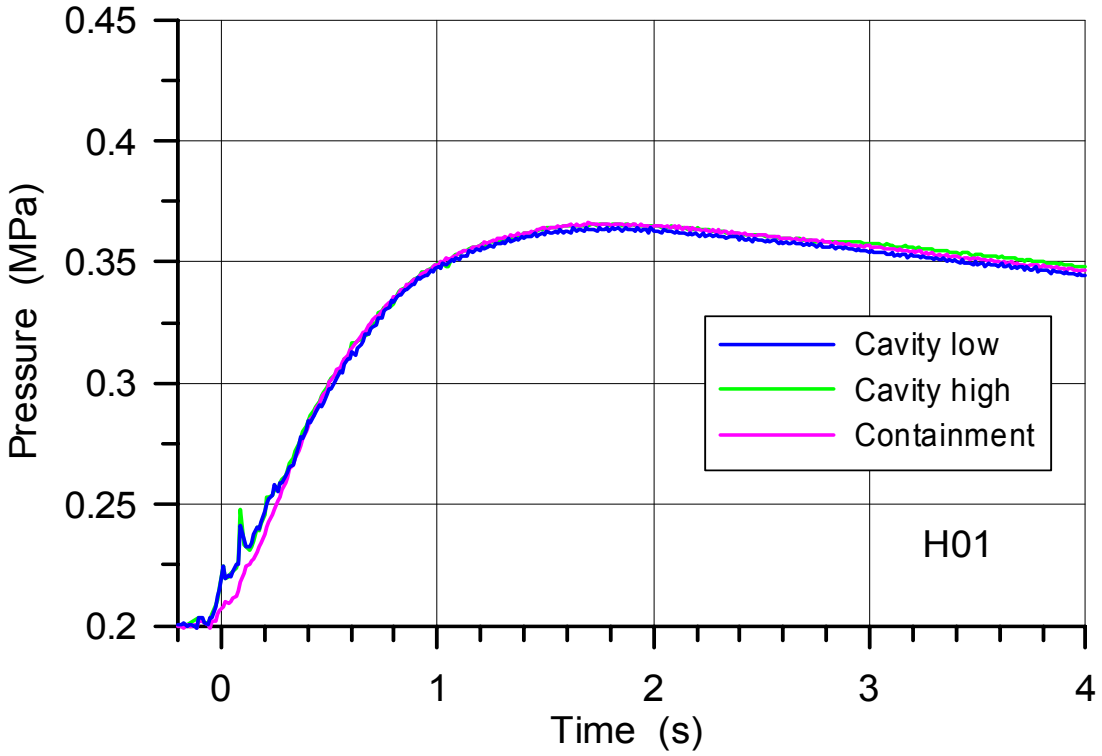

Fig. 31. Pressure in the cavity and containment in H01

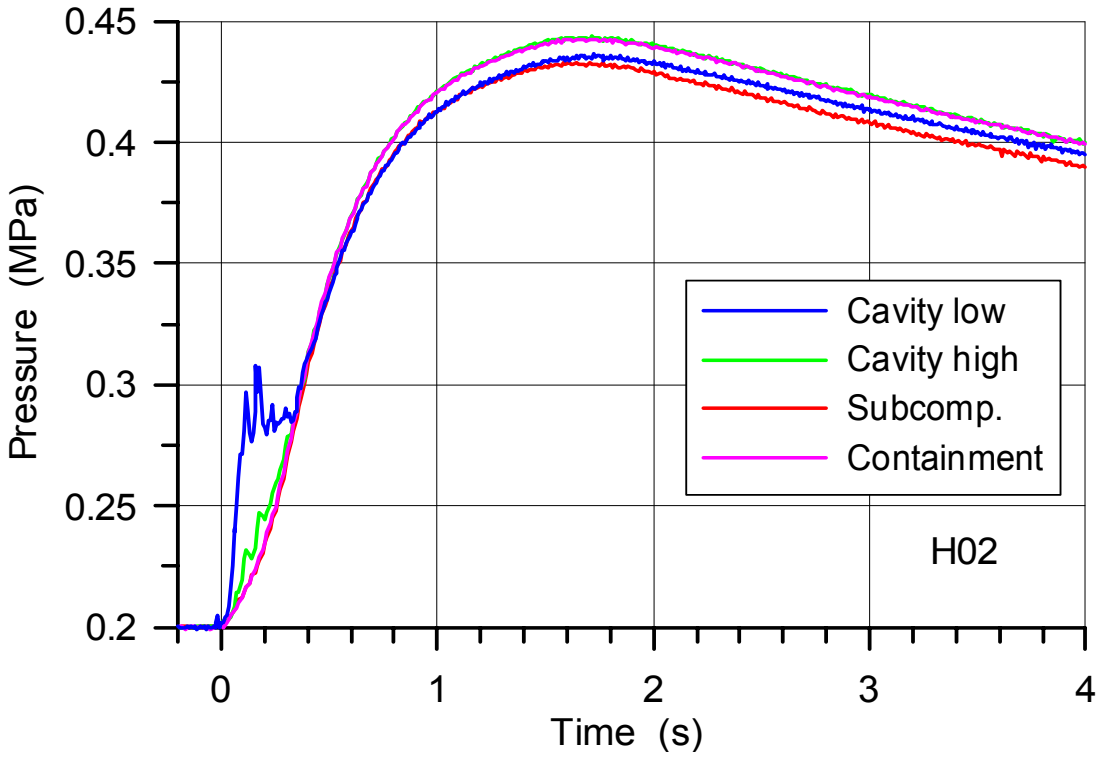

Fig. 32. Pressure in the cavity, subcompartment and containment in H02

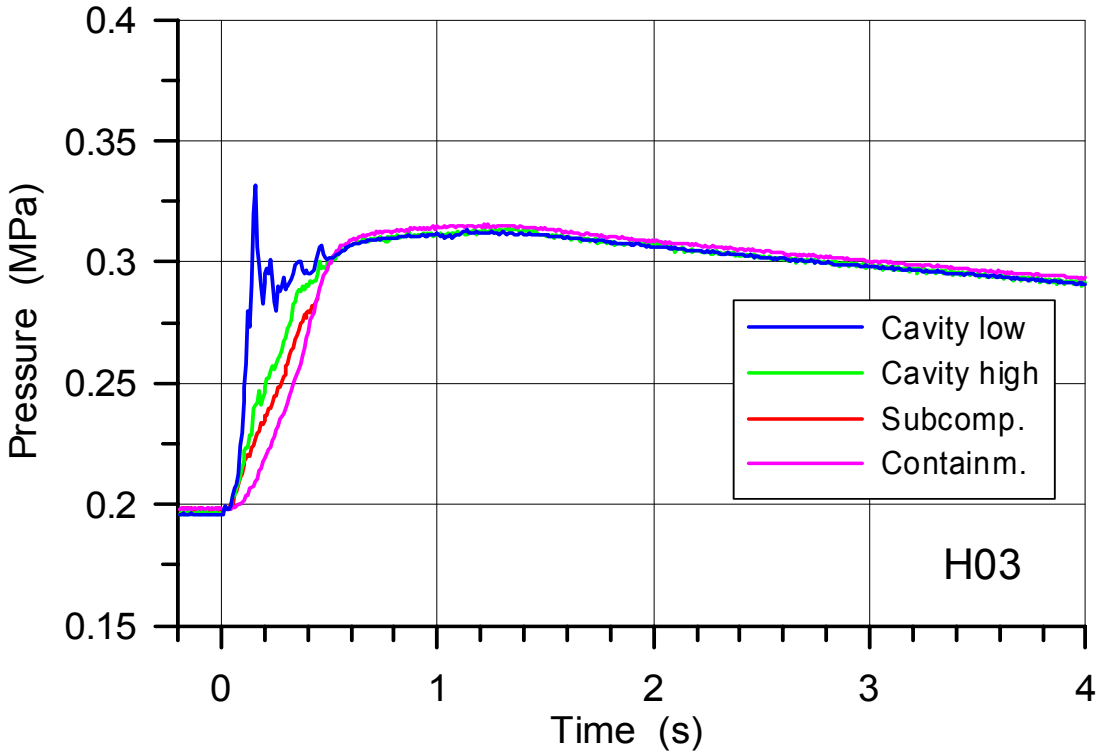

Fig. 33. Pressure in the cavity, subcompartment and containment in H03

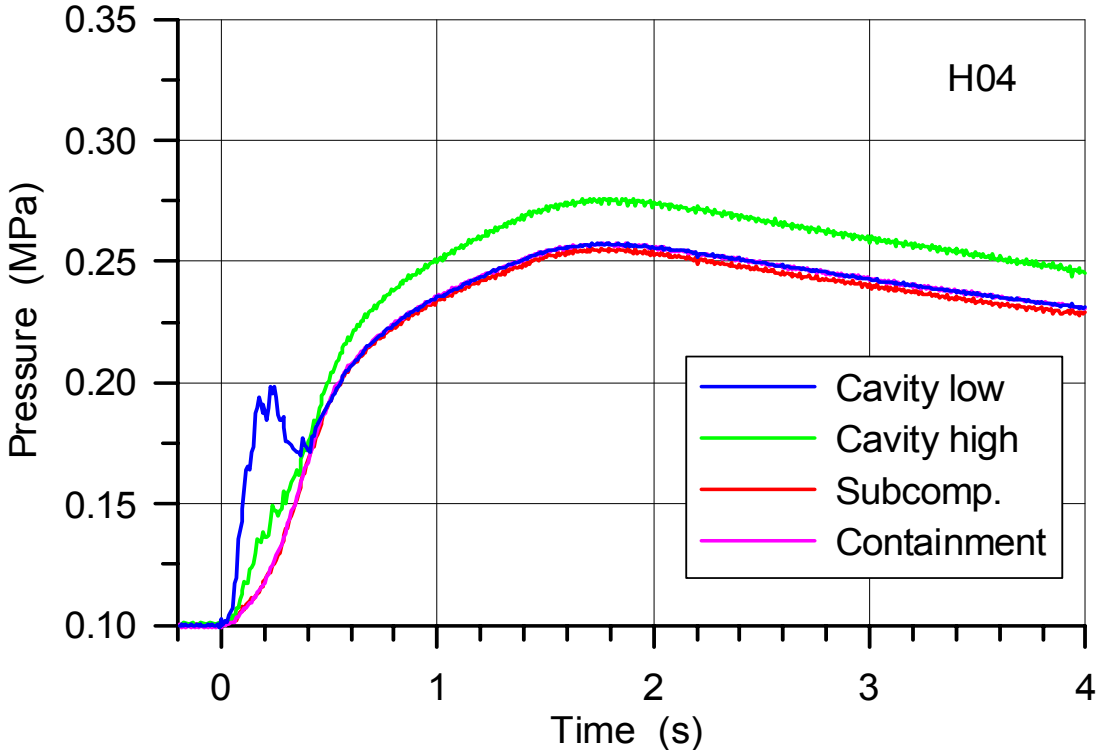

Fig. 34. Pressure in the cavity, subcompartment and containment in H04

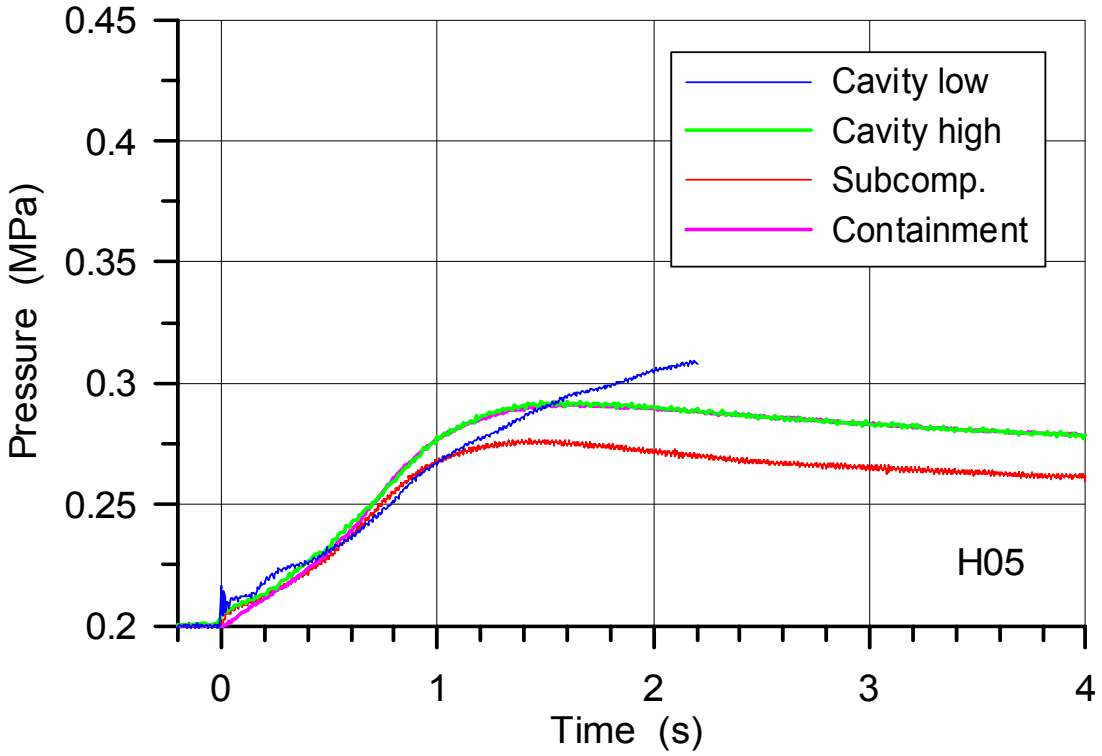

Fig. 35. Pressure in the cavity, subcompartment and containment in H05

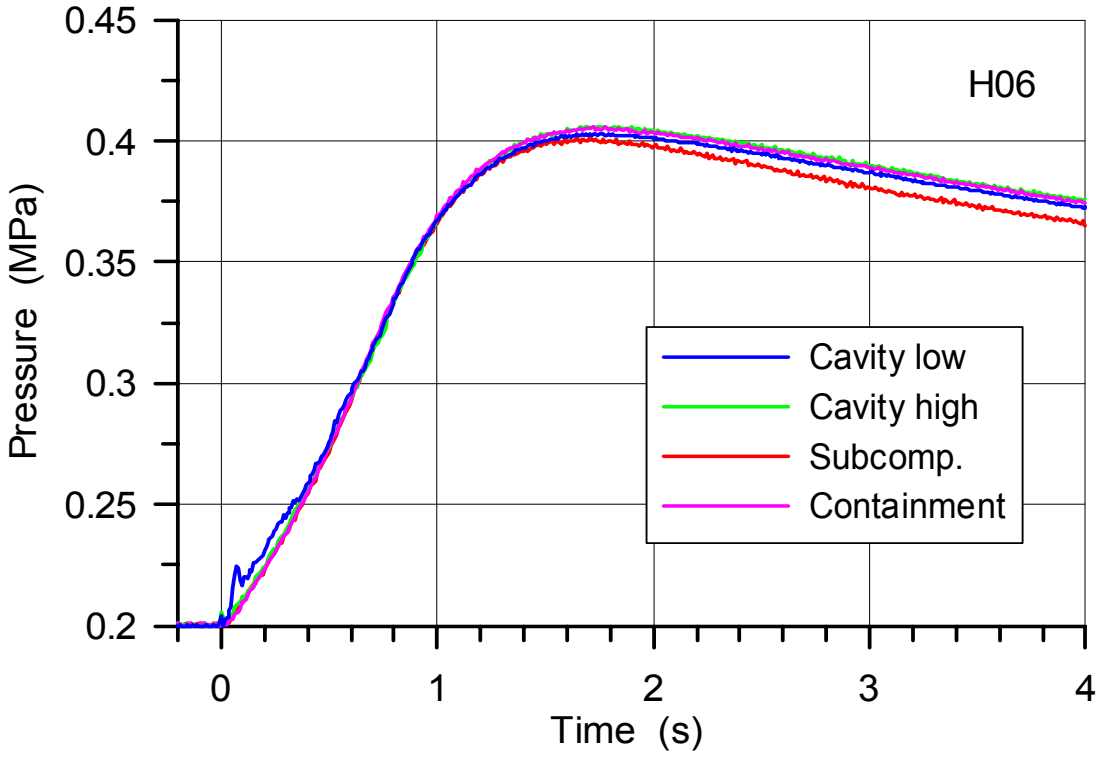

Fig. 36. Pressure in the cavity, subcompartment and containment in H06

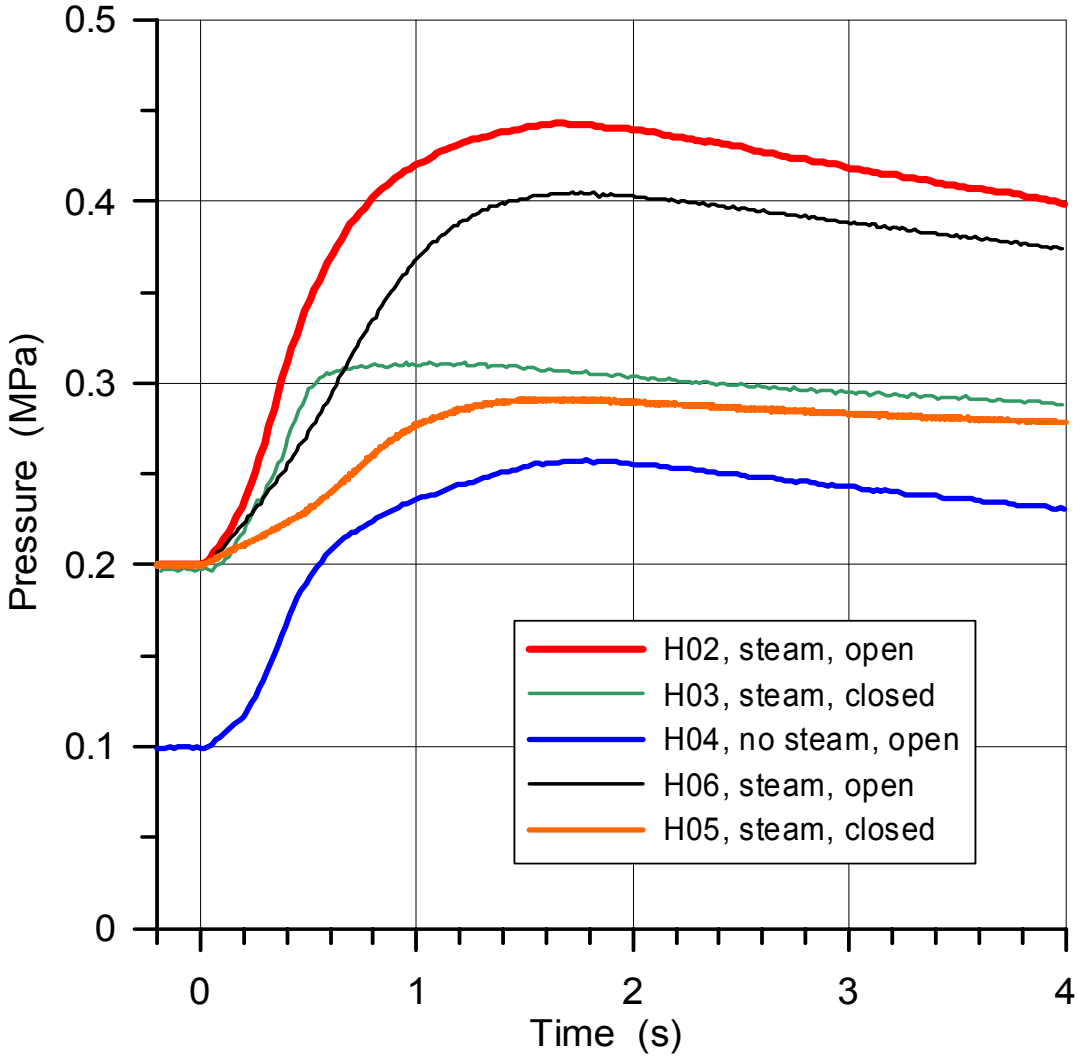

Fig. 37. Comparison of pressure rise in the containment
(H02, H03 and H06 pressures were adjusted to initial pressure of 0.2 MPa)

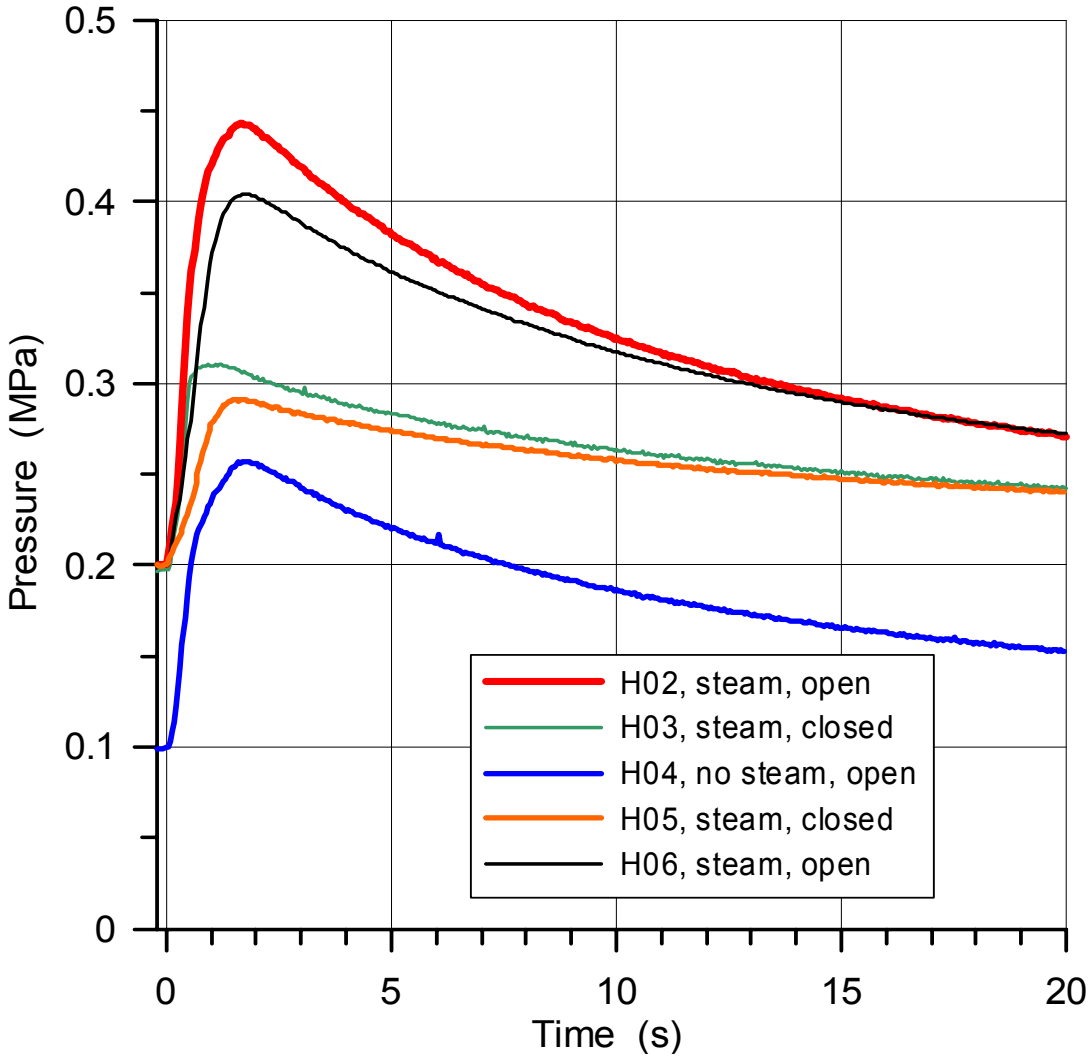

Fig. 38. Long term pressure histories in the containment
(H02, H03 and H06 pressures were adjusted to initial pressure of 0.2 MPa)

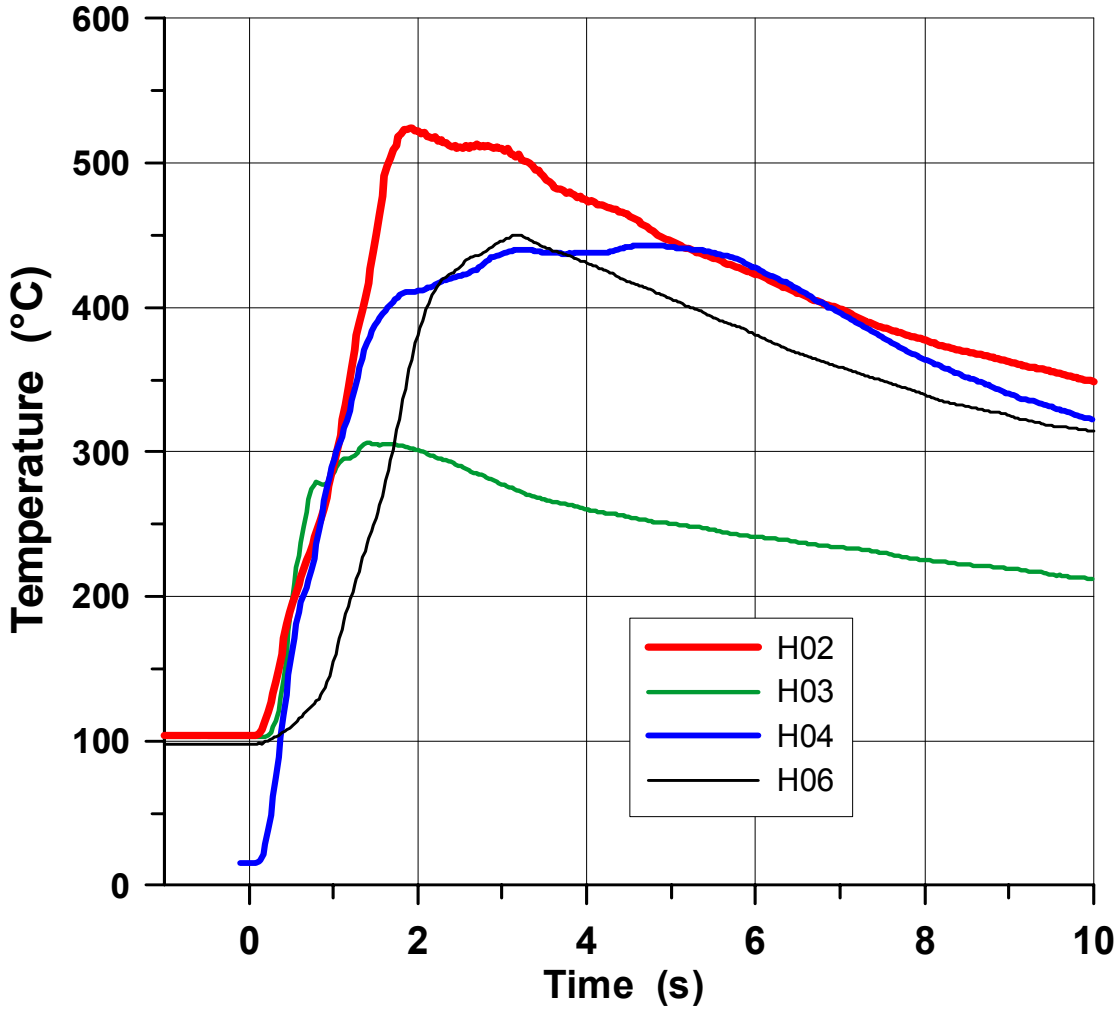

Fig. 39. Comparison of average containment temperatures

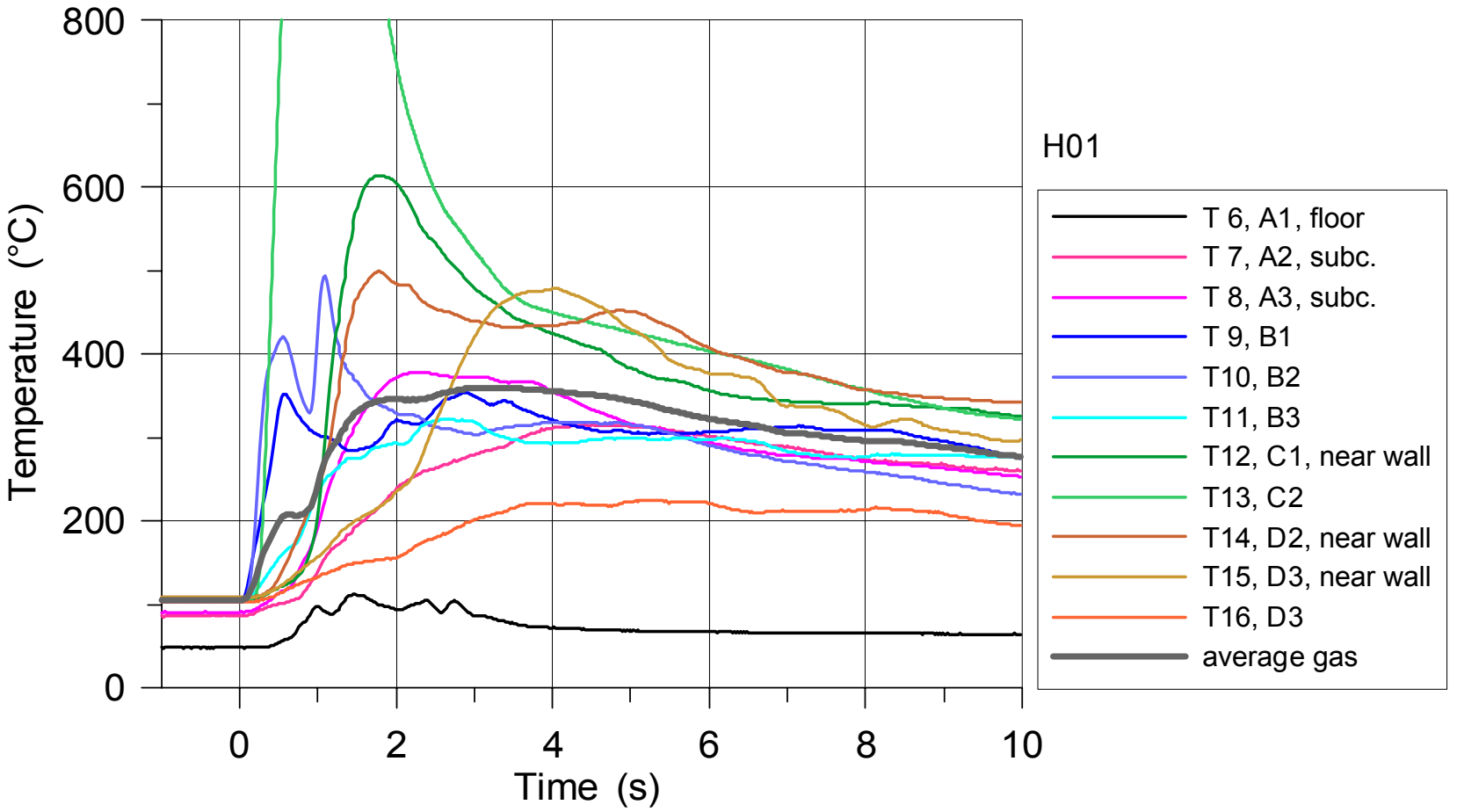

Fig. 40. Gas temperatures in the subcompartment and containment in H01

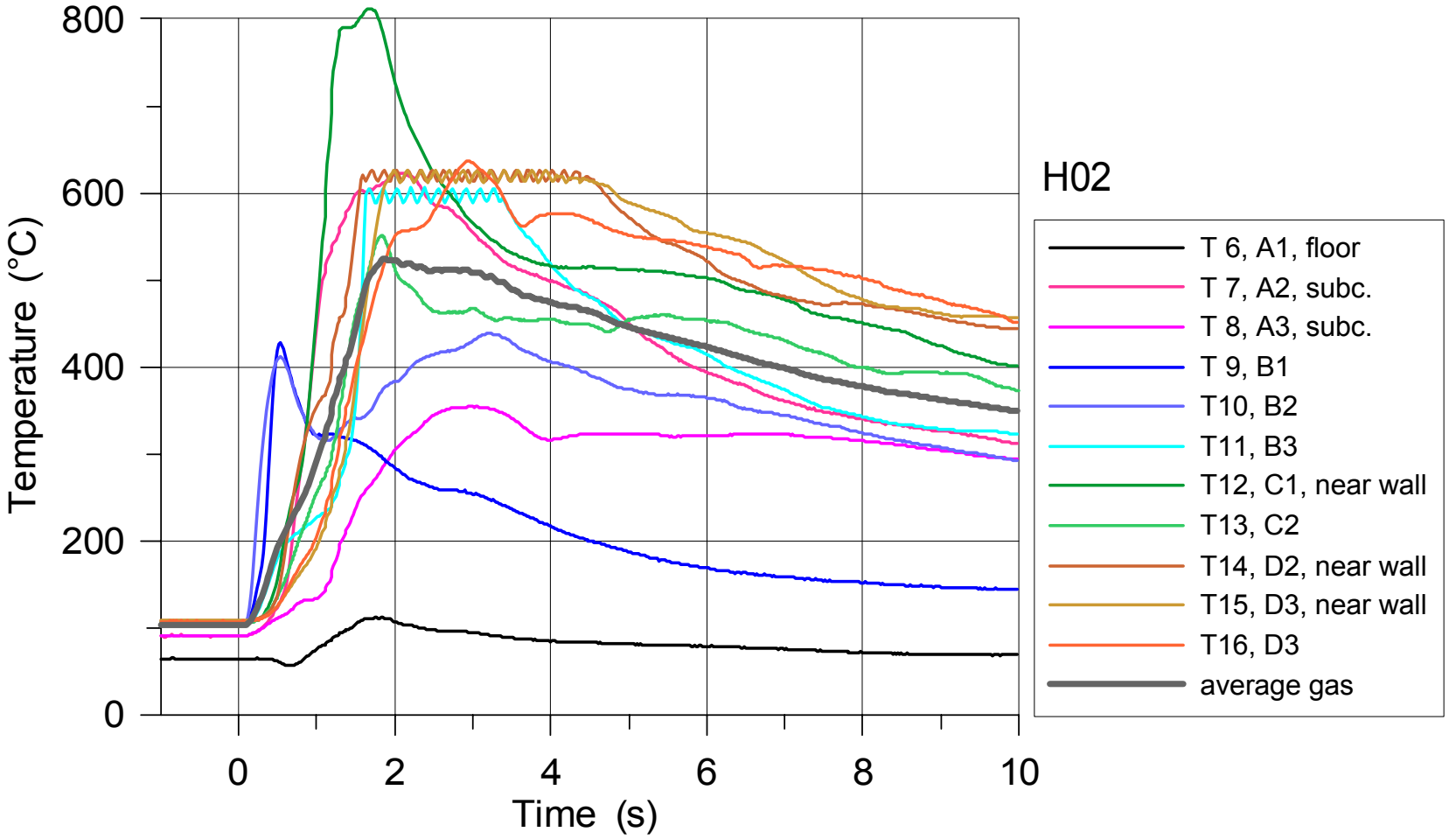

Fig. 41. Gas temperatures in the subcompartment and containment in H02

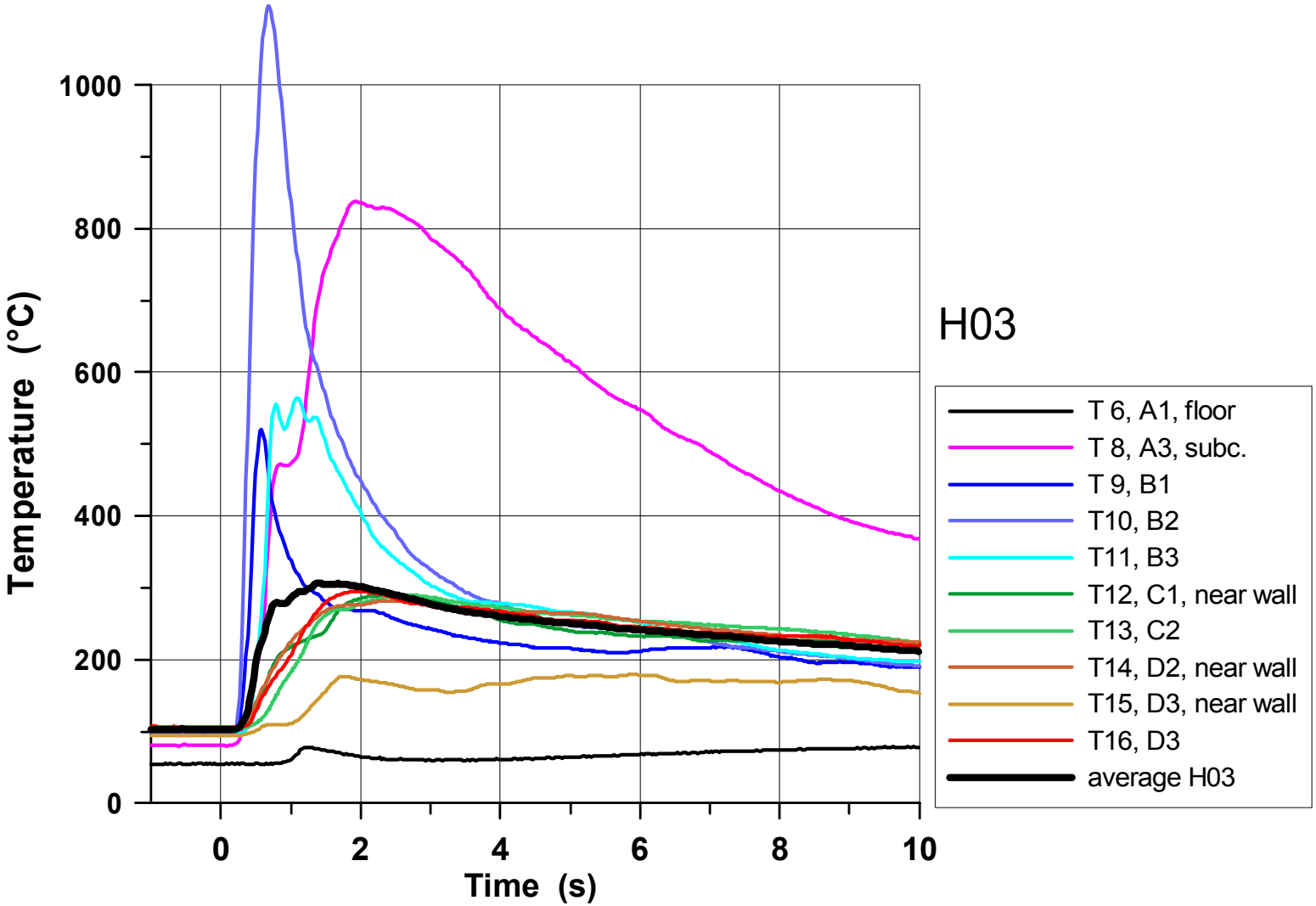

Fig. 42. Gas temperatures in the subcompartment and containment in H03

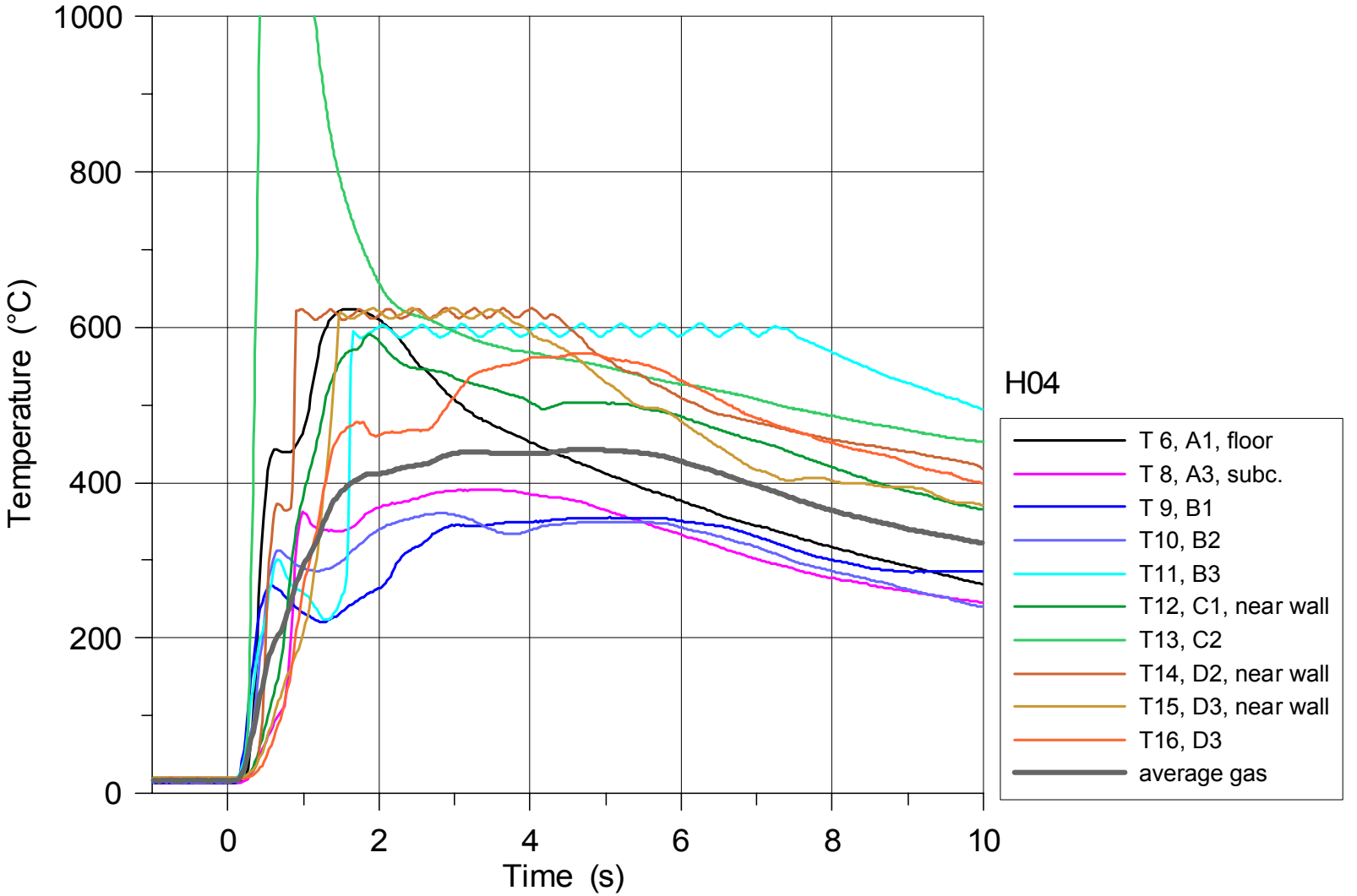

Fig. 43. Gas temperatures in the subcompartment and containment in H04

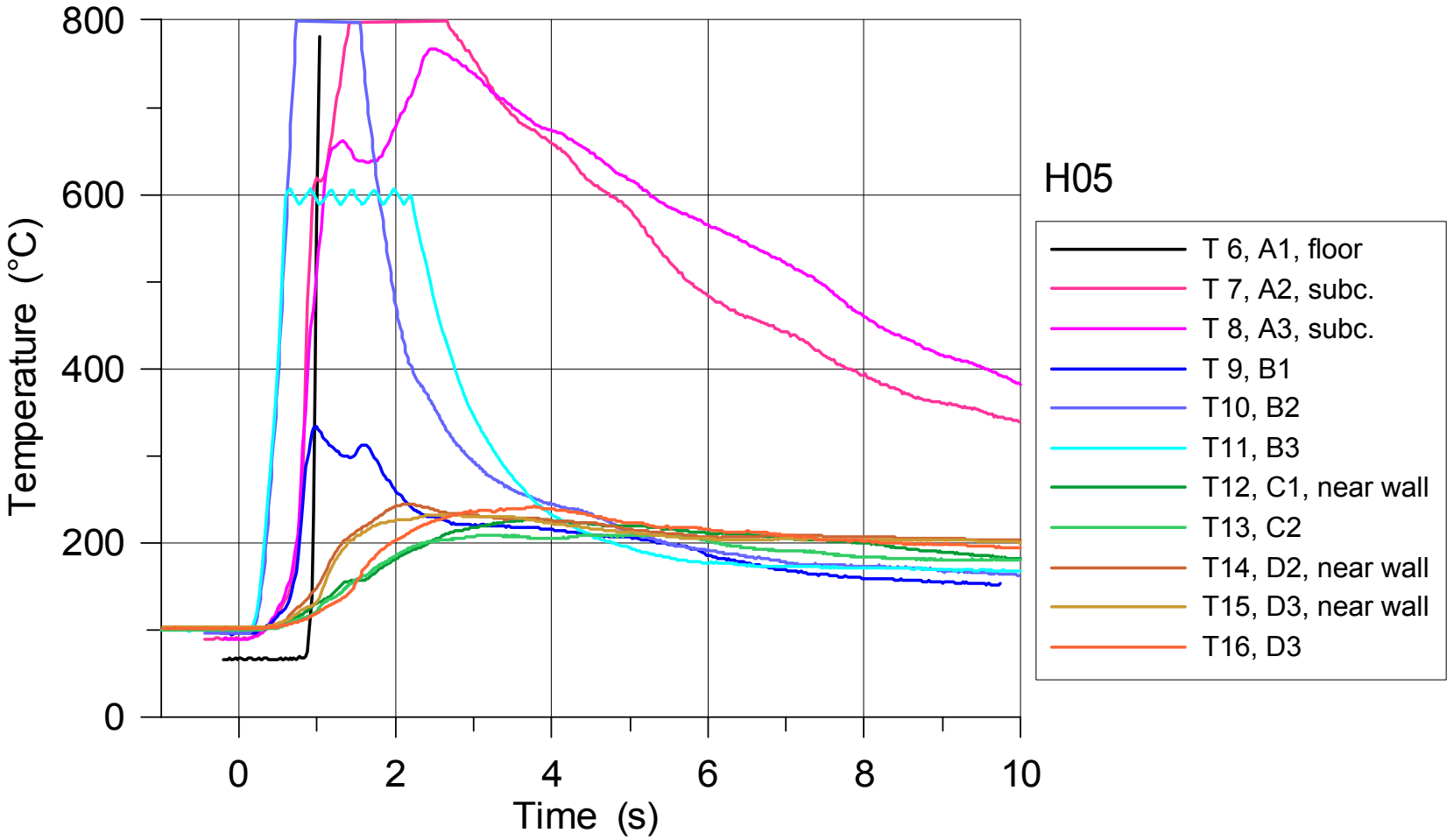

Fig. 44. Gas temperatures in the subcompartment and containment in H05

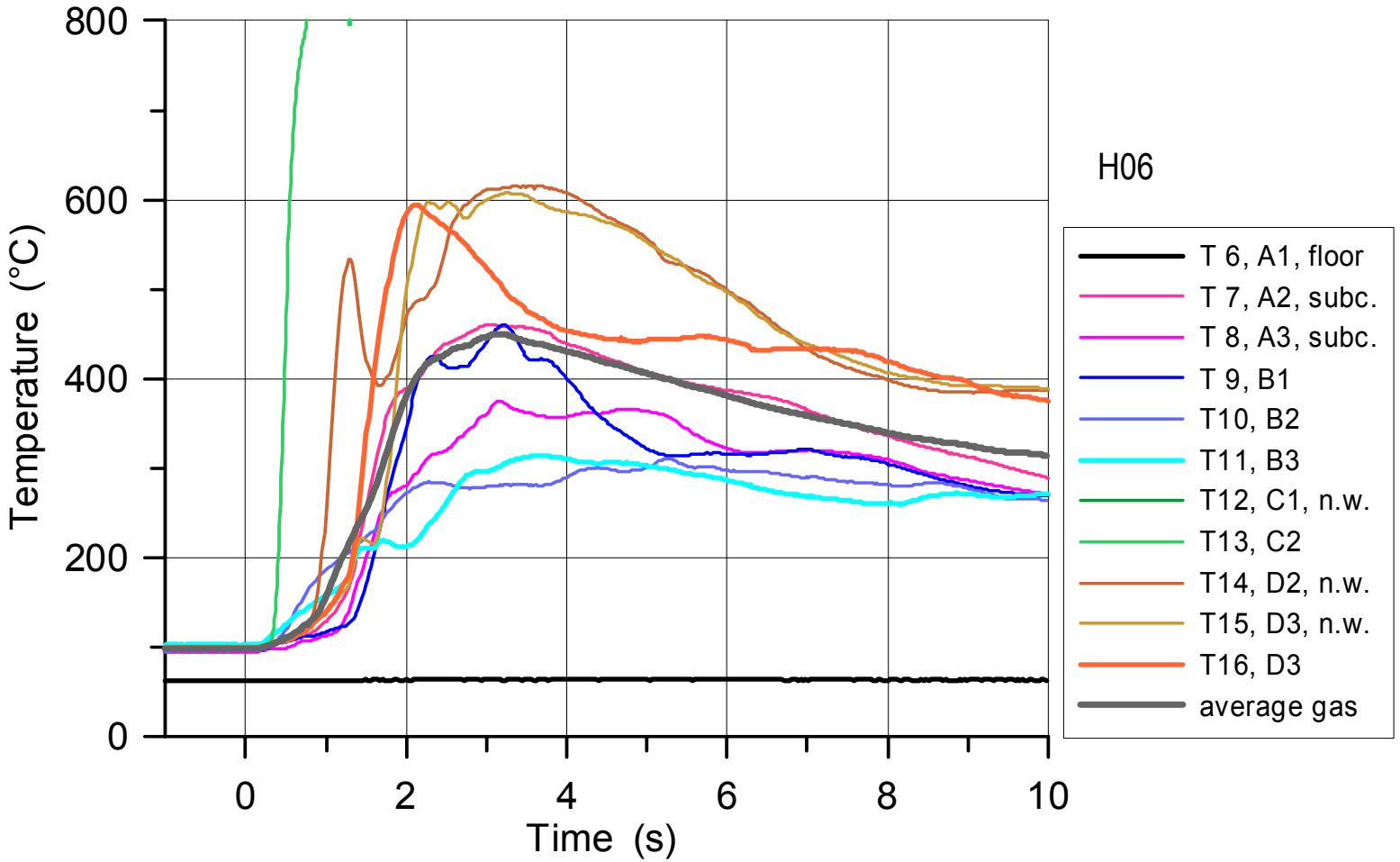

Fig. 45. Gas temperatures in the subcompartment and containment in H06

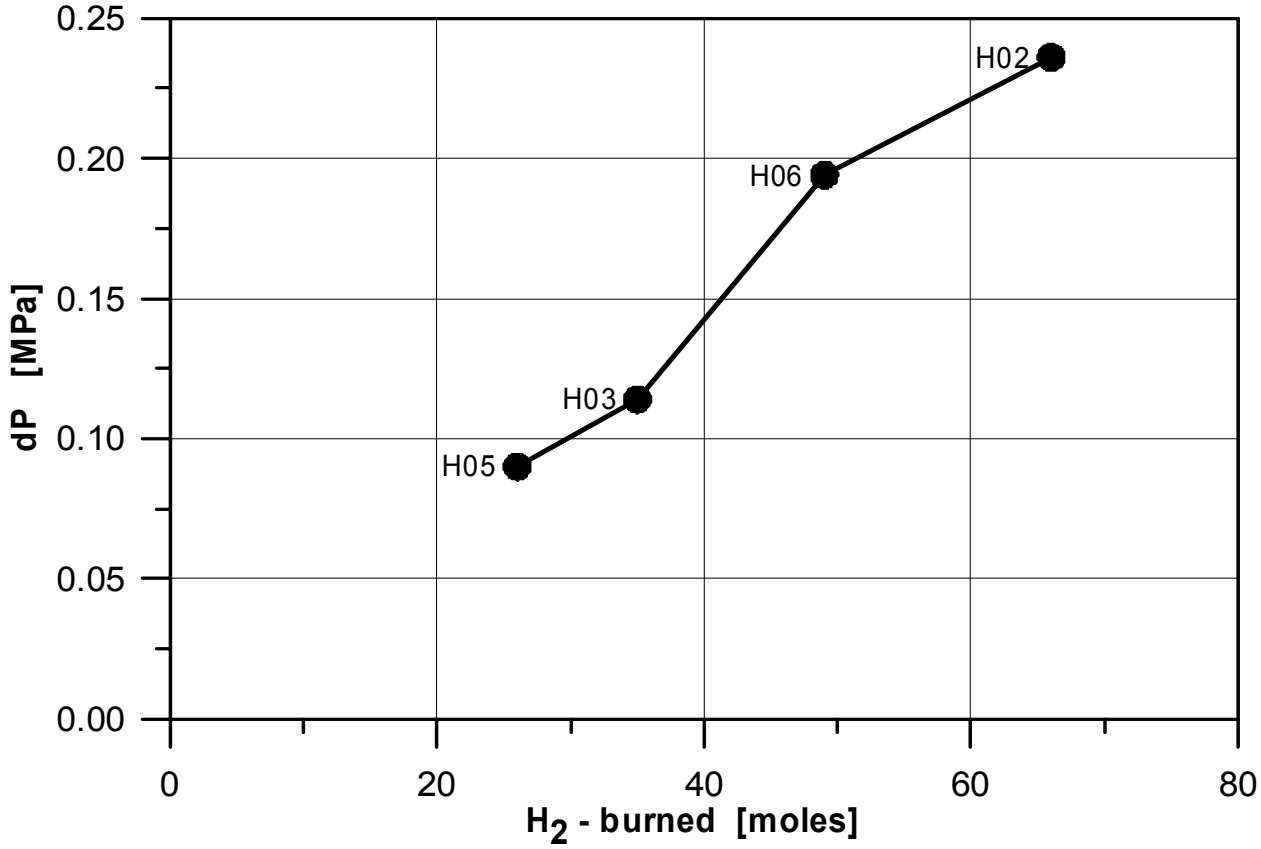

Fig. 46. Burned hydrogen versus pressure rise in the containment

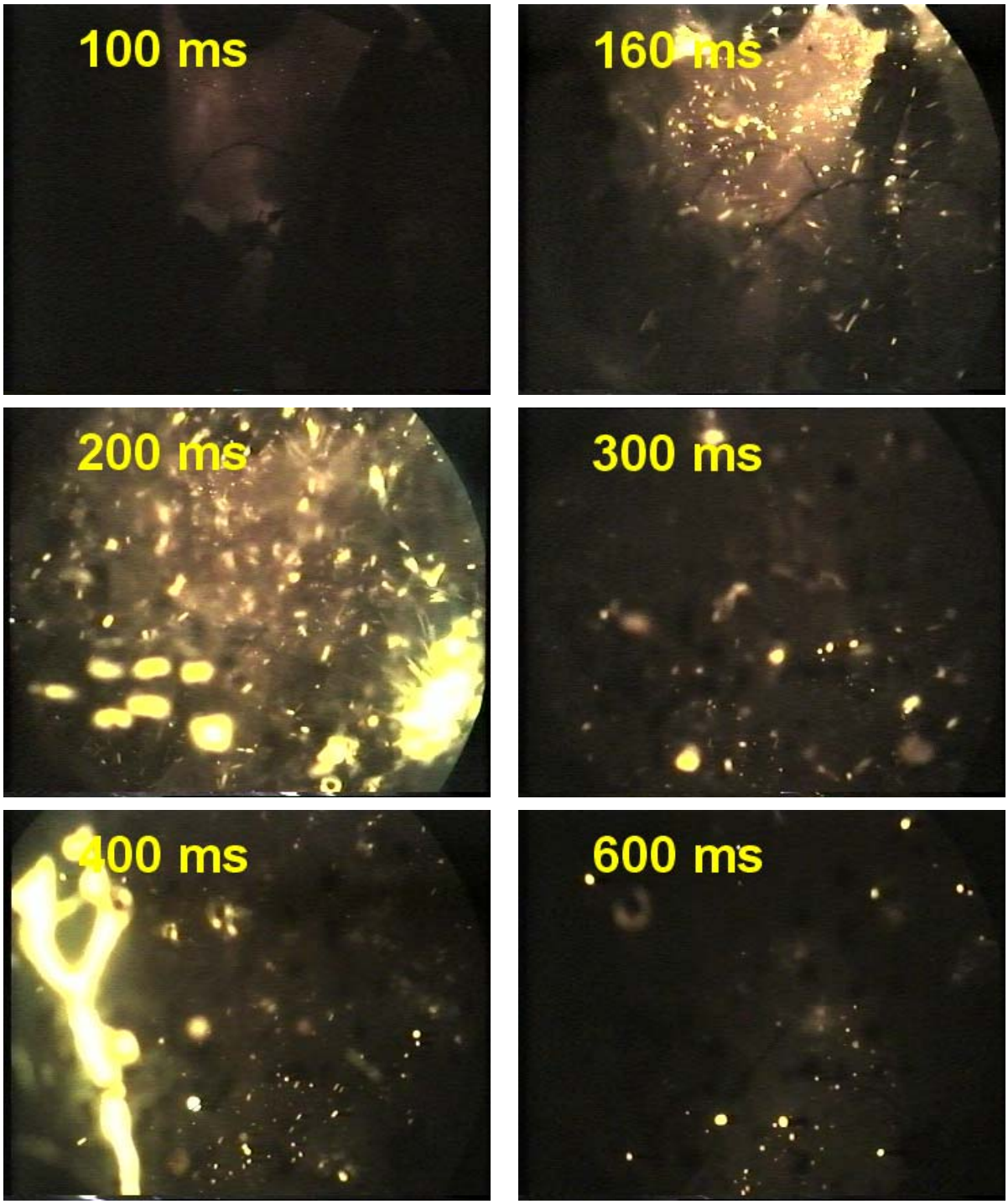

Fig. 47. Video pictures from subcompartment in test H02

(After 600 ms no more melt or flames can be seen)

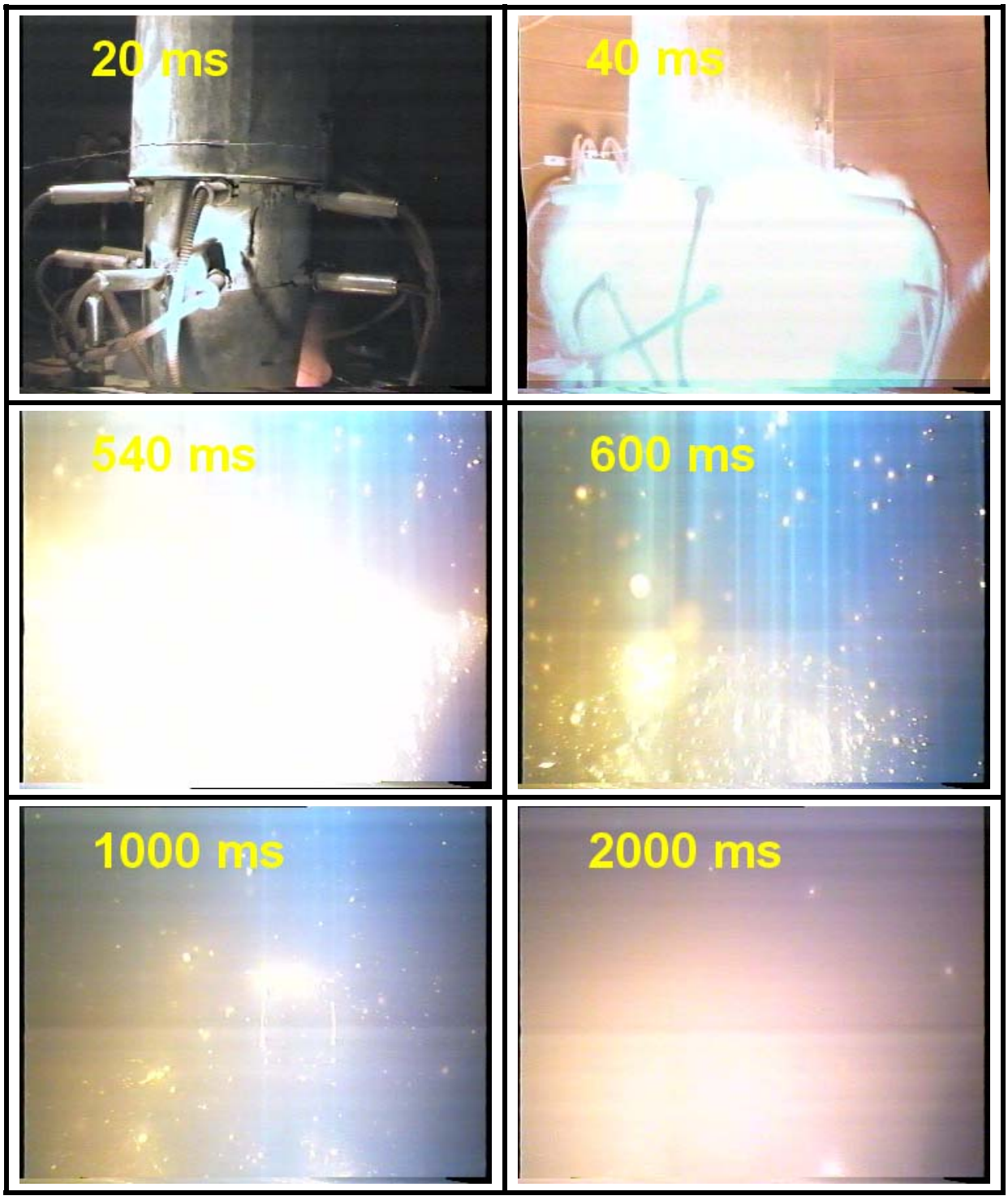

Fig. 48. Video pictures from containment near cavity exit from test H02

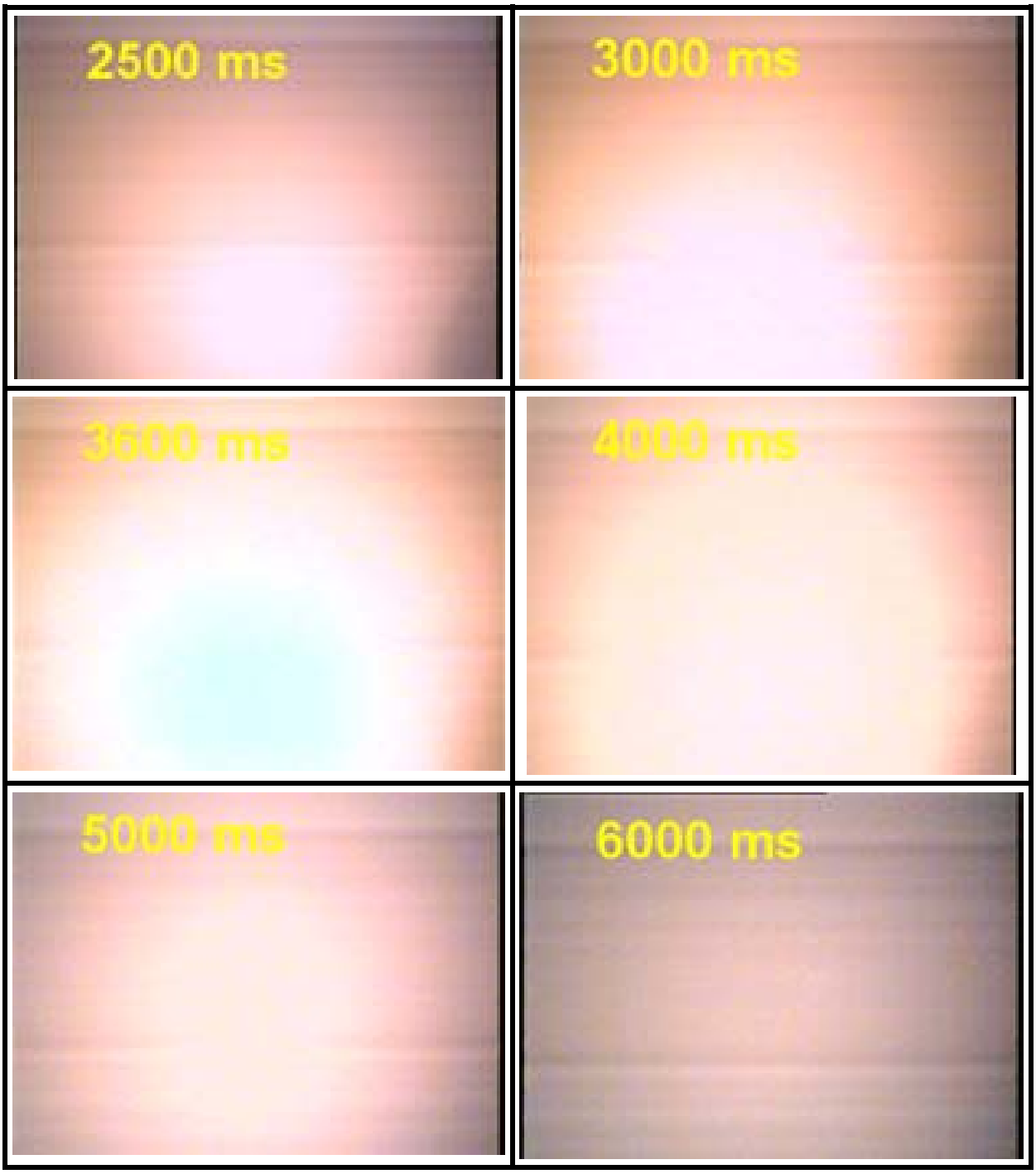

Fig.48. Cont.

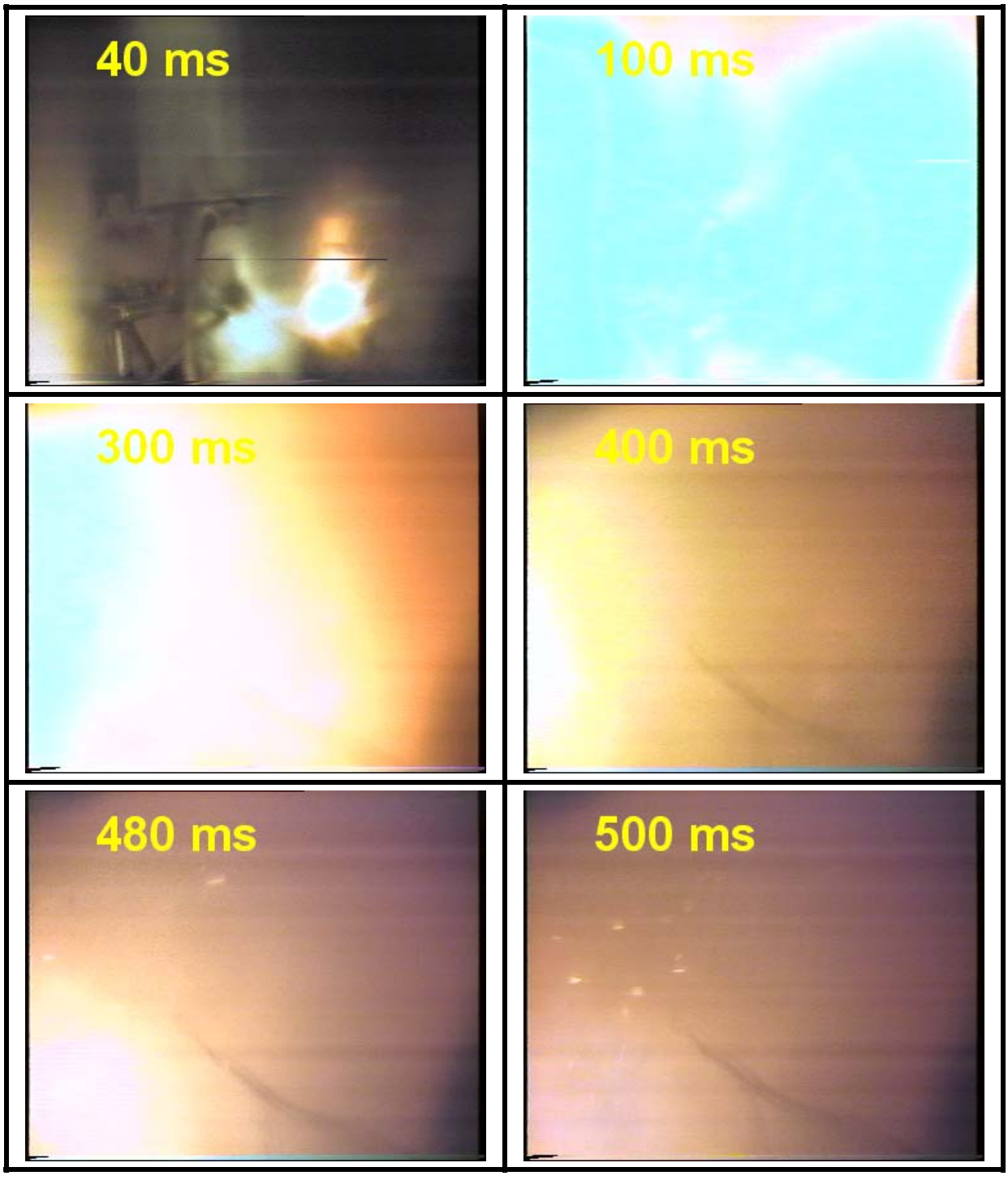

Fig. 49. Video pictures from containment compartment exit from test H03

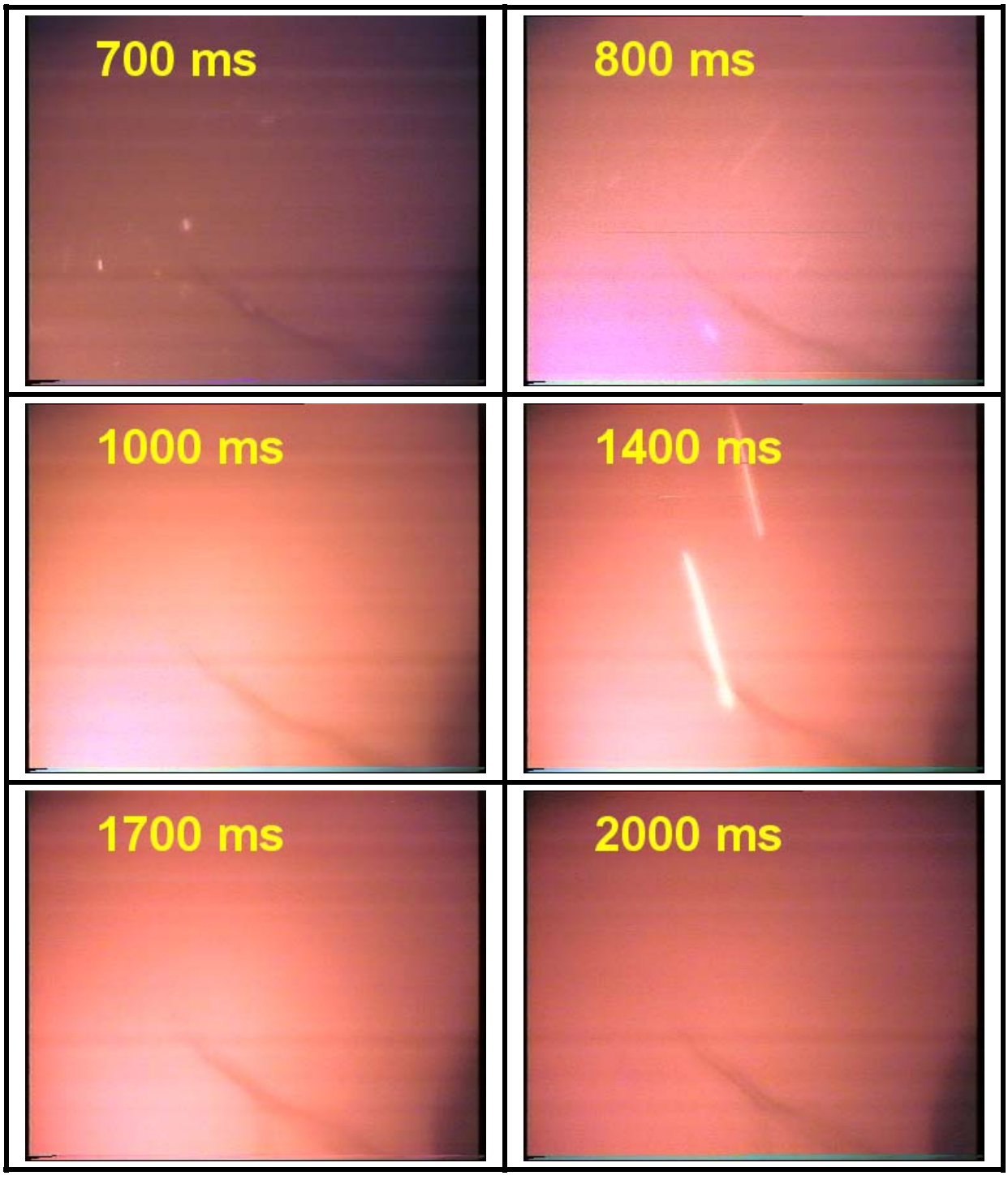

Fig. 49 cont.

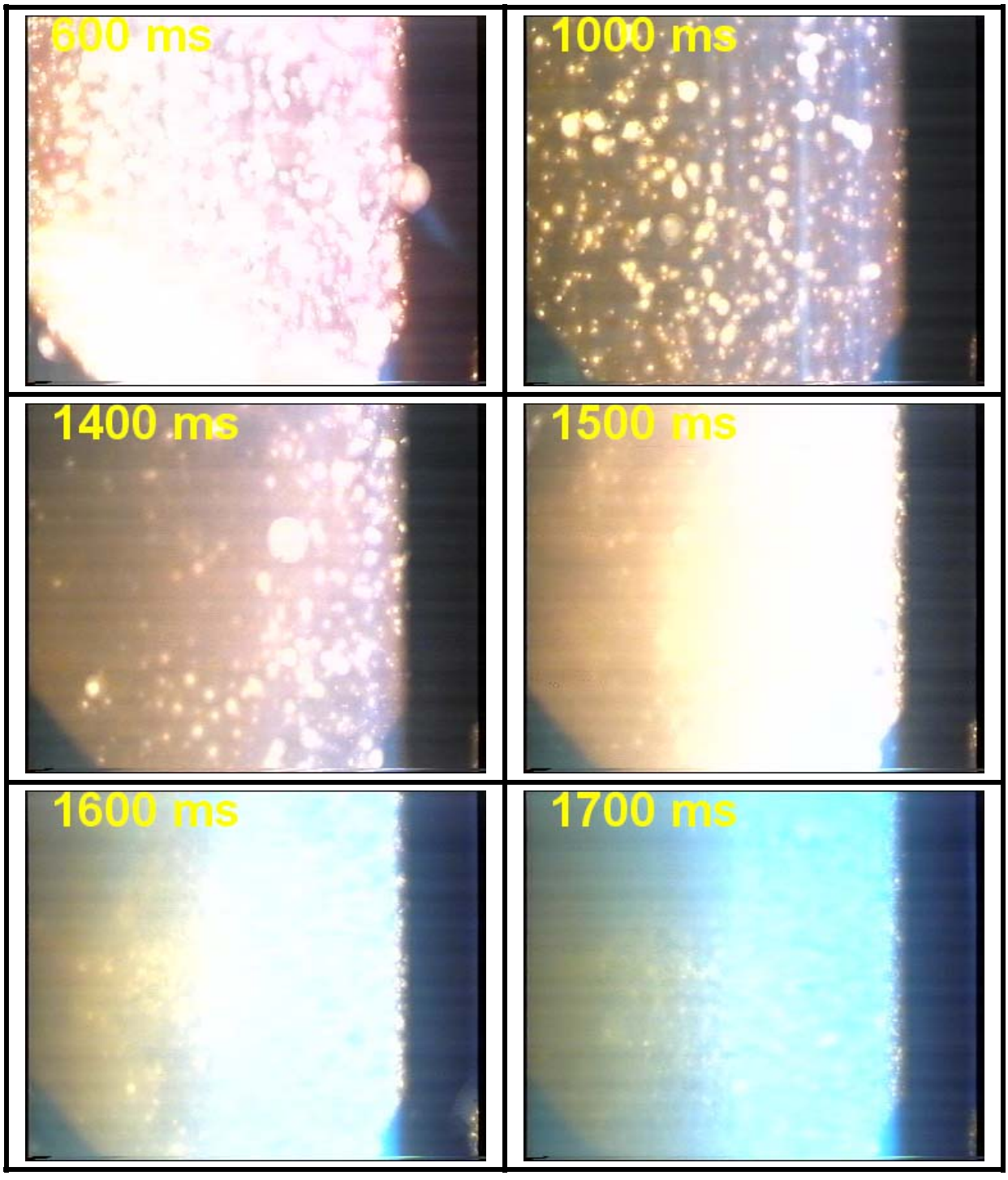

Fig. 50. Video pictures from containment near cavity exit from test H04

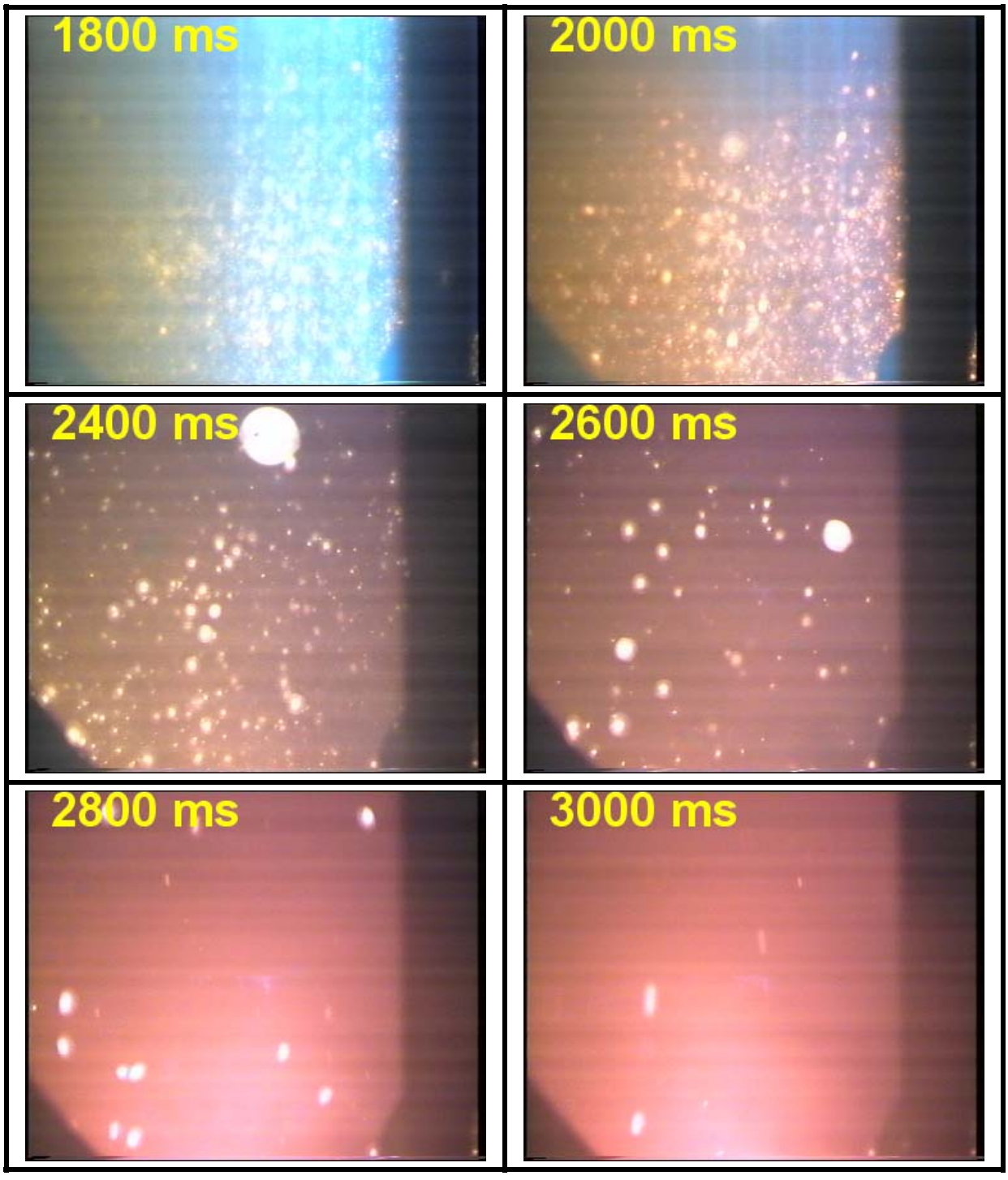

Fig.50. cont.

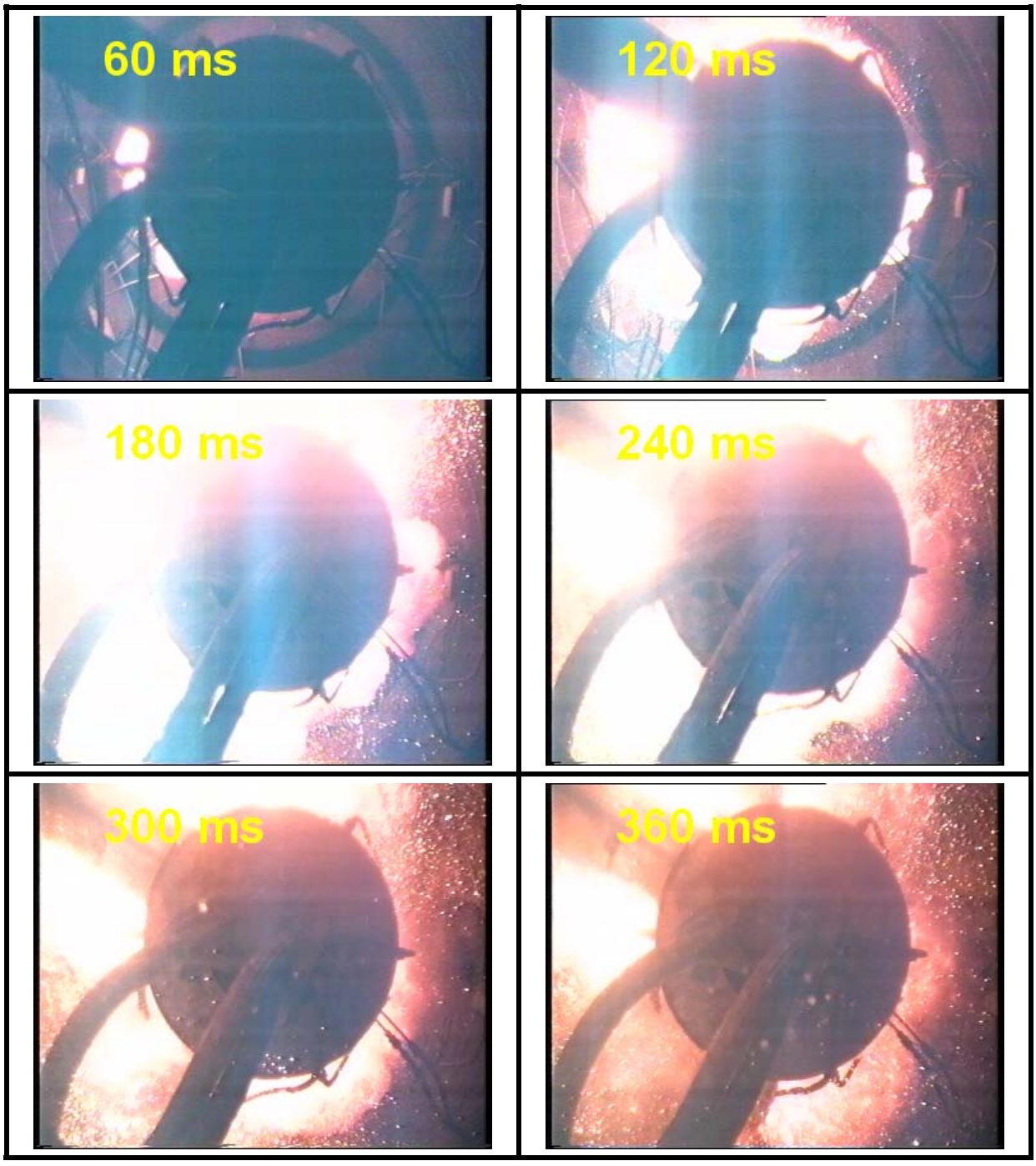

Fig. 51. View from top down to RCS-vessel and cavity exit in test H06

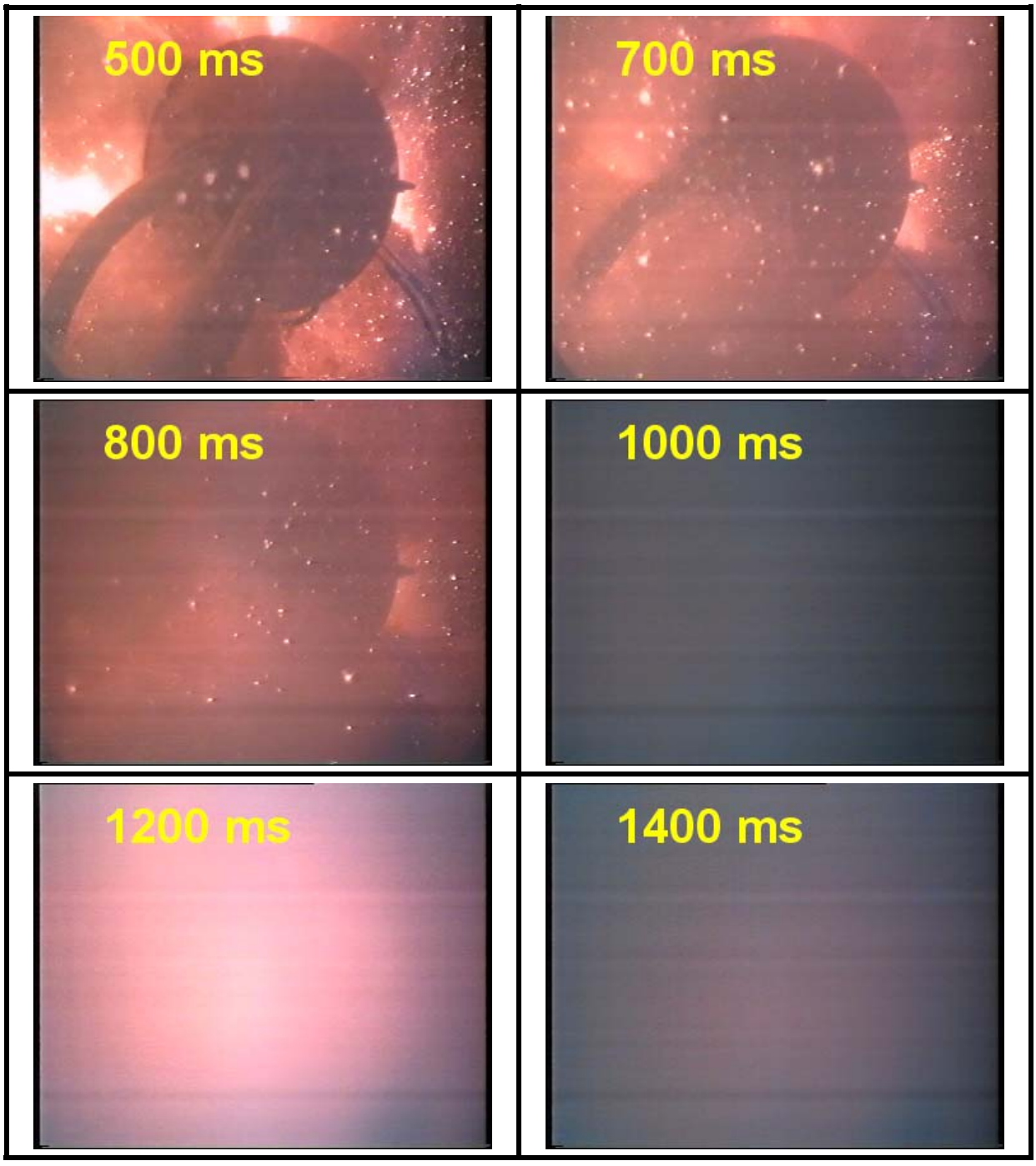

Fig. 51. cont., in times 900 ms < t < 1100 ms it was dark, in 1120 ms < t < 1240 ms a flame was observed

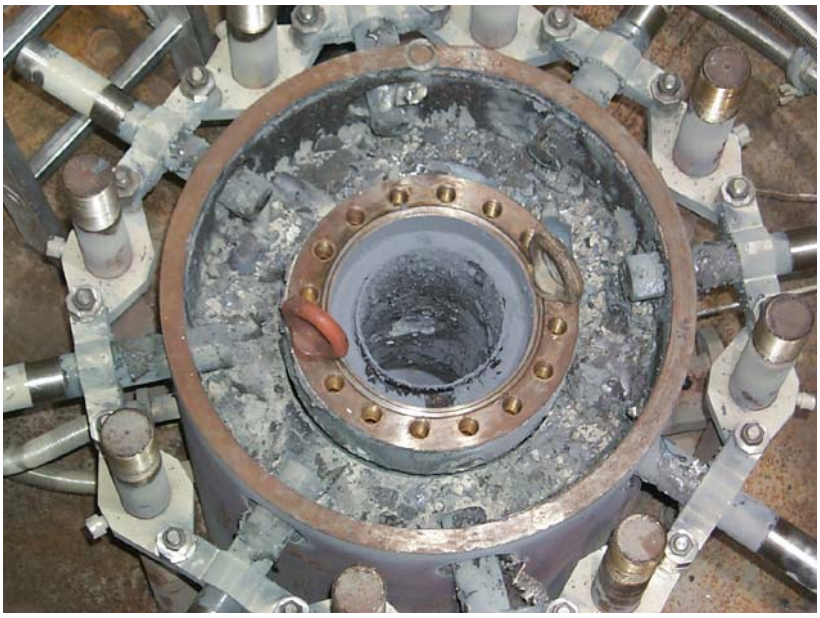

Fig. 52. Post test view of concrete cavity and RPV/crucible

Fig. 53. Post test view of concrete cavity

Fig. 54. Post test view of RPV lower head and hole

Fig. 55. Post test view at cavity exit and subcompartment cover

Fig. 56. Melt particles at containment wall

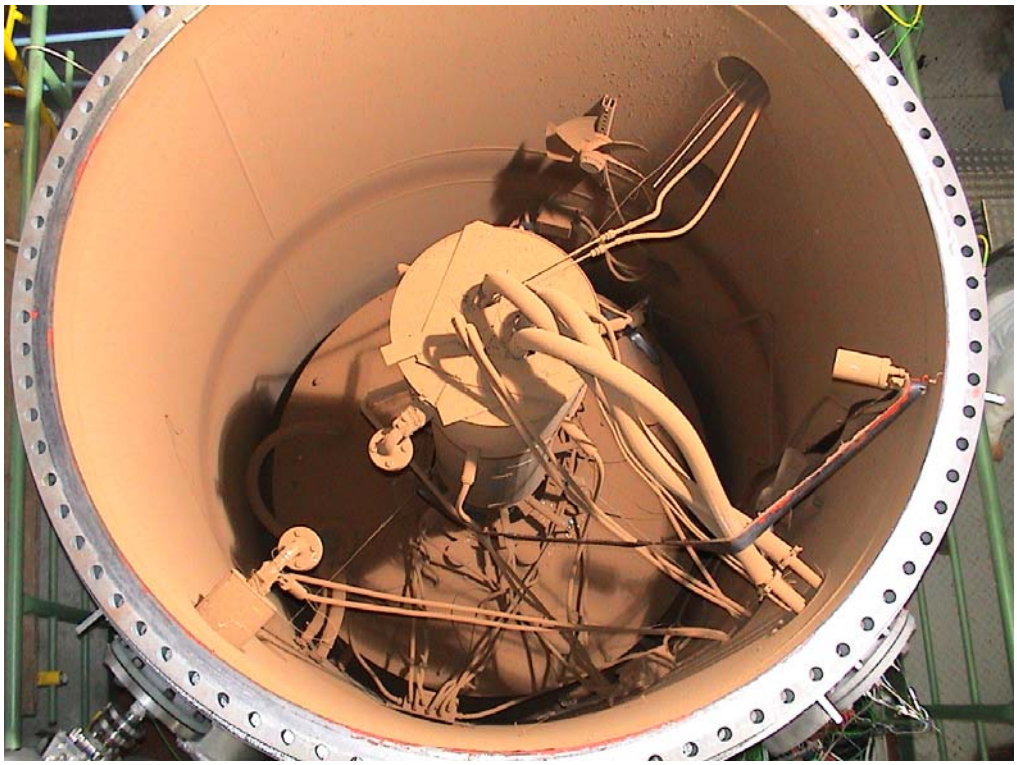

Fig. 57. Post test view into containment, test H04

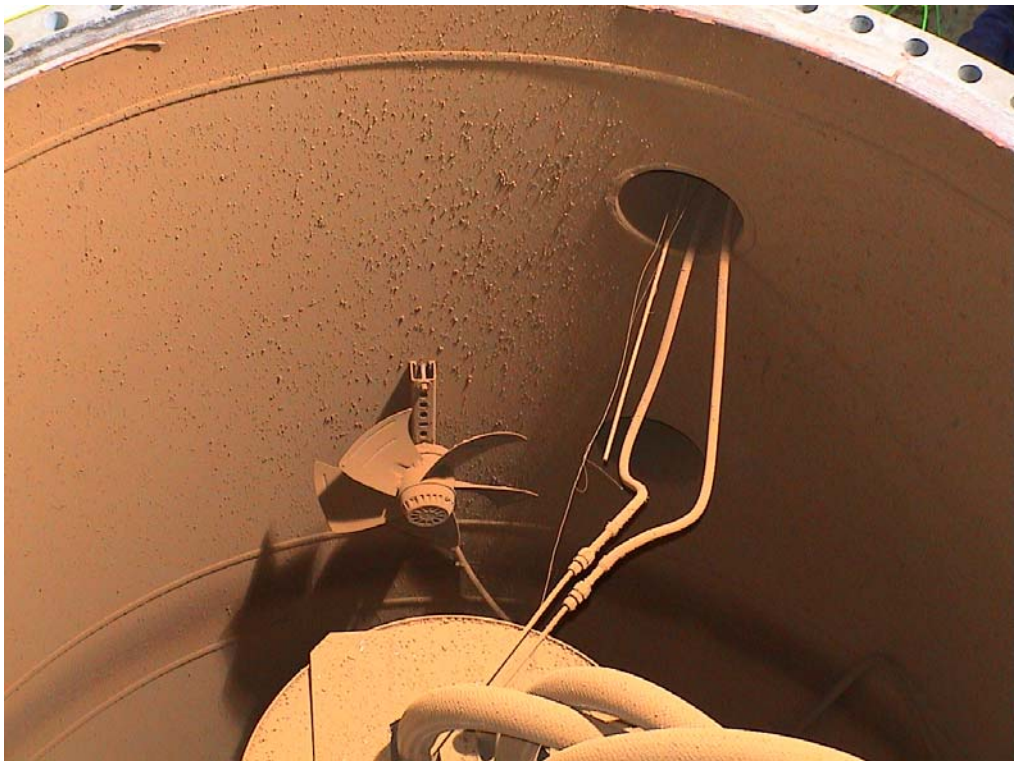

Fig. 58. Post test view into containment, test H04

Fig. 59. Post test view of containment top head, test H04

Fig. 60. Close up of melt debris at containment top head, test H04

7 > d > 5 mm

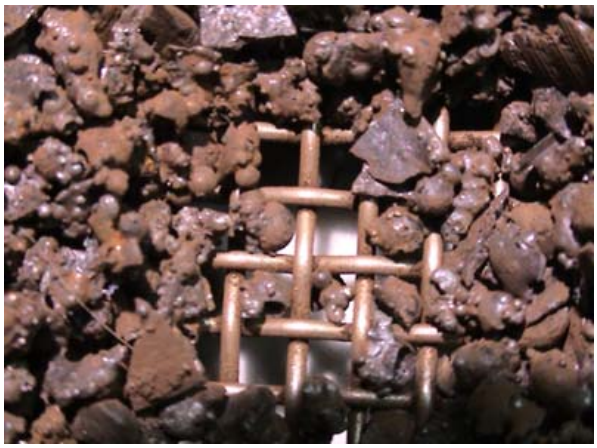

3.55 > d > 2.5

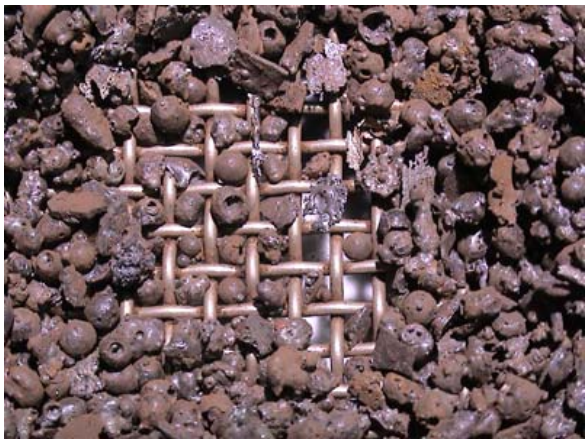

2.5 > d > 1.8

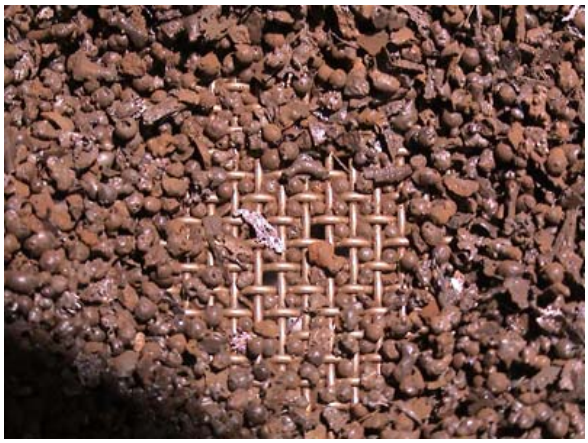

1.8 > d > 0.90

0.63 > d > 0.45

0.315 > d > 0.224

Fig. 61. Particle size fractions

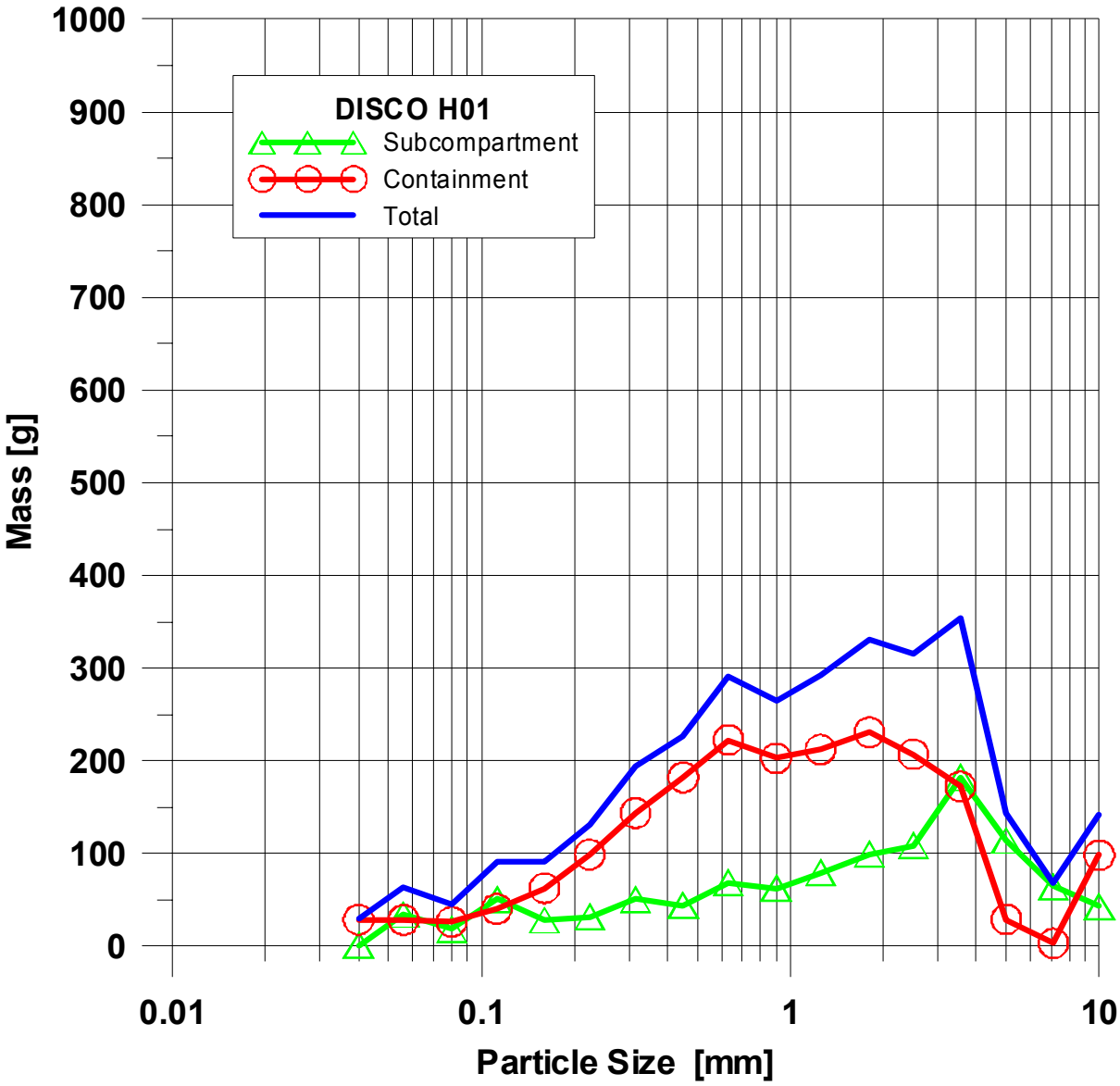

Fig. 62. Particle size distribution of debris in H01

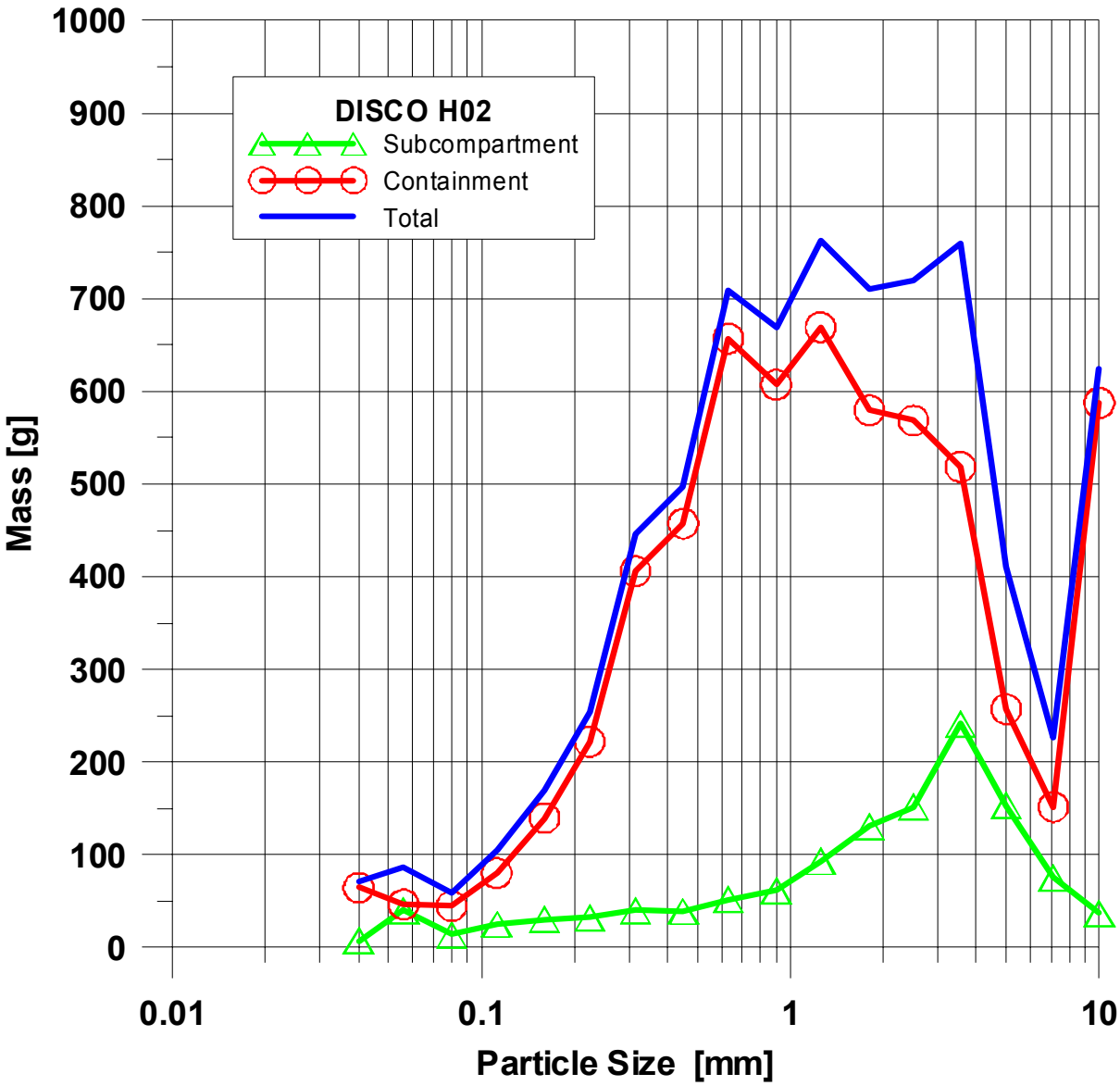

Fig. 63. Particle size distribution of debris in H02

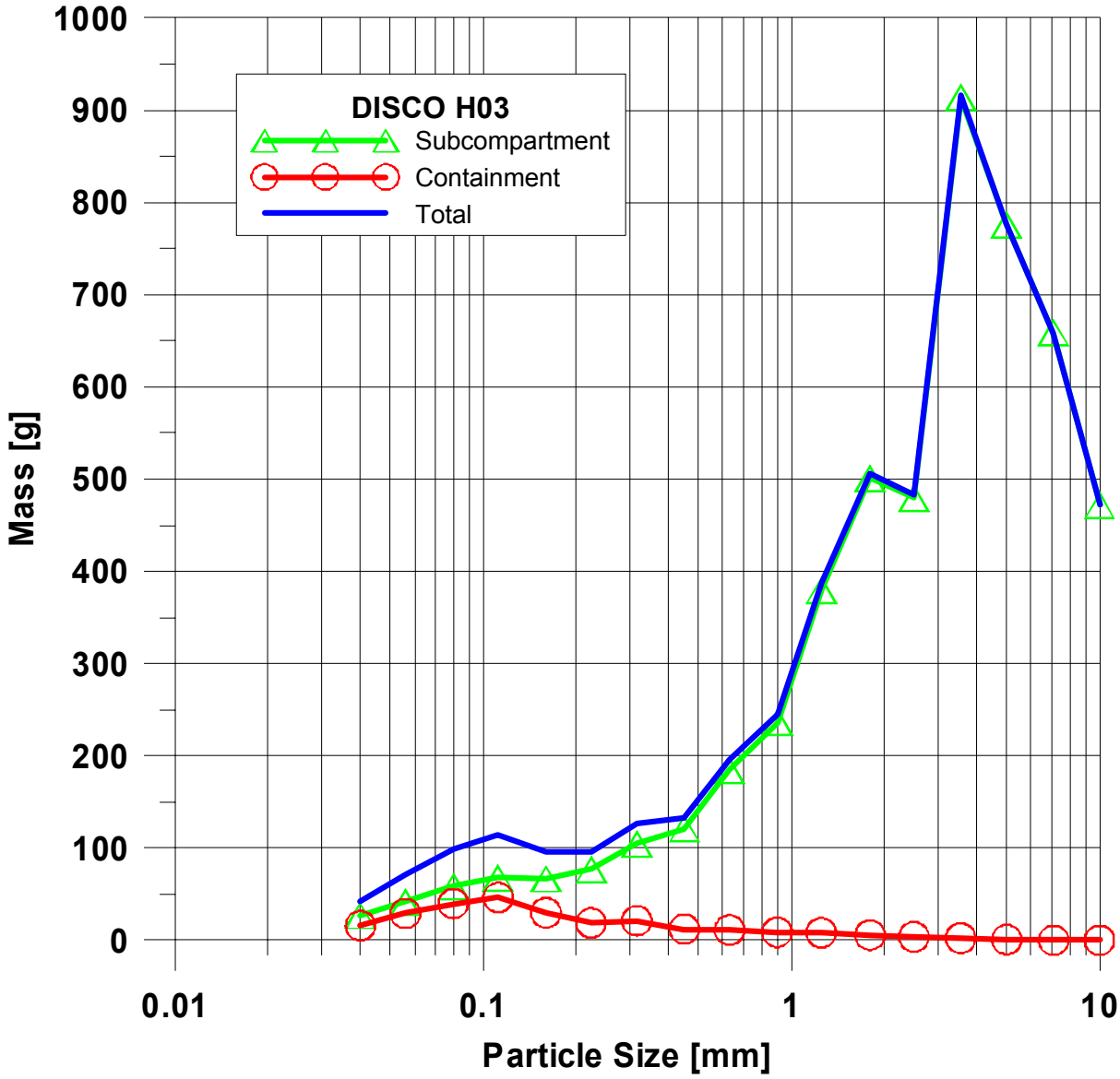

Fig. 64. Particle size distribution of debris in H03

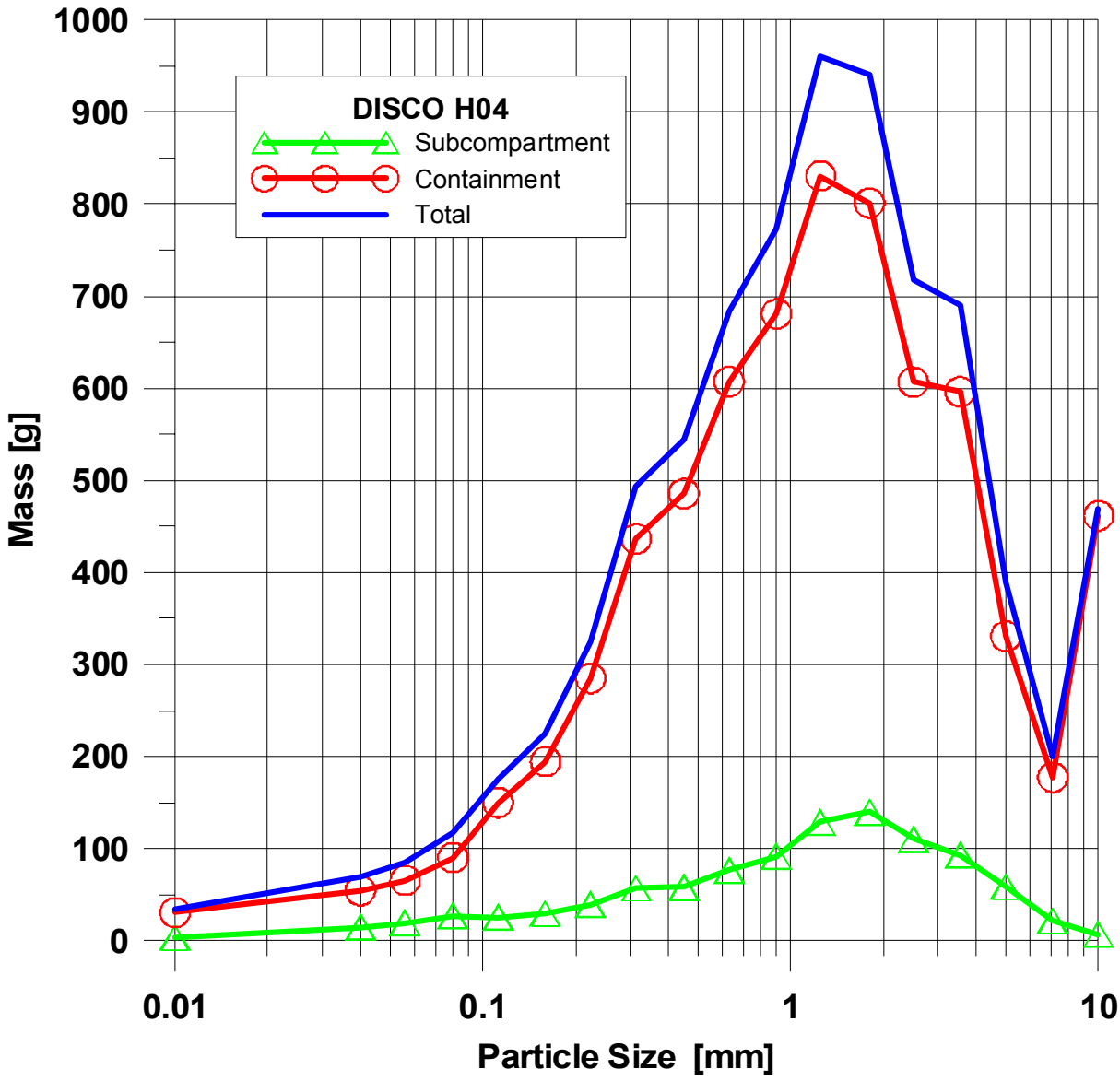

Fig. 65. Particle size distribution of debris in H04

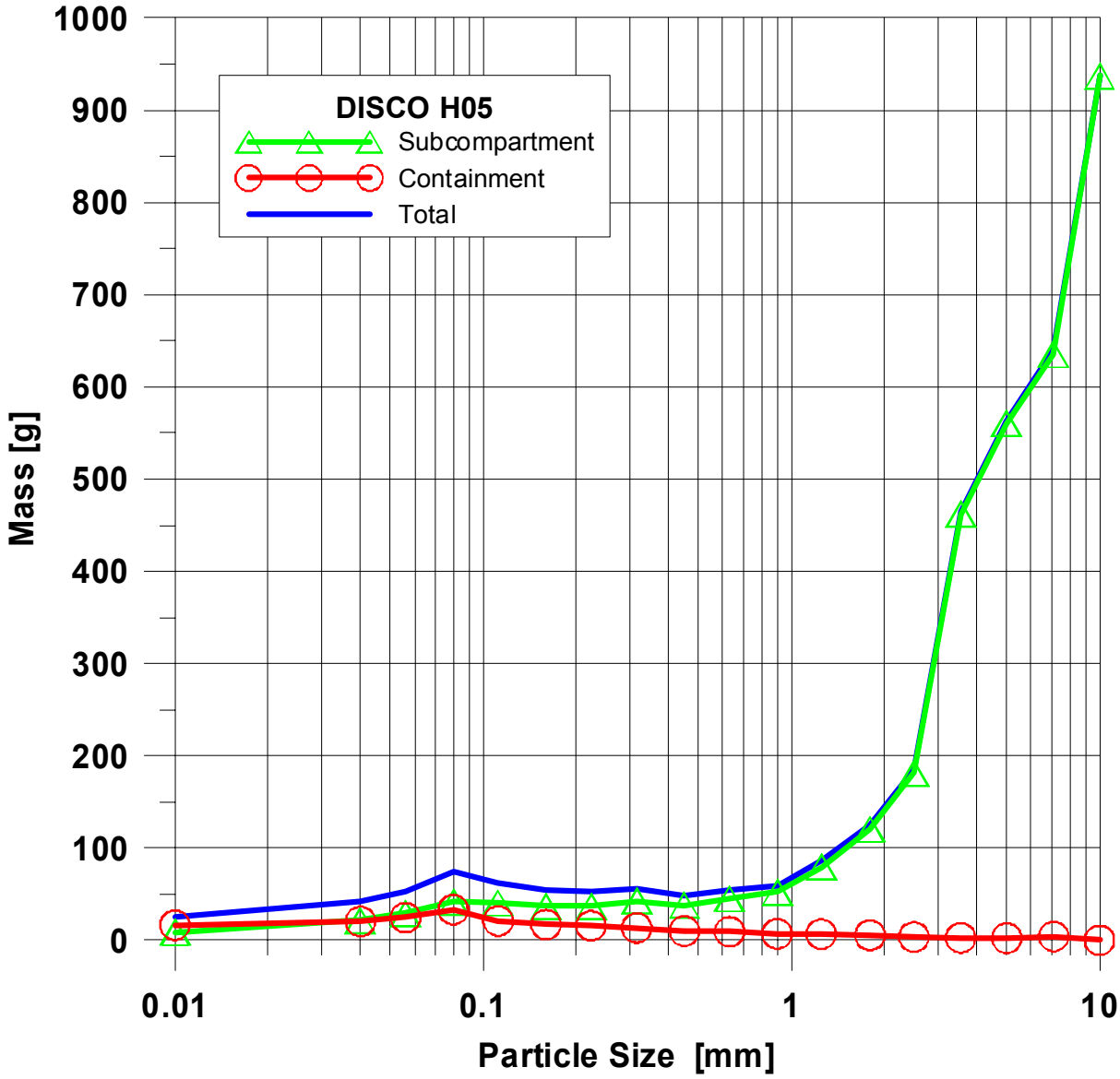

Fig. 66. Particle size distribution of debris in H05

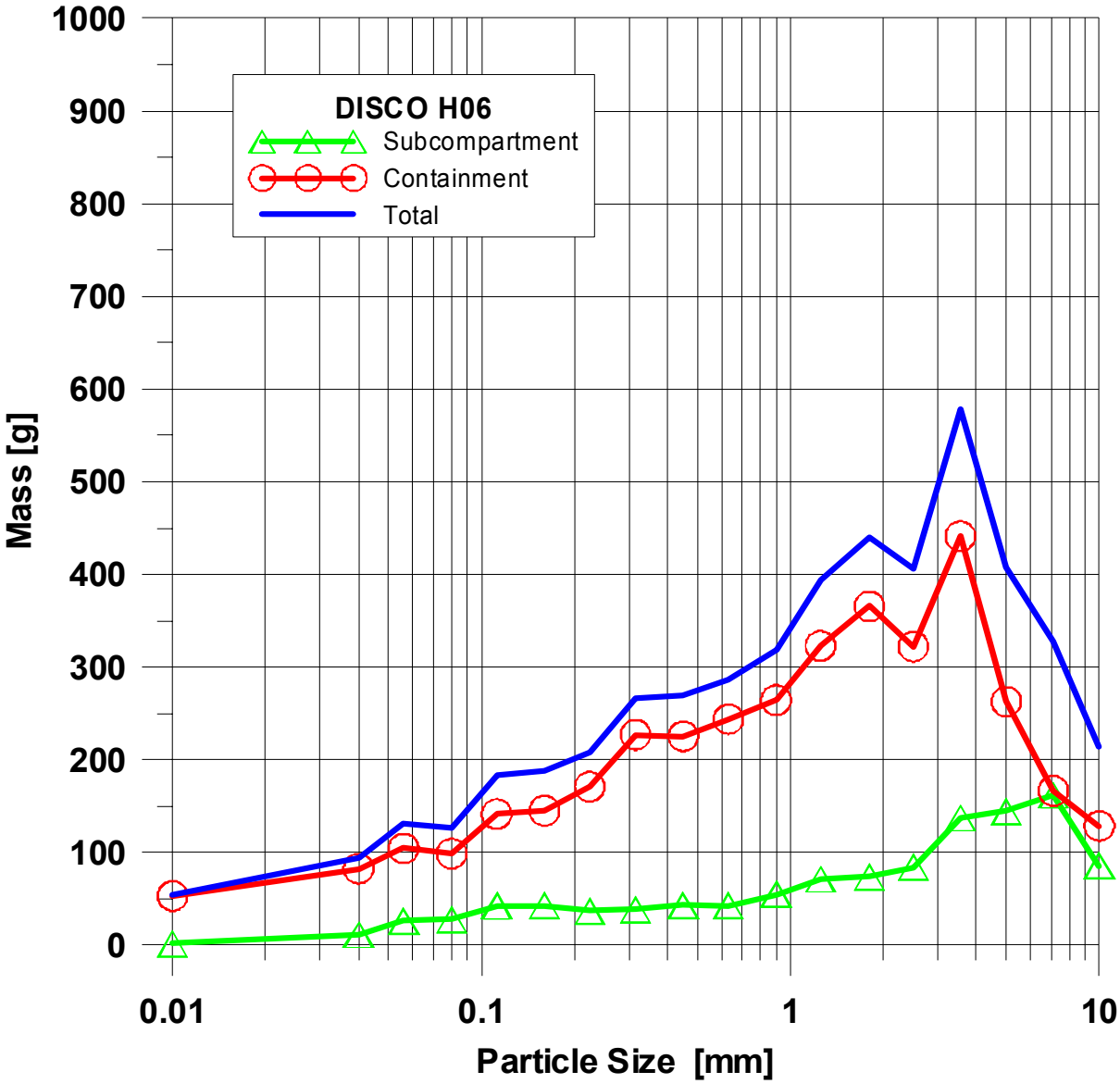

Fig. 67. Particle size distribution of debris in H06

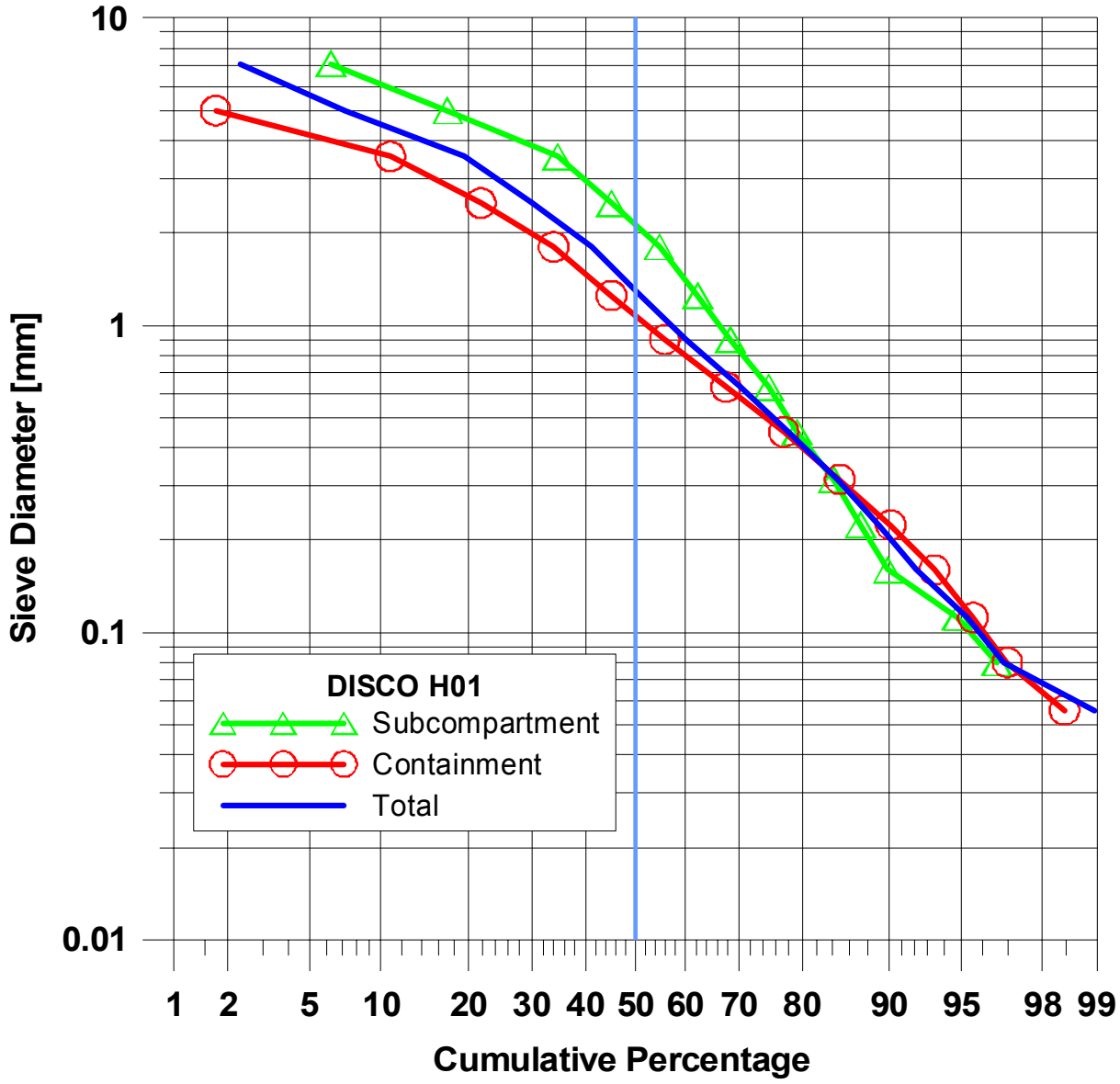

Fig. 68. Cumulative particle size distribution of debris in H01

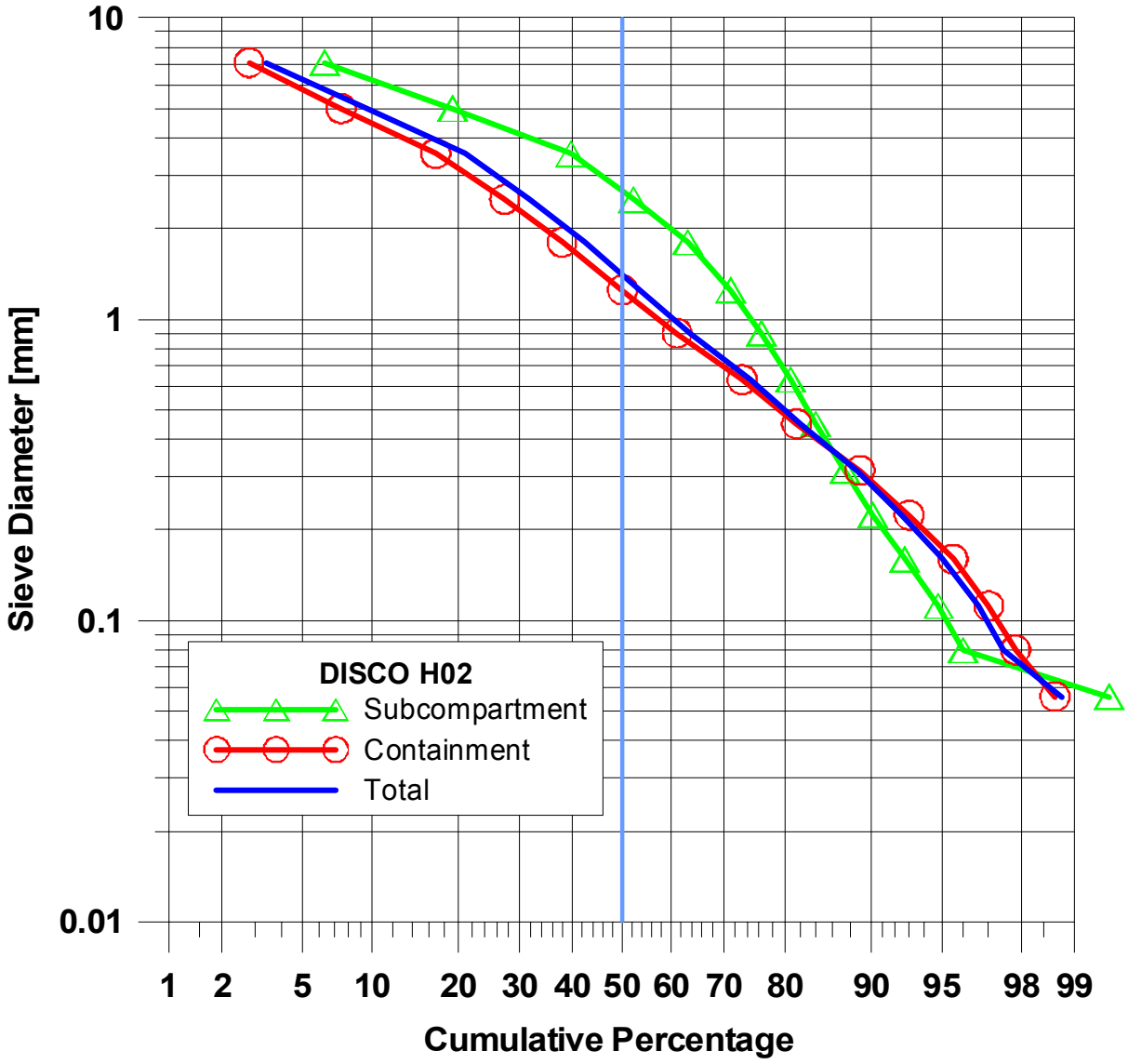

Fig. 69. Cumulative particle size distribution of debris in H02

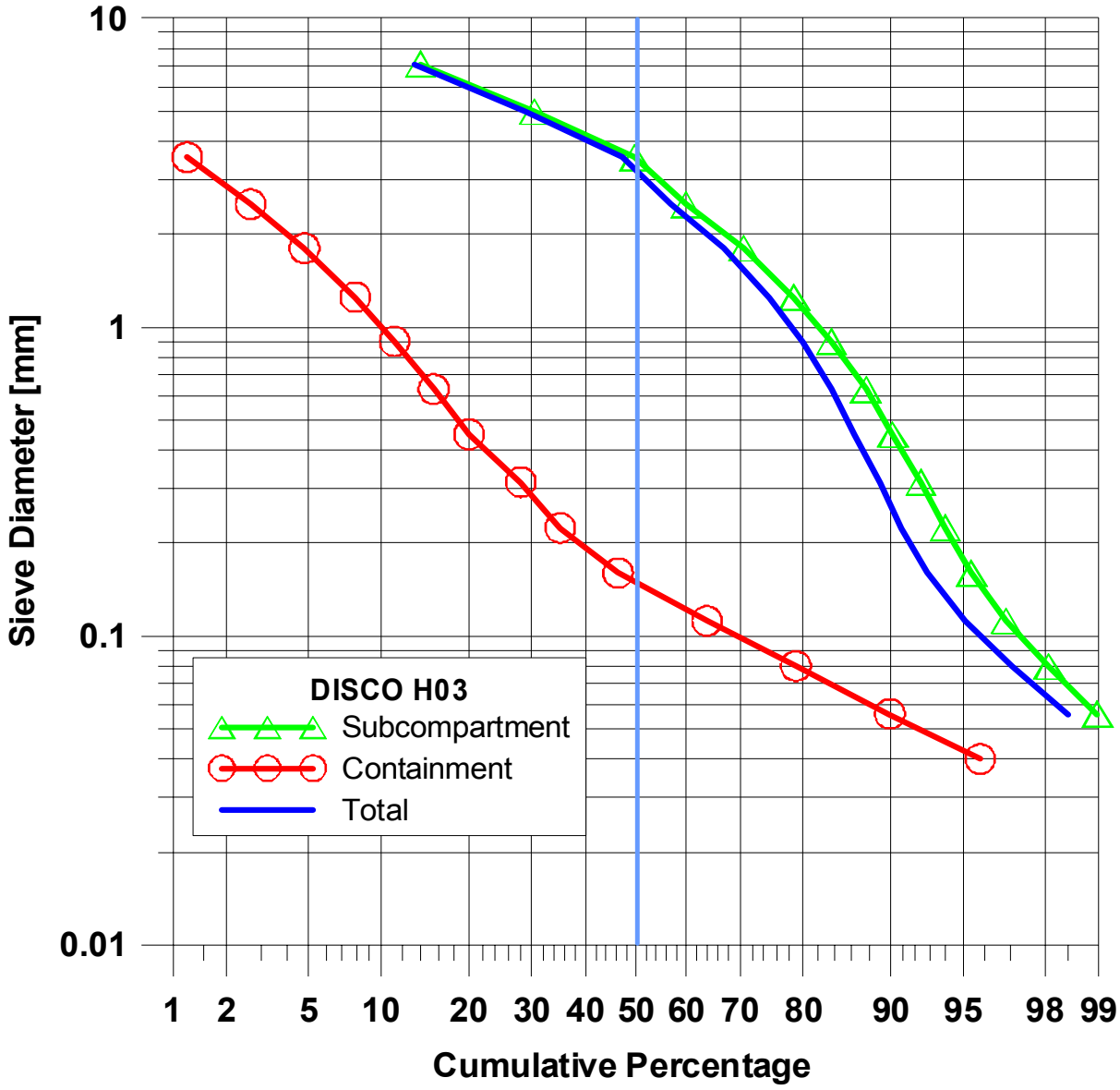

Fig. 70. Cumulative particle size distribution of debris in H03

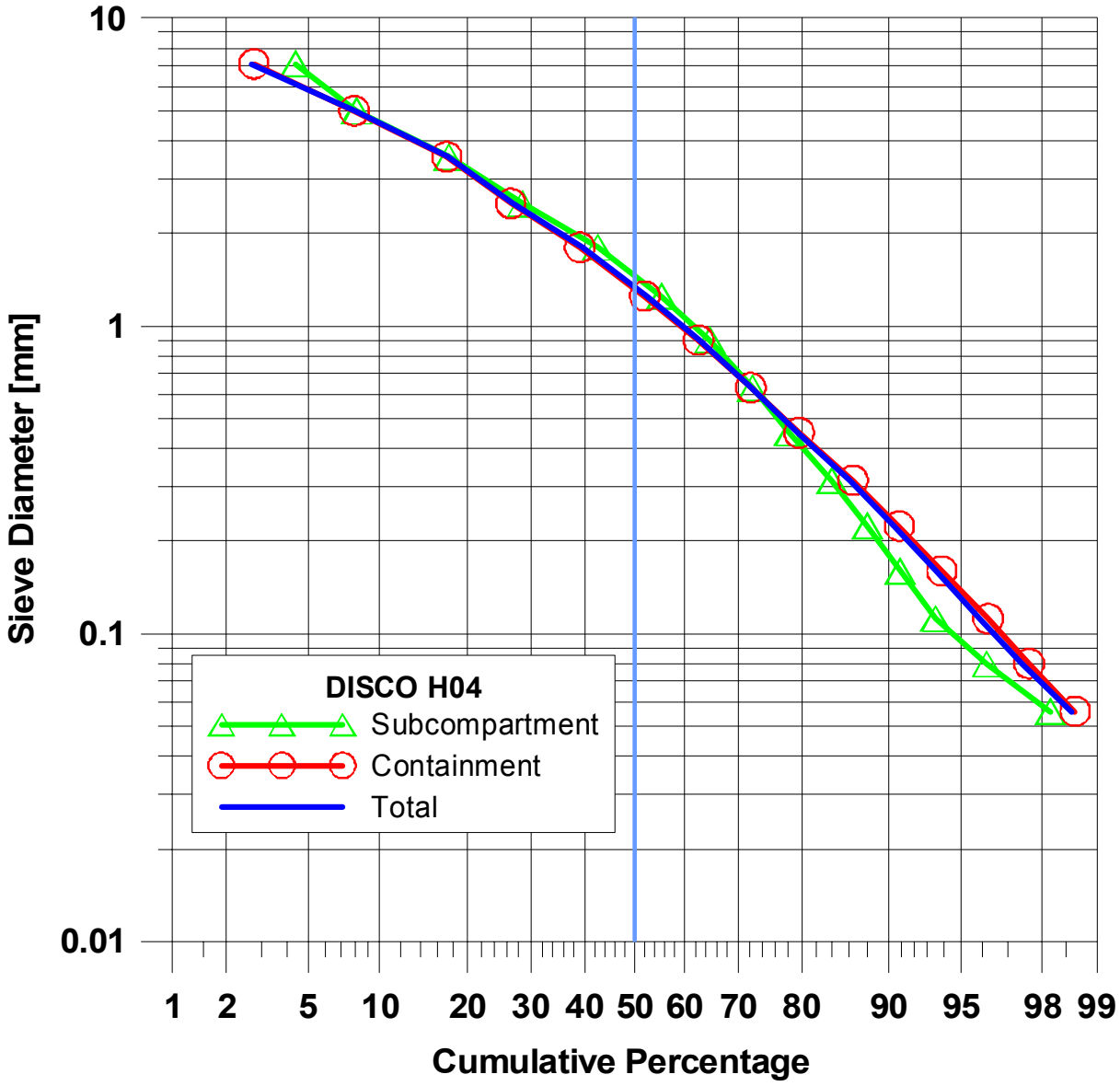

Fig. 71. Cumulative particle size distribution of debris in H04

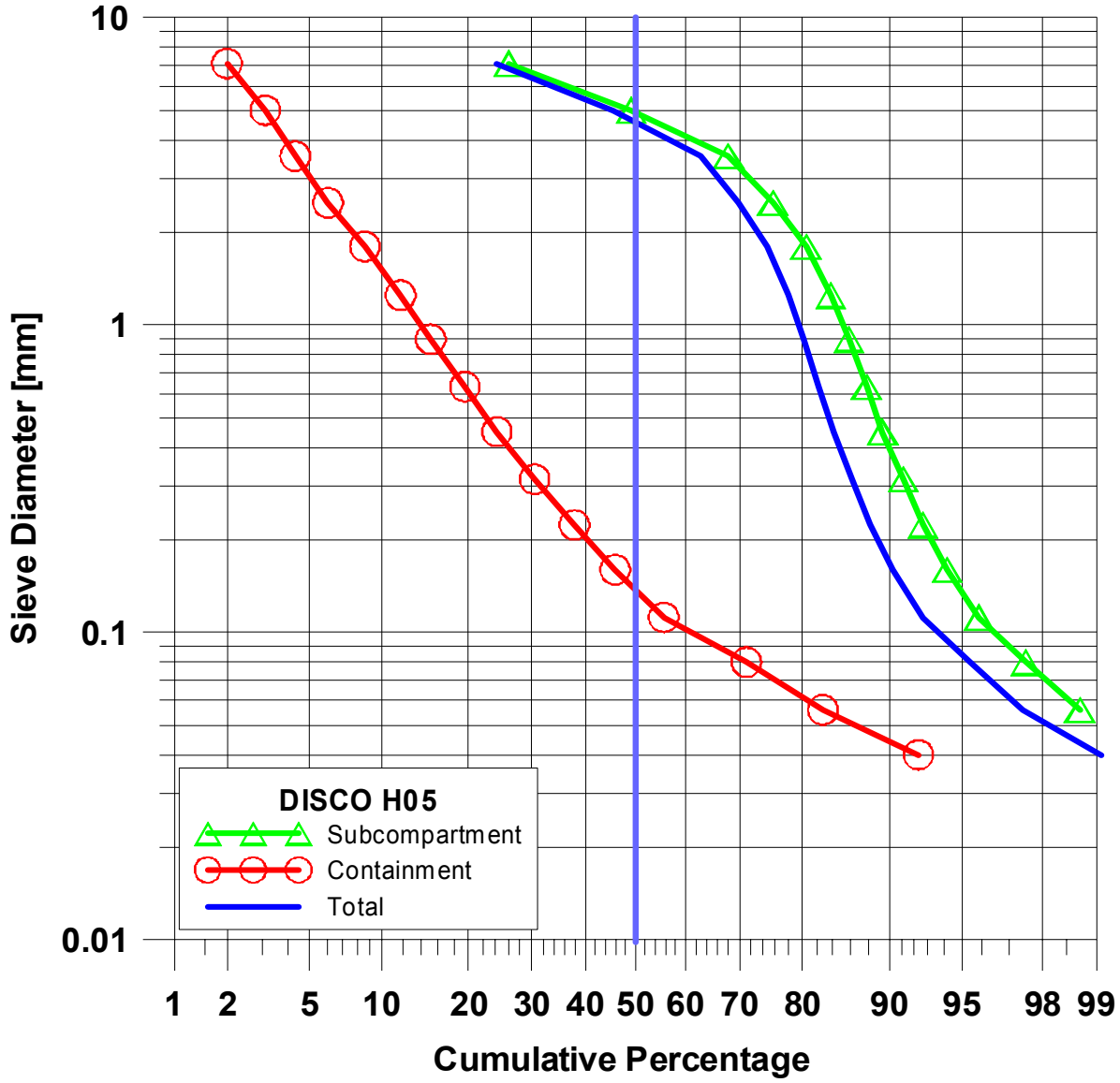

Fig. 72. Cumulative particle size distribution of debris in H05

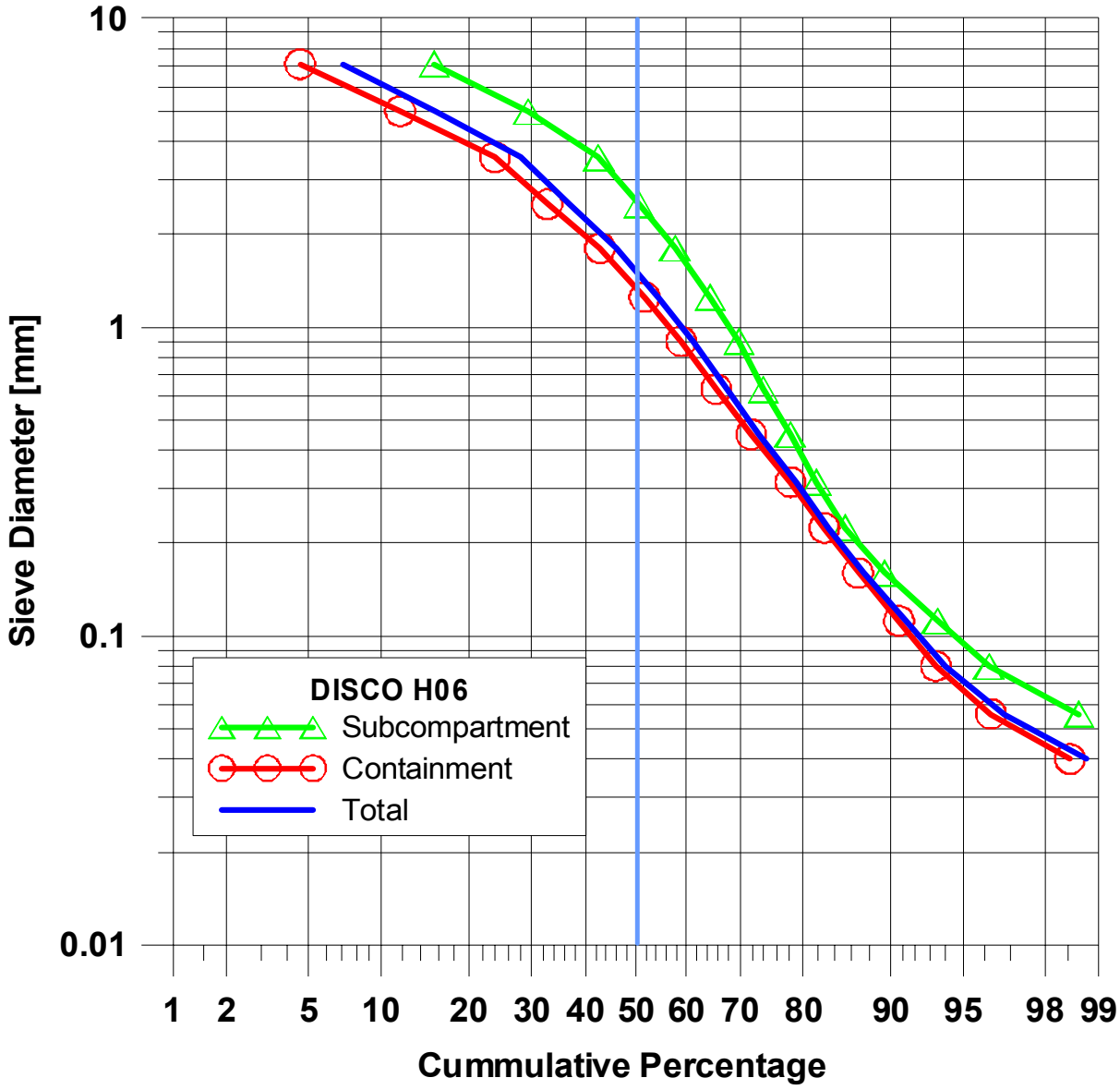

Fig. 73. Cumulative particle size distribution of debris in H06

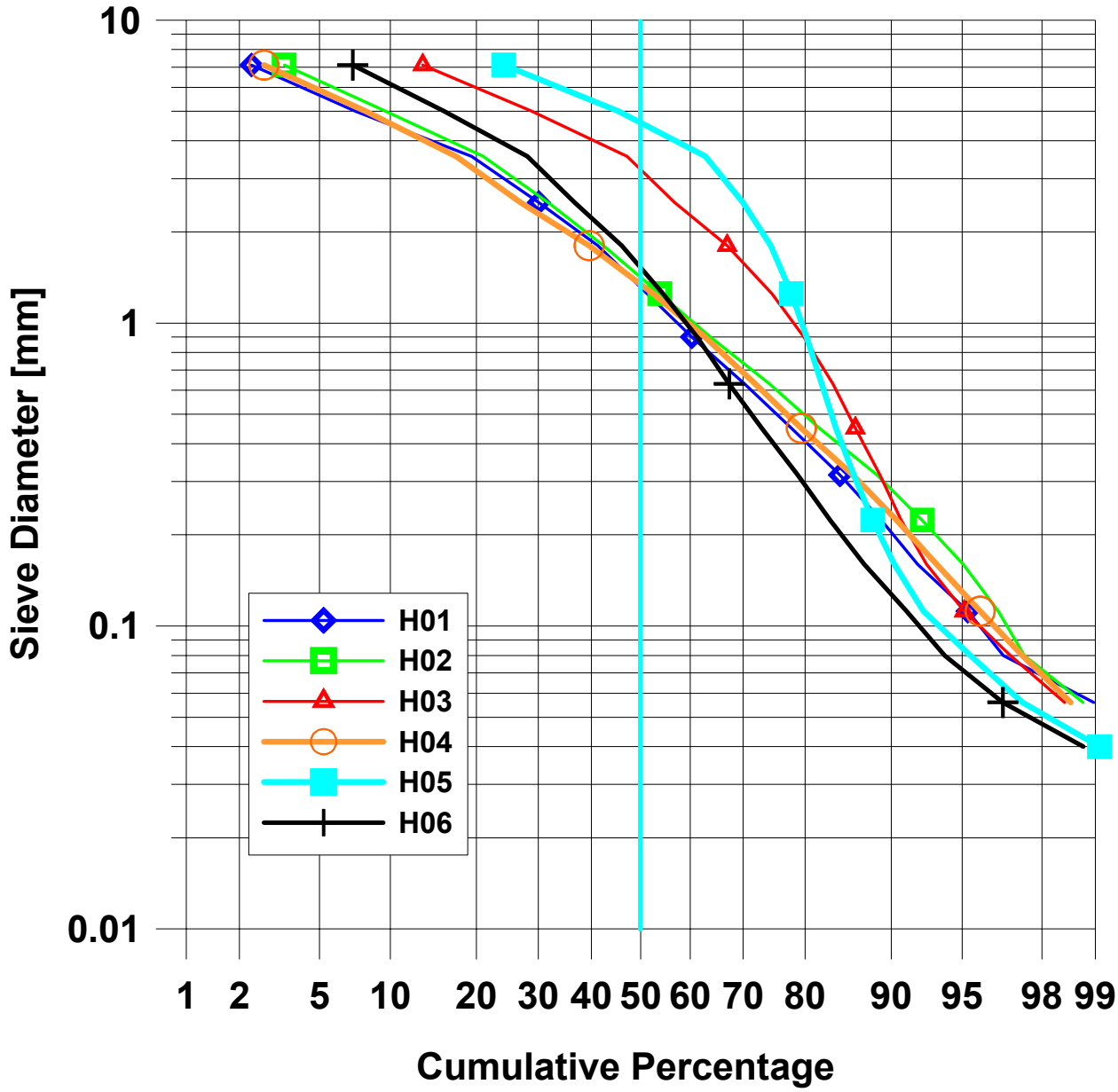

Fig. 74. Comparison of cumulative particle size distribution of debris

4 Conclusions

Six experiments were performed in the DISCO-H test facility to investigate DCH phenomena in a scaled geometry of a European reactor with a tight cavity. The test program is a continuation of a program conducted at the Sandia National Laboratories with different reactor geometries.

Because the system pressure at core melt accidents will be low in German plants, the experiments were run at RPV failure pressures below 22 bars. The conditions were chosen as close as possible to anticipated conditions during a severe accident. The melt was part metal part oxide, however at a lower temperature, and the atmosphere in the containment was air, steam and some hydrogen at elevated temperature and pressure. To determine the contribution of hydrogen combustion one test was performed with nitrogen and air only. All breaches were holes at the center of the bottom head, which lead to higher melt dispersal, but may be less likely than breaches at the side of the lower head.

The main results are the final location of the melt debris, the particle size distribution and the pressure histories in the cavity and the containment. The extrapolation of the experimental results to the prototypical case is done by applying a CFD code, that contains specific models to describe all fluid dynamic, thermal and chemical processes in sufficient detail [Wil02]. The models are validated by comparing the experimental data with code results.

The main conclusions from the experiments are summarized below.

1. The largest melt fraction that was dispersed out of the cavity was found in the experiment without steam (74%). The reason is probably the lower back pressure in the cavity and the higher density of nitrogen versus steam and hydrogen. (H04).

2. When the reactor cavity has no direct exit to the containment, more melt remains in the reactor pit (>50%) and only 2% reaches the containment. All the rest is trapped in the subcompartment (H03 and H05).

3. A smaller cross section of the hole leads to less dispersion (at the same failure pressure, H05 vs. H03).

4. Higher failure pressure (H06) only partly compensates the smaller hole in respect to melt dispersed from the cavity (H06 vs. H02).

5. The size of the debris particles ejected into the containment is small with a Sieve Mass Median Diameter (SMMD) smaller than 1.4 mm. With a closed pit it is only 0.15 mm. Larger particles are found in the subcompartment with a SMMD between 1.5 and 4.8 mm. No effect of pressure on particle size was found.

6. The maximum pressure in the containment was 0.44 MPa at 1.75 seconds after RPV failure. After 10 seconds it had decreased to 0.32 MPa. The pressure decreased although the hydrogen burned for up to 6 seconds.

7. With an open pit and hydrogen combustion the pressure rise is highest. Without a direct path into the containment less hydrogen is produced and burned. The pressure rise in the containment correlates to the amount of hydrogen burned. However, there is also a considerable pressure rise in the test without steam and hydrogen (H04), presumably because of the efficient heat transfer from the large amount of dispersed melt into the containment.

The experiments performed with nearly prototypical conditions in a small scale showed the importance of the direct path from the reactor pit to the containment. If that path does not exist, there will be a considerable ejection into the pump and steam generator rooms, but almost nothing into the open space of the containment. On the experimental scale the pressure increase will stay moderate and well below the design pressure of most containments. This applies for failures in the lower part of the RPV bottom head, at failure pressures between 10 and 20 bars. Without having done a hot test with lateral breaches yet, and no code calculations, we can only estimate the consequences of lateral breaches to be lower than those of more central breaches, taking the results from cold tests as reference. The comparison of two tests with and without steam, but both with hot melt, furnishes valuable data for model development concerning the effects of heat transfer, metal oxidation by air or steam and hydrogen production and combustion. All processes affect both, the melt dispersal, and the temperature and pressure load on the containment.

The experimental program is accompanied by analytical work with the objective to transform the experimental results to the prototypical case. The main tool is a multi-phase CFD-code to which specific DCH-models were added [Wil02]. The models used in the code are validated by comparison with experimental results [Wil01][Wil03]. An extrapolation out of the range of experimental parameters is necessary and a careful assessment of scaling is essential.

5 References

[Bla94] T.K. Blanchat, M.D. Allen, M.M. Pilch, R.T. Nichols, "Experiments to Investigate Direct Containment Heating Phenomena with Scaled Models of the Surry Nuclear Power Plant", *NUREG/CR-6152, SAND93-2519*, Sandia Laboratories, Albuquerque, N.M., (1994)

[Bla99] T. K. Blanchat, M.M. Pilch, R.Y. Lee, L. Meyer, and M. Petit, "Direct Containment Heating Experiments at Low Reactor Coolant System Pressure in the Surtsey Test Facility," *NUREG/CR-5746, SAND99-1634*, Sandia National Laboratories, Albuquerque, N.M., (1999).

[Mey03] L. Meyer, M. Gargallo, "Low Pressure Corium Dispersion Experiments with Simulant Fluids in a Scaled Annular Cavity", *Nuclear Technology*, **141**, pp. 257-274, 2003.

[Pil91] Pilch, M.M., "Adiabatic Equilibrium Models for Direct Containment Heating," presented at the 19th Water Reactor Safety Information Meeting, Washington, DC, SAND91-2407C, Sandia National Laboratories, Albuquerque, NM., October 1991

[Pil96] M.M. Pilch and M.D. Allen, 1996, Closure of the direct containment heating issue for Zion, *Nuclear Engineering and Design*, **164,** Issue1-3 , pp.37-60.

[Roth94] H. Roth-Seefried, A. Feigel, H.J. Moser, "Implementation of bleed and feed procedures in Siemens PWRs", Nuclear Engng. Design, 148 (1994), pp133-150

[Wil01] D. Wilhelm, 2001, Analysis of a Thermite Experiment to Study Low Pressure Corium Dispersion, Forschungszentrum Karlsruhe Report, FZKA 6602 (August 2001)

[Wil02] D. Wilhelm, "Chemical Reaction Models in a Code of the SIMMER-Family", Joint IAEA/NEA Technical Meeting on the Use of Computational Fluid Dynamic Codes for Safety Analysis of Reactor Systems, Including Containment, Pisa, Italy, 11-13 November, 2002

[Wil03] D. Wilhelm, 2003, Recalculation of corium dispersion experiments at low system pressure, NURETH-10, Seoul, Korea, October 5-9.